UNIVERSITE D'ABOMEY - CALAVI (UAC)

INSTITUT NATIONAL DE L'EAU

Registered under N° 5586-19/UAC/VR-AARU/SA

A DISSERTATION

Submitted

In partial fulfillment of the requirements for the degree of

DOCTOR of Philosophy (PhD) of the University of Abomey-Calavi (Benin Republic)

In the framework of the

Graduate Research Program on Climate Change and Water Resources (GRP-CCWR)

By

Oluwafemi Ebenezer ADEYERI

Public defense on: 12/04/2019

======

MODELLING THE HYDROLOGICAL RESPONSE OF KOMADOUGU-YOBE AREA OF THE LAKE CHAD BASIN TO CLIMATE CHANGE

======

Supervisors:

Agnidé Emmanuel LAWIN, Full Prof, University of Abomey-Calavi, Benin
Patrick LAUX, Associate Prof, Karlsruhe Institute of Technology, Campus Alpine, Germany

=====

Reviewers:

Philip OGUNTUNDE, Full Prof, Federal University of Technology, Akure, Nigeria
Sidéra Kodjovi EDJAME, Associate Prof, University of Lome, Togo
Aristide Barthelemy AKPO, Associate Prof, University of Abomey-Calavi, Benin

======

JURY

Jean Bio CHABI OROU	Full Prof, University of Abomey-Calavi, Benin	President
Philip OGUNTUNDE	Full Prof, Federal Uni. of Techn., Akure, Nigeria	Reviewer
Sidéra Kodjovi EDJAME	Associate Prof, University of Lome, Togo	Reviewer
Aristide Barthelemy AKPO	Assoc. Prof, University of Abomey-Calavi, Benin	Reviewer
Benjamin N'GOUNOU NGATCHA	Full Prof, University of Ngaoundere, Cameroon	Examiner
Agnidé Emmanuel LAWIN	Full Prof, University of Abomey-Calavi, Benin	Supervisor

Dedication

To him who sits on the throne whose mercies and kindness endure forever.

To my wife; Deborah, Son; Beethoven, Parents and Siblings for their love, encouragement and support.

Acknowledgements

This PhD work is realized in the framework of the West African Science Service Center on Climate Change and Adapted Land Use (WASCAL) and funded by the German Ministry of Education and Research (BMBF) in collaboration with the Benin Ministry of High Education and Scientific Research (MESRS).

I would like to acknowledge my supervisors; Prof. Agnidé Emmanuel Lawin (University of Abomey Calavi, Benin) and Dr Patrick Laux (Karlsruhe Institute of Technology (KIT), Campus Alpine, Germany) for the tremendous work in supervising and guiding me throughout this study. I would also like to acknowledge the Federal Ministry of Education and Research (BMBF), West African Science Service Centre on Climate Change and Adapted Land Use (WASCAL) and the Karlsruhe Institute of Technology (KIT) for the doctoral scholarship during this study. My appreciation goes to the Netherlands government for funding my scientific stay at the University of Twente.

My acknowledgement also goes to Prof Harald Kunstmann (KIT, Germany) for approving my stay at the KIT during the scientific visit and also for his overall contribution to the success of the programme. I acknowledge Dr Benjamin Lamptey (ACMAD, Niger) for his ideas and constructive criticism during the early stages of the research. My appreciation goes to Dr Joel Arnault (KIT, Germany) for his valuable ideas and inputs towards the realization of the research.

Sincere appreciations to Dr Peter Domonkos (University of Tarragona, Spain) for the provision of ACMANT package as well as the constructive discussions regarding the use of ACMANT as well as Dr Charles Perrin (National Institute of Science and Technology for Environment and Agriculture, France) for the fruitful discussion about the optimal usage of the hydrological model. Sincere appreciation also goes to Maurus Borne (KIT, Germany) for the python scripts used for some of the analysis, Dr Seyni Salack (WASCAL's competent center, Burkina-Faso) and Prof Charles Ichoku (NASA Goddard Space Center, USA) for the productive discussions.

I would also like to acknowledge the Committee of Space and Research (COSPAR) and Dr Ernesto Baeza (University of Valencia, Spain) for sponsoring and hosting me for a part of the research. My colleagues and the management and staff of the KIT Campus Alpine, WASCAL Graduate School on Climate Change and Water Resources are also acknowledged for their contribution towards this research. The reviewers of the research papers and the whole thesis are acknowledged for their valuable comments and suggestions.

Abstract
This study was carried out to investigate the hydrological response of the Komadougu-Yobe basin to climate change using daily observed data and outputs from regional climate models. Analyses carried out in this study include (a) the spatiotemporal trends and correlation in daily hydrometeorological variable as well as climate extremes, (b) the quantification and segregation of the contributory effects of precipitation variability and human influences on the variations in river discharge, (c) the calibration of and conceptual hydrological model using six evolutionary optimization methods and three combined objective functions over the study area. Results from this study showed an increasing trend of climate extremes, temperature, precipitation and river discharge. The distribution of LULC also affected the volume of river discharge. However, the impact of human activities and precipitation variability on river discharge was seen to be equally shared in the basin. Furthermore, the applied model parameters' optimization methods showed reasonable abilities to simulate runoff with a satisfactory level of accuracy towards more accurate representation of the river discharge in the basin in the context of climate change, climate extremes and water resources. Therefore, the attempts in this study to characterize areas in the river basin with the potential risk of climate extreme events will serve as a useful resource for assessments of the potential impacts of climate change on human, ecosystems, water resources.

Keywords: climate change, water resources, hydrological modelling, homogeneity, bias-correction, landuse landcover.

Synthèse de la Thèse

Résumé

Le présent travail analyse la réponse hydrologique du bassin du Komadougu-Yobe au changement climatique en utilisant les données d'observations journalières de même que des sorties des modèles climatiques régionaux. Dans un premier temps l'analyse des tendances et des inter-corrélations des variables hydrométéorologiques et des extrêmes climatiques a été faite. Ensuite, les effets contributeurs d'une part des variabilités de précipitation et de l'influence humaine d'autre part sur la variation des débits ont été quantifiées puis séparés. De plus, le calage et la validation d'un modèle hydrologique conceptuel ont été faits sur la zone d'étude en utilisant six méthodes d'optimisation évolutionnaire avec trois fonctions objectives combinées. Il en résulte une tendance à l'augmentation des extrêmes climatiques de même que la température, les précipitations et les débits. La distribution de l'utilisation des terres aussi affecte les débits. Cependant, les impacts des activités anthropiques et de la variabilité des précipitations sur les débits sont équitablement partagés dans le bassin. De plus, l'optimisation des paramètres du model hydrologique utilisé montre une aptitude du modèle à simuler les débits avec un niveau satisfaisant. Ainsi, le présent travail fait dans le but de caractériser la zone potentielle a risques climatiques extrêmes dans le bassin servira d'outils d'évaluation des potentiels impacts des changements climatiques sur l'homme, les écosystèmes et les ressources en eau.

Mots clés : Changement climatique, ressource en eau, modélisation hydrologique, homogénéité, correction de biais, utilisation des terres.

Introduction

Le bassin du lac Tchad (LCB) a connu des changements drastiques de couverture des terres et une mauvaise gestion de l'eau au cours des 50 dernières années. Les sécheresses successives dans les années 1970 et 1980 ont abouti à une pénurie d'eau de surface et souterraines. Les impacts hydrologiques de ces fluctuations climatiques ne sont pas assez bien compris, car ils nécessitent des études à de plus petite échelle, avec des systèmes d'observation de haute résolution afin d'établir un lien entre les grandeurs climatiques et hydrologiques. Le bassin du Komadougu-Yobe (KYB) est un sous bassin du grand bassin du lac TChad. Ce bassin est drainé par deux principaux sous-systèmes. Le premier sous-système représente la rivière Yobe, qui est formée par les tributaires Hadejia et Jama'are, qui créent la plaine d'Hadejia-Nguru à leur confluence. Le second sous-système est la rivière Komadougu-Gana, qui a toujours été considérée comme un affluent de la rivière de Yobe. La zone active du bassin qui fournit de l'eau de surface au lac Tchad et à son bassin est située en dehors des limites conventionnel du

bassin dans les états de Kanjo, Bauchi et du Plateau. La partie centrale du bassin contient l'une des plus importantes zones humides du pays.

Avant la sécheresse des années 1970 et 1980, le bassin du Komadougu-Yobe contribuait à d'importante quantité d'eau de la partie nord du lac Tchad. Les sécheresses répétées des années 1970 et 1980 ont entraîné des modifications de l'environnement, qui ont conduit à un certain déclin de l'agriculture, l'élevage et de la pêche impactant ainsi le bien-être socio-économique des personnes vivant dans le bassin. Au cours des dernières décennies, le changement climatique et les activités anthropiques ont été les causes de la modification du cycle hydrologique dans ce bassin transfrontalier. Cela a conduit à une pression sans précédent sur les ressources en eau douce, ce qui a incité les décideurs à rechercher des méthodes de gestion de la crise. Cette étude est réalisée pour étudier la réponse hydrologique du bassin du Komadougu-Yobe au changement climatique afin de comprendre l'interaction entre le changement climatique et la disponibilité des ressources en eau douce dans le bassin.

Zone d'étude

Le KYB est situé au sud du désert du Sahara, dans la région sahélienne de l'Afrique. L'élévation du bassin est comprise entre 285 et 1750m. Il a une superficie de 150 000 km2 et représente près de 35% du bassin du lac Tchad. Il est drainé par les rivières d'Hadejia et Jama. Les pertes d'eau les plus importantes dans ces rivières sont par infiltration de même que l'évaporation et les prises d'eau. La saison des pluies s'étale en moyenne de Mai à Octobre. Les précipitations annuelles moyennes varient entre 300 à 1200 mm, alors que la température moyenne annuelle est de 29°C. Le système climatique dans ce bassin est régi par deux principaux systèmes de vent ; la saison sèche gouvernée par le vent du Nord-est qui apporte la poussière et du sable du Sahara et la saison de pluie gouvernée par le vent de sud-est qui apporte l'humidité de l'océan Atlantique. La moyenne annuelle de l'évaporation potentielle dans le bassin varie entre 1800 mm et 2400 mm. Le bassin est caractérisé par la présence d'épisodes de sécheresse grave ainsi qu'une forte variabilité climatique.

Matériel et méthodes

Cette étude a utilisé l'ensemble des données observées aux stations météorologiques aux points de grille de même que les sorties des modèles climatiques régionaux. Les données d'observations sont : la pluie journalière, le débit journalier à la station de Diffa et les températures minimales et maximales quotidiennes. Les données de grille de 10 km de résolution ont été obtenues à partir des archives de l'Université de Princeton (PGF) au Royaume-Uni tandis que les données CORDEX (Coordinated Regional climate Downscaling Experiment) ont été fournies à 50 km de résolution à partir des modèles climatiques régionaux. Les données des stations observées ont été collectées à l'Agence Météorologique Nigériane (NiMet) et à la station hydrologique de Diffa.

Les données d'observations et celles maillées ont été utilisées dans l'évaluation de l'impact du changement climatique sur les périodes historiques. Elles ont également servi à corriger les modèles climatiques de façon à minimiser l'écart entre les variables climatiques observées et simulées à l'échelle journalière. Cela a été exécuté par l'application d'une transformation des sorties de modèles climatiques de sorte que l'amplitude et la répartition de la variable transformée se rapprochent de celle de l'observation à un point donné. Après la correction des biais, les sorties des modèles climatiques ont été utilisées pour projeter les phénomènes climatiques extrêmes à l'avenir dans le bassin. Par la suite, la détection des périodes de changement brusque a été faite. Ces changements brusques pourraient avoir été causés par un repositionnement d'instrument de mesure ou de lecture ou aussi d'une délocalisation etc. Ces points de changement brusque ont été corrigés, fournissant ainsi un ensemble de données de haute qualité qui est nécessaire à l'analyse. Une première partie de ce travail a été consacrée à l'étude des tendances spatio-temporelles et l'analyse de l'homogénéité de la pluviométrie sur le bassin à l'aide des données du l'Agence Météorologique Nigériane (NiMet) de même que celles maillées à 10 km de résolution obtenu de l'Université de Princeton (PGF) pour la période 1979 et 2015. Les données analysées à l'échelle annuelle et saisonnière (saisons sèches et humides), ont été soumis au test de Mann-Kendal modifié qui consiste à la détection de tendance après application du test d'autocorrélation sérielle. Le test d'homogénéité a été réalisé à l'aide du test de Pettitt, Buishand, du test d'homogénéité normale Standard et celui de van Belle et Hughes. La deuxième partie a été consacrée à l'évolution spatio-temporelle des précipitations journalières observées, du débit, des températures minimale et maximale sur la période 1971-2013 dans le bassin du Komadougu-Yobe (KYB). Dans cette analyse, des changements importants dans le temps ont été détectés et corrigés en utilisant l'algorithme de Caussinus-Mestre adaptés pour les réseaux d'homogénéisation de la température (ACMANT). Le test de Mann-Kendall et la pente de Sen sont utilisés pour estimer la tendance et l'amplitude de changement de tendance sèche et humide à l'échelle de la saison. La troisième partie a fait l'objet de la quantification et la ségrégation des effets contributeurs de la variabilité des précipitations et de l'influence des activités humaines sur les variations de débit à l'aide de pluies journalières et de débits journaliers entre 1971 et 2013. Le double cumul de masse (DMC) a été utilisé pour la détermination des points de rupture causés par ces deux effets. Ensuite, une quatrième partie a été consacrée à l'analyse de l'occurrence des extrêmes climatiques passés et de projections futures à l'aide du test de régression et la statistique F. Les indices climatiques extrêmes considérés sont : les fréquences de journées chaudes (TX90p), nuit fraîche (TN10p), nuit chaude (TN90p). De plus il a été considéré l'indicateur de durée des épisodes chauds (WSDI), l'amplitude thermique diurne (DTR), maximum de 5 jours de précipitations (RX5day), le nombre de jours consécutifs sec (CDD), le nombre de jours de consécutifs humide (CWD), la précipitation des jours très humides (R95P), la précipitation des

jours extrêmement très humides (R99P), et les précipitations totales annuelles (PRCPTOT). Ces extrêmes ont été analysés sur la période historique (1971-2017 ; 1971-2005), dans le futur proche (2020-2050) et le futur lointain (2060-2090) sur la base des deux scénarios d'émissions RCP4.5 et 8.5. Cette analyse s'est faite à deux échelles temporelles et spatiales. Une cinquième partie a pris en compte le calage du modèle hydrologique conceptuel du Génie Rural à 5 paramètres au pas de temps journalier (GR5J) à l'aide de six méthodes d'optimisation, à savoir l'Optimization-Multi local (OLM), l'évolution différentielle (DE), la méthode multi-objectifs d'optimisation d'essai de particules (MPSO), Algorithme Mimétique avec des chaînes de recherche locale (MALS), la fonction d'Evolution-Rosenbrock complexes mélangées (SCE-R), l'approche Bayesienne de Monte Carlo par chaîne de Markov (MCMC) et les trois fonctions objectives combinées (minimisant RMSE, maximisant les NSE et KGE) sur la zone d'étude.

La méthode d'étalonnage multi-objectifs vise à quantifier les ajustements afin de maximiser ou minimiser un certain nombre de fonctions objectifs, trouver un ensemble représentatif de la solution optimum de Pareto, ainsi que la définition d'une solution unique qui maximise ou minimise une préférence spécifique et indépendante. Les calages à objectifs multiples sont d'un grand avantage car ils garantissent les résultats souhaités dans les applications hydrologiques. L'avantage d'utiliser les diverses méthodes d'optimisation réside dans sa capacité à évaluer la qualité des phases de l'optimisation de solutions telles que les précisions, leur diversité et les cardinalités.

Résultats et Discussion

Les résultats de cette étude ont montré une tendance croissante des phénomènes climatiques extrêmes de température, de précipitations et de débit. Il est observé une augmentation latitudinale (diminution) de la température du bassin (précipitations) aux latitudes supérieures. Il a été également remarqué une augmentation de la température et des précipitations dans le bassin. La tendance annuelle de température est présentée à la Figure 1.

Il y a une corrélation négative entre le débit et les températures plus chaudes. La corrélation entre les variables considérées à différentes saisons est présentée à la Figure 2. Les résultats de la répartition en pourcentage des classes LULC apportées ont montré qu'il y a eu une augmentation des sols nus et des plantations de 1975 à 2013, avec une diminution de la couverture forestière et des prairies. L'agriculture irriguée a augmenté de 1975 à 2000 avant de diminuer à partir de 2000 à 2013. La variation relative de la distribution des classes LULC pour trois périodes à savoir 1975-2000, 2000-2013 et 1975-2013 a montré qu'entre 1975 et 2000, il y a une augmentation dans toutes les classes sauf à l'utilisation des forêts et prairies avec les variations relatives de -10 % et -20 % respectivement.

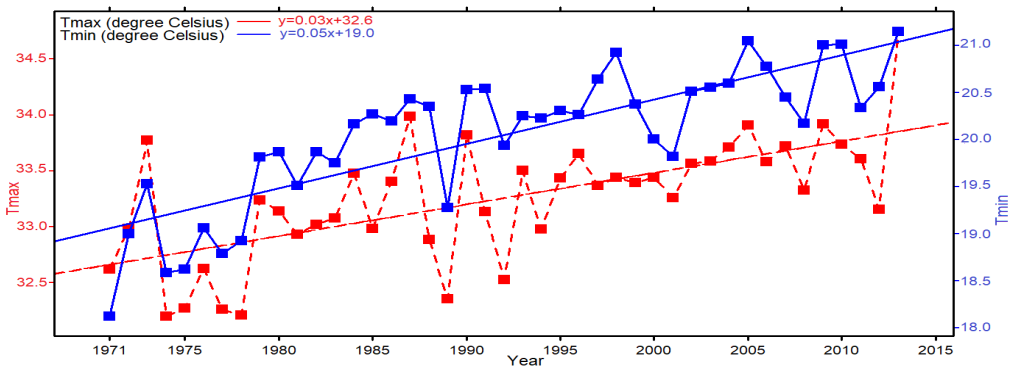

Figure 1: Tendance annuelle de température maximale et minimale sur le KYB entre 1971 et 2013

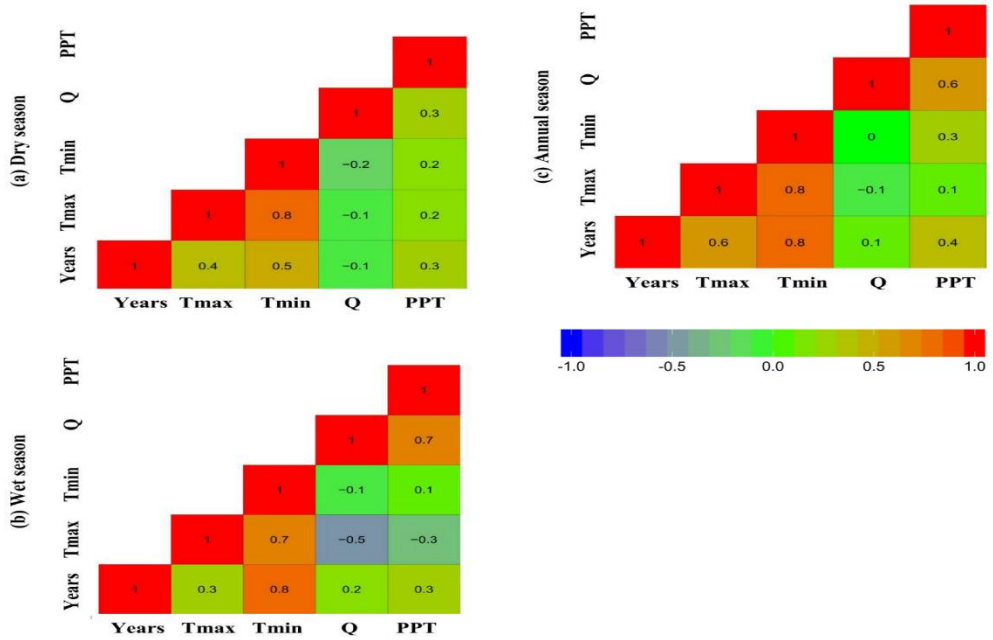

Figure 2: Graphe de corrélation des variables hydrométéorologiques ; (a) pendant la saison sèche, (b) saison humide, et (c) saison annuelle

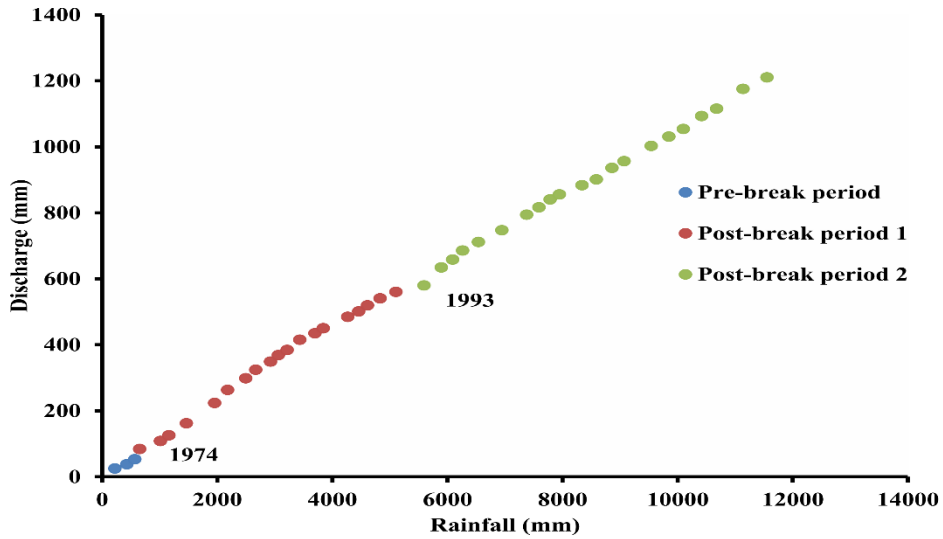

Figure 3: Relation entre débit de la rivière et de DMC précipitations entre 1971 et 2013

Tableau 1: Impact des activités humaines et la variabilité des précipitations sur le débit de la rivière

Année	Le débit moyen observé (mm)	Impact de la pluie (%)	Impact des activités humaines (%)
1971-1973	17.7	17.7	
1974-1992	26.7	20.9	35.6
1993-2013	31.0	25.4	58.5
1974-2013	28.9	23.3	49.8

Entre 2000 et 2013, les forêts et prairies montrent également une tendance à la diminution. Cependant, il y a une diminution de l'agriculture irriguée (-10 %). Cet écart présente une variation relative positive de 17,6 % enregistrée entre 1975 et 2000. Pour l'ensemble de la période, c'est-à-dire de 1975 à 2013, il y a une diminution constante de la forêt et des prairies bien qu'il y ait eu des gains dans d'autres classes d'utilisation des terres.

Dans l'ensemble, la plantation a obtenu le gain le plus élevé de 41 % tandis que les savanes ont connu un taux de perte de 38 %. La distribution de l'utilisation des terres affecte également le débit. En effet, le débit a augmenté avec la réduction de l'agriculture irriguée, forêt et prairie. De plus, lors de l'utilisation du DMC pour établir la relation entre débit de la rivière et les précipitations, il apparait une ligne droite sans déflexion, illustrant une condition de non existence d'influences extérieures. Cependant, le résultat de DMC a identifié trois grands points d'arrêt en 1974 et 1993, suggérant que les changements de débit n'étaient pas seulement dus à la variabilité des précipitations, mais aussi de l'influence de l'homme. Ces points de rupture correspondent aux années pendant lesquelles les différents barrages et l'irrigation à grande échelle est devenu pleinement opérationnel. Le point de changement année est présenté à la Figure 3. D'autres analyses sur l'ensemble de la période post-rupture a montré que l'impact des activités humaines et la variabilité des précipitations sur le débit de la rivière a été vu pour être partagé également dans le bassin. C'est présenté dans le Tableau 1.

Les indices de température extrême considérés montrent une tendance significative au réchauffement du bassin. Il y a une tendance à l'augmentation de jours très humides et extrêmement humides. En raison de la variabilité spatiale des précipitations, les indices de précipitations semblent suivre les différentes tendances à différents intervalles de temps en vertu des deux RCP. En effet, tous les indices de précipitation totale annuelle, de jours très humides, extrêmement très humides, et maximum 5 jours de pluie suivent une tendance négative en considérant un futur proche bien que cette tendance soit non statistiquement significative pour toutes les stations sous les projections RCP4.5 et 8.5. Cependant, cette tendance est plutôt positive pour tous les indices sous les deux scénarii pour un futur lointain. Ceci représente donc une intensification des événements extrêmes à l'avenir.

L'amplitude de l'évolution de la chaleur extrême est plus grande que celle de froid extrême. En conséquence, les distributions des extrêmes de chaleurs associées à l'augmentation de la température journalière changeraient plus rapidement que les extrêmes de fraicheurs. L'augmentation des tendances positives dans les précipitations annuelles totales et les tendances positives dans l'intensité des événements coïncidents avec les tendances positives de chaleur extrême. Les détails des modifications dans l'ampleur et de la tendance des événements extrêmes à l'échelle de temps considérée sont présentés au Tableau 2. M représente la grandeur tandis que T représente la tendance moyenne.

Tableau 2: Changements dans l'ampleur et de la tendance des événements extrêmes

Indices	Historique-Futur proche	Historique-Futur lointain	Futur proche-Futur lointain
Dtr	-T/-M	-T/ +M	-T/ +M
Tx10p	-T/ +M	-T/ +M	-T/ +M
Tx90p	+T/-M	+T/-M	+T/-M
Tn10p	-T/ +M	-T/ +M	-T/-M
Tn90p	+T/ +M	+T/-M	+T/-M
Wsdi	+T/-M	+T/ +M	+T/ +M

En ce qui concerne la modélisation hydrologique, l'étalonnage appliqué au KYB a montré les capacités du modèle à simuler l'écoulement avec un degré de précision satisfaisant. Les résultats de la statistique des flux ne sont pas universellement cohérents puisque certaines méthodes d'optimisation surestiment constamment alors que d'autres sous-estiment la représentation de flux. Par exemple, la MCMC a sous-estimé la durée maximale du pic de débit par -2 jours tandis que MALS surestimé par +13 jours. Pour le cas particulier de KYB, nous avons constaté que le DE et le SCE-R sont les meilleures méthodes. Le calcul multi-objectif pour l'évaluation de méthode d'optimisation pour atteindre les solutions optimales de Pareto MALS a montré le plus grand nombre d'expositions d'itérations alors que LOMS avait le plus grand nombre de simulations pour les deux périodes d'étalonnage. La plus faible des itérations et des simulations ont été approchés par le SCE-R dans tous les cas. La comparaison de la période de calcul et la mesure de performances de SCE-R indique l'équilibre entre la précision de la période de calcul et de simulation. Cependant, la combinaison de fonctions multi-objectifs et multi-techniques d'optimisation pour les ensembles de Pareto optimales n'ont pas seulement améliorer la stabilité des paramètres du modèle au cours de l'étalonnage, mais aussi améliorer la capacité d'optimisation des algorithmes d'étalonnage les rendant plus précis et robuste pour la représentation du débit de la rivière dans le bassin dans le contexte du changement climatique, les extrêmes climatiques et les ressources en eau.

Conclusion

Cette étude a porté sur la réponse hydrologique du bassin transfrontalier du Komadougu-Yobe de l'Afrique de l'Ouest face aux changements climatiques. Il y a une tendance croissante générale de température et des précipitations dans l'ensemble du bassin. Cette augmentation de la température pourrait réduire la disponibilité des pâturages à l'alimentation du bétail, avec une incidence sur le rendement des cultures et intensifier l'impact des sécheresses. D'autre part, l'augmentation des précipitations en raison de la reprise des pluviométries sahéliennes pourrait relancer les zones humides dans le bassin afin de maintenir l'équilibre de la chaîne alimentaire et préserver de l'écosystème. Cependant, l'excès d'eau pourrait entraîner des inondations, de sorte que les exploitations agricoles, les produits agricoles et les propriétés soient affectés. De plus, il y a eu une tendance croissante des événements extrêmes dans le bassin. Afin de représenter avec précision la réponse hydrologique du bassin au changement climatique, une solide stratégie de modélisation hydrologique a été développée pour prendre en compte les propriétés hydrologiques de la zone d'étude face à des extrêmes climatiques. La combinaison des fonctions multi-objectifs et multi-techniques d'optimisation pour les ensembles de Pareto optimal pour la modélisation hydrologique n'est pas seulement pour améliorer la stabilité des paramètres du modèle au cours de l'étalonnage dans le KYB, mais aussi pour améliorer la capacité d'optimisation des algorithmes d'étalonnage pour les rendre plus précis et robuste à représenter les débits dans le bassin dans le contexte du changement climatique, les extrêmes climatiques et les ressources en eau. Les impacts environnementaux associés à l'augmentation des événements climatiques extrêmes et les activités anthropiques pourraient entrainer en particulier des coûts économiques pour des zones vulnérables (comme de la zone d'étude) en Afrique de l'Ouest. Par conséquent, les tentatives faites dans cette étude pour caractériser les zones dans le bassin du fleuve avec le risque potentiel d'événements extrêmes climatiques servira à l'évaluation des impacts potentiels des changements climatiques sur les écosystèmes, les ressources en eau, et par conséquent améliorer la préparation à l'adaptation régionale, la planification des stratégies et la prise de décisions.

Table of Contents

List of Acronyms

ACMANT	Adapted Caussinus-Mestre Algorithm for homogenising Networks of Temperature series
AMMA	African Monsoon Multi- disciplinary Analyses
AOGCM	Atmospheric-Ocean General Circulation Model
CDD	Consecutive Dry Days
CORDEX	Coordinated Regional climate Downscaling Experiment
CV	Coefficient of Variation
CWD	Consecutive Wet Days
DMC	Double Mass Curve
DE	Differential Evolution
DMN	Direction de la Meteorologie Nationale
DTR	Diurnal Temperature Range
ENSEMBLES	ENSEMBLE-Based Predictions of Climate Changes and their Impacts
GCM	Global Climate MModel
GHG	Green House Gas
GR5J	modèle du Génie Rural à 5 paramètres au pas de temps Journalier
HYPE	Hydrological Predictions for the Environment model
IDW	Inverse Distance Weighted
ITCZ	Inter-Tropical Convergence Zone
KGE	Kling-Gupta Efficiency
KYB	Komadougu-Yobe Basin
LOMS	Local Optimization-Multi Start
LOWESS	Locally Weighted Scatterplot Smoothing
MALS	Memetic Algorithm with Local Search Chains
MCMC	Bayesian Markov Chain Monte Carlo
mHm	Mesoscale Hydrological Model
MK	Mann-Kendall
MMK	Modified Mann-Kendall
MPSO	Multi-objective Particle Swarm Optimization
NAO	North Atlantic Oscillation
NiMET	Nigerian Meteorological Agency

NSE	Nash-Sutcliffe Efficiency
NSGA	Non-Dominated-Sorting-Genetic-Algorithm
PRCTOT	Annual Total Precipitation
R95P	Very Wet Days
R99P	Extremely Wet Days
RCA	Rossby Centre Regional Atmospheric Model
RCM	Regional Climate Model
RCP	Representative Concentration Pathways
RMSE	Root Mean Square Error
RR	Precipitation Amount
RX5DAY	Maximum 5-Days Precipitation
SCE-R	Shuffled Complex Evolution-Rosenbrock's function
SNHT	Standard Normal Homogeneity Test
TN	Minimum Temperature
TN10P	Cool Night Frequency
TN90P	Warm Night Frequency
TX	Maximum Temperature
TX90P	Warm Day Frequency
WAM	West African Monsoon
WSDI	Warm Spell Duration Indicator
X1	maximum capacity production store
X2	inter-catchment exchange coefficient
X3	maximum capacity routing store
X4	unit hydrograph
X5	inter-catchment exchange threshold

List of Figures

List of Tables

"The first law of success is concentration- to bend all the energies to one point and to go directly to that point, looking neither to the right nor to the left- William Mathews".

CHAPTER 1: General Introduction

The general introduction section is outlined as described below. Section 1.1 focussed on the context and the problem statement, section 1.2 presented the state of art, section 1.3 described the research questions, section 1.4 focussed on the objectives of the thesis while section 1.5 focussed on the hypothesis. Section 1.6 focussed on the novelty, section 1.7 described the scope of the thesis, section 1.8 discussed the expected results and the outline of the thesis is presented in section 1.9.

1.1 Context and problem statement

The Komadougu-Yobe Basin (KYB) had witnessed intensive grazing, desertification and improper water management practices, which had altered the hydrological processes in the basin.

The KYB is one of Nigeria's most important agricultural basins and currently produces food and cash crops including sorghum, rice, millet, groundnuts, wheat, cowpeas and vegetables under both upland and irrigated farming. The farming system in, especially the high population density zones of the basin including the Kano-Close-Settled Zone (KCSZ) which is described as a zone practicing intensive agricultural (Tanko 2007). There are also the productions of livestock, trees which yield fruits, edible leaves, silk, cotton and firewood. Fishing is also an important activity of the people in the basin.

The drought of 1970s and 1980s coupled with uncoordinated water resources management and the increasing population have led to the degradation of the natural resources of the basin (Uluocha and Okeke 2004). For instance, sheet and wind erosion leading to formation of sand dunes, fertility reduction and drying-up of some floodplains/wetlands have been observed. In the field of livestock and fisheries, herds have been decimated and fish stocks have diminished (Uluocha and Okeke 2004).

The climatic instability characterized by occurrence of three drought periods coupled with the construction of dams upstream has led to the need for more water for people downstream. However, the hydrology of the basin is complex. Both the Hadejia and Jama'are river systems are 'gaining' rivers until they cross the geological divide between the basement complex and the Chad formation after which their flows begin to decrease. As the demand for water increases due to the soaring population and varying climatic conditions, there is need for good and sustainable management practices for the dwindling water resources. To achieve this, there

is the need for accurate information from timely hydro-climatological, remote-sensing data and projections of future climate.

In most cases, these data are not easy to come-by or do not even exist at all. This is a major gap. This proposed study will contribute towards building capacity to address this gap. This study will develop capacity to address the data gap by exploiting the suitability of different climate models and their ensembles to replicate the in-situ climatic scenarios so as to extrapolate the findings to the part of the basin with paucity of data. The climate model output will in turn be used to drive a selected hydrological model so as to study the interface between climate and water. This is important for the study area because of its strategic location and utmost importance to the surrounding communities. The study will allow decision makers and stakeholders to better evaluate the performance of irrigation systems based on the better understanding of climate change and to also propose relevant adaptation strategies in the basin as a result of the increased knowledge gained.

1.2 State of art

Lake Chad Basin (LCB) has experienced drastic changes of land cover and poor water management practices during the last 50 years (Li et al. 2007). The successive droughts in the 1970s and 1980s resulted in the shortage of surface water and groundwater resources. This problem of drought and water shortage has a devastating implication on the natural resources of the LCB with great consequence on food security, poverty reduction and quality of life of the inhabitants (Babamaaji and Lee 2014) . The combined effects of climate variability and increased human unsustainable water consumption led to a significant change of the water balance of the Lake Chad drainage basin. In turn this situation has resulted in the shrinkage of the lake (Coe and Foley 2001). During the last 50 years, West Africa has been subject to significant precipitation variability, characterized both by large interannual fluctuations and by periods of long-lasting droughts, such as during the period 1970-1990. Numerous studies have described this variability and its controlling factors, more often at large space–time scales (Le and Galle 2005) hydrological impacts of these climatic fluctuations are not as well understood, because they require studies at smaller scales, with high-resolution observing systems, to link the climatic and hydrological scales (Lebel and Ali 2009). Numerous studies have been conducted for the problems of Lake Chad. It is agreed that the lake levels have fluctuated considerably over the past decades in response to the climate variability and environmental degradation (Buma et al. 2016; Coe and Foley 2001). (Buma et al. 2016) investigated the hydrological variability associated within the LCB from January 2003 to December 2013; they found that the discharge in this area is governed by surface water of the lake.

The Komadougu-Yobe Basin (KYB) is a sub-basin of the larger Lake Chad Basin. The basin is drained by two main river sub-systems. The first sub-system, the Yobe River, is formed by

the Hadejia and Jama'are tributaries, which create the Hadejia-Nguru floodplain at their juncture. The second sub-system is the Komadougu Gana (or Missau) River, which historically has been seen as a tributary of the Yobe River (Muhammad et al. 2015a). The active watershed basins that supply surface water to the basin and the Lake Chad are located outside the limit of the conventional basin in Kano, Bauchi and Plateau States (Sobowale et al. 2010b). The middle part of the basin contains one of the country's most significant wetlands.

Prior to drought of 1970s and 1980s, it contributed substantial volume of water to the northern pool of Lake Chad. The repeated droughts of the 1970s and 1980s have resulted in significant environmental changes, which in turn led to some decline in agriculture, livestock and fisheries as well as threatened the socio-economic well-being of people living in the basin (Tafida and Galtima 2016). During the last 30 years, parts of Komadougu-Yobe Basin (KYB) have been at the forefront of watershed development aimed at tackling the challenges of poverty alleviation and more recently environmental sustainability. The period witnessed unprecedented development at the upper reaches of the basin, which led to significant socio-economic advances but this was at a cost of several environmental degradation and some socio-economic dislocations (Tafida and Galtima 2016).

However, previous studies have only focused on the past and present changes in the hydrological components of the KYB (Lopez et al. 2016; Muhammad et al. 2015; Odunuga et al. 2011b; Tafida and Galtima 2016; Uluocha and Okeke 2004) using the available datasets which are most time limited and prone to inaccuracies (Buma et al. 2016), some other studies tried to fill in the gap of unavailability of dataset by using different remote sensing and satellite data (Onamuti et al. 2017) without a detailed investigation of what future hydrology of the KYB will look like under different climate scenarios. For example (Ejieji et al. 2016; Odunuga et al. 2011b) found out that at there is a decrease in precipitation amount from the upstream (the south of the basin) to the downstream northern part of the basin. The reduction of flow at Hadejia River between 1964-1973 and 1979-1989 was attributed to the construction of the dams (Tiga and Challawa), blockage of the river by Typha weeds, and droughts (Odunuga et al. 2011b). There was also a reduction in flow of Jama'are River, which is an uncontrolled river. Unlike the Hadejia, the reduction in the flows of Jama'are is attributed to droughts, evapotranspiration and losses due to anthropogenic activities (Odunuga et al. 2011b).

Specifically, this study shall account for the changes in the climate and surface runoff as well as quantifying the water yield through modelling, remote sensing and statistical techniques and will also project the future climate and surface runoff response of the Komadougu Yobe area of the Lake Chad basin to climate change scenarios using climatic and hydrological models.

1.3 Research questions

The relevant research questions discussed in this study are;

1 Are there changes in the trend and magnitude of river discharge, precipitation and temperature in the Komadougu-Yobe basin?
2 What is the impact of climate and human activities on the hydrological regime of the basin?
3 Are there traces of climate extreme conditions as a result of climate change in the basin both in the historical and future time scales?
4 Is there a way to improve the hydrological model parameters for optimal representation of river discharge in the basin?

1.4 Thesis objectives

1.4.1 Main objective

The aim of the research is to model the hydrological response of the Komadougu-Yobe area of the Lake Chad Sub-Basin to climate change.

1.4.2 Specific objectives

The specific objectives of this research are to:

1. analyse the trend in meteorological variables as well as climate extremes in the basin,
2. assess the impact of human activities and precipitation variability on the river discharge, and
3. model the river discharge of the basin using multi-objective functions and multi-optimization techniques.

1.5 Hypothesis

The hypotheses to verify in this thesis are presented below.

Hypothesis 1 (H1); human activities alter the flow of river or discharge in the basin,

Hypothesis 2 (H2); the effect of climate change is evident on the hydrological cycle of the basin.

1.6 Novelty

Limited hydrological and climatic data of sufficient quality have hindered sound research and in-depth investigations of the basin's hydrology. The spatial distribution of the existing observational network for hydro-climate data especially the climatic data are inadequate, being too thinly spread and located in big cities. In most cases the stream gauges are without proper rain gauge representation upstream of the catchment outlets. Thus, assessments of water resources through hydrological models or further hydrological studies are often difficult and not well enough supported by data. In view of this, there is a need to integrate the Earth Observation (EO) data but the EO data must be validated by in situ data. The EO data could be

used for “proof of concept” until in situ data becomes available. This will aid the modelling of water resources especially in areas with little or no in-situ data and quantify the water yield and at a spatial scale.

Furthermore, the scarcely available data sets are in some cases in-homogenous, hence, to accurately understand the climate change impact on water resources in the basin, there is need for the data set to be homogenized. In addition, to further understand the future climate extreme events at a basin scale, there is need to accurately downscale climate model outputs to be able to represent the inherent properties of the basin. The above-mentioned points have been lacking in the KYB, hence, they were clearly analysed and interpreted in this thesis. This will improve our understanding of the water budget partitioning which is essential in appreciating the dynamics of the basin both in space and time and under a changing climate.

This thesis is my own unaided work except as stated in the acknowledgements. No other person’s work has been used without due acknowledgment in the main text of the report. It has not been submitted before for any degree or examination at any other universities.

1.7 Scope of the thesis

This thesis focuses on the test, detection and correction of abrupt change points in observation time series. Other elements include the trend detection in meteorological variables in the basin, quantification and segregation of the impacts of human activities and precipitation variability on the basin’s stream flow, analysis of precipitation and temperature extremes in the basin at both historical and future time slices under two emission representative pathways. Additionally, the scope includes the combination of multi-objective functions and multi-optimization techniques to improve the hydrological model’s parameters stability in representing the actual stream flow in the basin. However, due to time constraints, the projection of the stream flow response to future climate has been advertently left out from the thesis.

1.8 Expected results and benefits

At the end of this thesis, trends in meteorological variables as well as climate extremes in the basin are analysed, the impact of human activities and precipitation variability on the river discharge are assessed, and the modelling of the river discharge of the basin using combined multi-objective functions and multi-optimization techniques to improve the hydrological model’s parameters stability is carried out.

Overall, this study will increase our understanding of climate change based on which relevant adaptation strategies in the basin could be drafted.

1.9 Outline of the thesis

The thesis is written in paper format.

Chapter 1 is an overview of the vulnerability of the KYB to human activities and the effect of climate change. This chapter explored the drought episodes and its effect on the livelihood in the KYB. Furthermore, the problem statement, justification of study, objectives as well as the expected results is covered.

Chapter 2 covers the description of the study area, flow characteristics under different climate scenarios and the experimental set up.

Chapter 3 investigated the spatio-temporal trends and homogeneity analysis of precipitation over the Komadougu-Yobe basin using data from Nigerian Meteorological Agency (NiMet), Department of National Meteorology Niger (DMN) and a 10 km resolution gridded observation data from Princeton University (PGF) for the period 1979 and 2015.

The data, analysed at the annual and seasonal (wet and dry seasons) timescales, were subjected to Mann-Kendal including modified Mann-Kendall trend test after testing for autocorrelation. Test for homogeneity was performed on the data using Pettitt's, Buishand's, Standard Normal Homogeneity Test and van Belle and Hughes' test.

Chapter 4 described the spatiotemporal trends in daily observed precipitation, river discharge, maximum and minimum temperature data between 1971 and 2013 in the Komadougu-Yobe Basin (KYB). Significant change points in time series were detected and corrected using Adapted Caussinus–Mestre Algorithm for homogenising Networks of Temperature series (ACMANT) algorithm. Mann-Kendall test and Sen's slope is used to estimate the trend and magnitude change at dry, wet and annual season time scales.

Chapter 5 explicated the variations in river discharge as a result of the contributory effects of precipitation variability and human influences using daily precipitation and discharge data between 1971 and 2013.

Chapter 6 explained the occurrence of climate extreme over the study area both in the past as well as the future projections. The climate extreme indices considered are the warm day frequency (tx90p), cool night frequency (tn10p), warm night frequency (tn90p), warm spell duration indicator (wsdi), diurnal temperature range (dtr), maximum 5-days precipitation (rx5day), consecutive dry days (cdd), consecutive wet days (cwd), very wet days (r95p), extremely wet days (r99p), and annual total precipitation (prctot).

Chapter 7 elucidated the use of combined multi-objective functions and multi-optimization techniques to improve the hydrological model's parameters stability and the algorithms' optimization to represent the runoff in the basin.

Chapter 8 and 9 summarizes the results and concluded the thesis.

CHAPTER 2: Study area and data presentation

The description of the study area and data is presented in this section. Section 2.1 described the study area, section 2.2 described the climate of the basin, section 2.3 focussed on the flow characteristics while section 2.4 presented the dams in the basin. Section 2.5 focussed on the water use and ecosystem, section 2.6 and 2.7 described the data used and the experimental set up respectively.

2.1 Study Area

The Komadougu-Yobe (Figure 4) is a sub-basin of the larger Lake Chad Basin. It is situated in the Sudan-Sahel zone of northeast Nigeria and southeast Niger covering an area of 148,000 km^2, out of which 84,138 km^2 is in Nigeria (57% of basin area) with a population of over 10 million people. It represents approximately 35 percent of the conventional basin of Lake Chad. The Nigerian sector of Komadougu-Yobe Basin (KYB) accounts for 95% of the basin's total contribution to the lake (Odunuga et al. 2011b).

The basin is drained by two main river sub-systems. The first sub-system, the Yobe River, is formed by the Hadejia and Jama'are tributaries, which create the Hadejia-Nguru floodplain at their juncture junction. The second sub-system is the Komadougu Gana (or Missau) River, which historically has been seen as a tributary of the Yobe River (Muhammad et al. 2015a).

The Hadeja wetlands are composed of swamp, grassland, and woodland created by the passage of the Hadeja and Jama'are Rivers. The area flooded annually by river discharge, supports various socioeconomic activities and provides a favorable environment for migratory species.

The climatic features of the basin are made up of three different types ranging from the north east to the southwest (IUCN 2011):

(i) Sahelo-sudanian climate, with an average annual precipitation of between 300 to 600 mm corresponding to an area of mixed cropping and livestock activities;

(ii) Sudano-sahelian climate, with an average of 600 to 900 mm of precipitation suitable for cultivation of maize, cotton, cowpeas and rice; and

(iii) Sundan-savannah climate, with 900-1200 mm of mean annual precipitation suitable for varied crops and fisheries.

2.2 Climate

Due to the global positioning of the basin, the precipitation period varies from one location to the other. The average annual precipitation ranges between 300 to 1200mm (IUCN 2011).

Precipitation is seasonal and limited to between May and October in the Nigeria portion, shorter than that in the Niger sector. This highly seasonal nature of the precipitation is the result of the annual migration of the Inter-Tropical Convergence Zone (ITCZ). Annual potential

evaporation tends to vary between 1,800 mm and 2,400 mm across the basin, though lower rates are recorded at Jos on the raised Plateau (IUCN 2011).

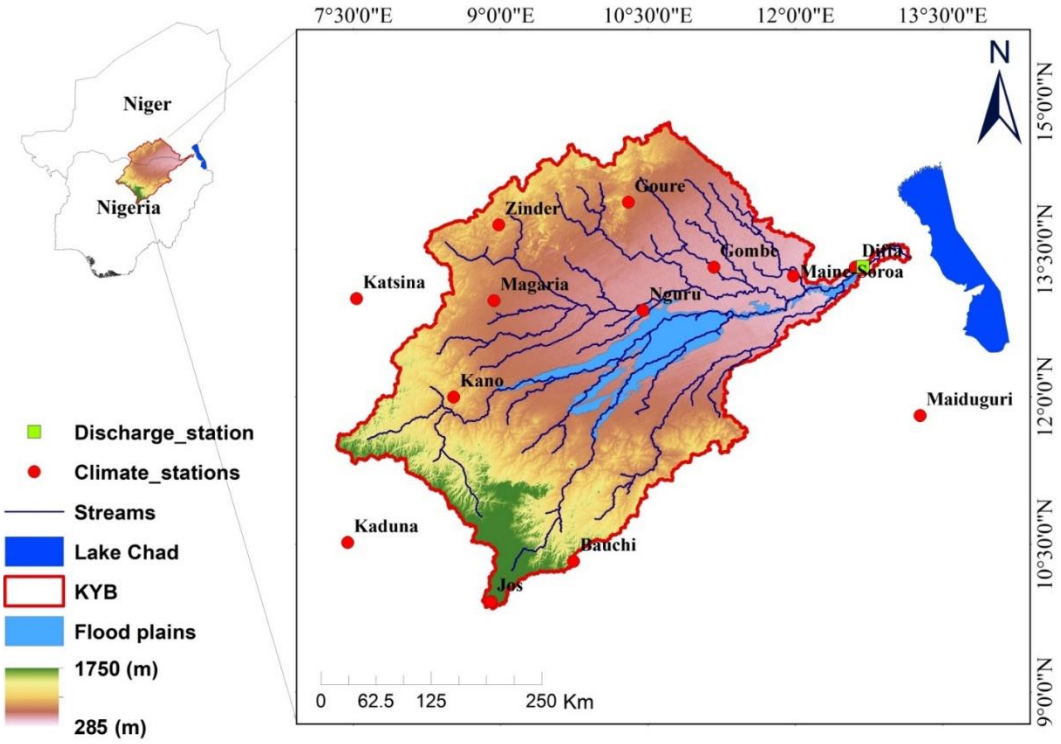

Figure 4: The Komadougu-Yobe Area of the Lake Chad Basin

A notable feature is the climatic instability characterized by occurrence of three drought periods in the last century. The droughts were characterized by significantly below average precipitation and a shift southward of the average isohyets occurring in the early 1950s, 1970s and particularly the 1980s. To this spatial overall deficit there is often some temporal irregularity of precipitation (Thompson and Polet 2000). Across the basin, the mean annual temperature is 27.9°C when observed between 1951and 1990. The temperature has increased by more than 0.7ºC with characteristic rates of warming more than 0.15ºC per decade. There are two main winds; the south easterly monsoon wind which brings moisture from the Atlantic Ocean in the rainy season and the north easterly harmattan wind which brings sand-dust from the Sahara desert during the dry season (Warner 2004). Annual potential evaporation fluctuates between 1,800 mm and 2,400 mm across the basin (IUCN 2011). The basin's climatic instability in the last century is attributed to the occurrence of three drought episodes (Thompson and Polet 2000).

2.3 Flow Characteristics

The basin is drained by two river sub-systems, flowing into the Lake Chad as the Yobe River. The uplands are made up of impermeable basement complex. Due to the impermeable

basement complex as well as the intense precipitation, the runoff is very rapid. The annual flow ends in September. However, the construction of dams and irrigation projects, as well as LULC change and climate variability, has modified the pattern of downstream river discharge.

2.4 Dams

Dams and reservoirs have impacts on the Komadougu-Yobe river flow. There are three principal dams in the basin as well as large scale irrigation projects. The first dam, the Tiga Dam, was completed in 1974 while others became operational in 1993 (Oyebande 2001).

2.5 Water use and ecosystem degradation

Inappropriate land and water management practices in the basin have changed the seasonal flow to a perennial flow regime. This has resulted in the invasion of reeds and weeds such as Typha in some of the river reaches, which block streams and flooding of channels causing changes in the wetland ecosystems that communities have historically relied upon to deliver regular water services. With the exception of the year 2001, natural flooding of the Yobe River floodplains has been very limited in recent years and irregular and low flows in the Yobe River have affected the small- and large-scale irrigation schemes along the rivers with many of them now abandoned. Fishing, farming and herding livelihoods have been adversely affected and the scarcity of water has led to conflict over the available resources.

2.6 Data used

2.6.1 Climate Models

The atmospheric-ocean general circulation models (AOGCMs) is essential in providing projections for future climate under different climate change scenarios. The AOGCMs have a resolution of 100-250km. The AOGCMs are very coarse which makes it difficult to meet the requirement of many users demanding high resolution outputs to produce regional climate projections. Various international projects had focused on downscaling output from AOGCMs using the Regional climate models (RCMs) to generate relatively high resolution, multi-model ensembles of present and future climate. These include the Prediction of Regional Scenarios and Uncertainties for Defining European Climate Change Risks and Effects (Christensen and Christensen 2007) and ENSEMBLE-Based Predictions of Climate Changes and their Impacts (van der Linden and Mitchell 2009) for Europe; the North American Regional Climate Change Assessment Program (Mearns et al. 2009) for North America; and ENSEMBLES–African Monsoon Multi- disciplinary Analyses (van der Linden and Mitchell 2009) for West Africa. (Nikulin et al. 2012) stated that each of these projects has made significant contributions to downscaling efforts over their specific region, but there has been very limited international

coordination of such projects and therefore limited transfer of knowledge between projects and regions.

The Coordinated Regional climate Downscaling Experiment (CORDEX) (Giorgi et al. 2009; Jones et al. 2011), aims to fill this gap by coordinating international efforts in regional climate downscaling. CORDEX is organized in a similar manner to the Coupled Model Intercomparison Project phase 5 (CMIP5) for global model simulations, with predefined regions, grids, experiment protocols, output variables, and output format facilitating easier analysis of possible future regional climate changes, not only by the scientific community, but also by end-user communities at regional and local levels (Nikulin et al. 2012). (Kim et al. 2014) expressed that the CORDEX program incorporates GCM and RCM model evaluation, uncertainty assessment of climate simulations and construction of multi-model ensembles. It is anticipated that Africa will benefit from the CORDEX program.

The CORDEX program aims to provide high-resolution regional climate change projections using a wide range of greenhouse gas (GHG) emission scenarios to support impact assessment and decision making at the regional level. (Nikulin et al. 2012)analysed in details the present-day CORDEX simulations using ERA-Interim reanalysis at the boundaries focusing on precipitation climatology. They concluded that the multi-model ensemble mean generally outperforms any individual RCM simulation in line with previous studies (Diallo et al. 2016; Dosio 2017; Gbobaniyi et al. 2014). They also found out that the Rossby Centre regional atmospheric model (RCA) which is a RCM, simulates a north-ward jump in precipitation from the Gulf of Guinea to the Sahel region, at roughly the correct time of the year. The RCA, however do not propagate WAM precipitation sufficiently far north when driven by a single GCM. The multi-model average smooths these diverse biases and presents the best simulated WAM precipitation. A study by (Akinsanola et al. 2018) found out that RCA exhibit the most reasonable intensity among the RCMs over West Africa but different bias magnitudes in the frequency and mean precipitation climatology. According to (IPCC 2013) report, the present-day warming and the increased variability of precipitation are likely to be exacerbated in future climate with large regional variations and different degrees of confidence. This will greatly affect the hydrological cycle and component of any basin since the source of the hydrological cycle is the precipitation. In this regard, (IPCC 2013) states that there is low to medium confidence in the robustness of projected regional precipitation change over Africa in general until a larger body of regional results become available through, for example CORDEX.

For this study, the outputs of eight CIMP5 GCMs from the CORDEX-Africa project and their ensembles downscaled by Sveriges Meteorologiska och Hydrologiska institute, Sweden Regional climate model (SMHI-RCA4 RCM) is used. In the CORDEX Africa project, the simulations have been performed for 1961-2005 (with historical forcing) and for 2006-2100

under different Representative Concentration Pathways (RCP) scenarios (Moss et al. 2010). In RCA4, the RCP scenarios are expressed as changes in equivalent carbon dioxide concentrations as interpolated from one year to the next (Kjellström et al. 2016). The resolution is 50 km. Table 1 below presents the list of CMIP5 GCMs.

Table 1: CIMP5 GCMs used as boundary conditions (Kjellström et al. 2016)

No	Modelling Centre	Model name
1	Canadian Centre for Climate Modelling and Analysis	CanESM2
2	Centre National de Recherches Météorologiques/Centre Européen de Recherche et Formation Avancée en Calcul Scientifique	CNRM-CM5
3	EC-EARTH consortium	EC-EARTH
4	NOAA Geophysical Fluid Dynamics Laboratory	GFDL-ESM2M
5	Met Office Hadley Centre	HadGEM2-ES
6	Atmosphere and Ocean Research Institute, National Institute for Environmental Studies and Japan Agency for Marine-Earth Science and Technology	MIROC5
7	Max Planck Institute for Meteorology	MPI-ESM-LR
8	Norwegian Climate Centre	NorESM1-M

2.6.2 RCM outputs and Bias correction

Hydrological models are often used to simulate the impact of future climate conditions on hydrologic processes. However, (Teutschbein and Seibert 2012) state that simulations of temperature and precipitation often show significant biases due to systematic model errors or discretization and spatial averaging within grid cells, which hampers the use of simulated climate data as direct input data for hydrological models. Bias correction procedures are used to minimize the discrepancy between observed and simulated climate variables on a daily time step so that hydrological simulations driven by corrected simulated climate data match simulations using observed climate data reasonably well. The underlying idea is to identify biases between observed and simulated historical climate variables to parameterize a bias correction algorithm that is used to correct simulated historical climate data. Bias correction methods are assumed to be stationary, i.e. the correction algorithm and its parameterization for current climate conditions are assumed to be valid for future conditions as well. Thus, the same correction algorithm is applied to the future climate data. However, it is unknown how well a bias correction method performs for conditions different from those used for parameterization.

A good performance during the evaluation period does not guarantee a good performance under changed future conditions. (Teutschbein and Seibert 2012) provide a detailed discussion and state that a method that performs well for current conditions is likely to perform better for changed conditions than a method that already performs poorly for current conditions.

To project the future climate response and the stream flow characteristics of the basin, the bias-corrected output from RCA is used for the climate and stream flow analysis under two forcing scenarios (RCPs 4.5 and 8.5) (Table 2). This will quantify the effect of a future warming climate on the stream flow characteristics of the basin.

The hydrological model used is *le modèle du Génie Rural à 5 paramètres au pas de temps Journalier* (GR5J).

Table 2: Representative concentration pathways

RCP	Climate	Reference
8.5 (very high baseline emission scenarios)	CO_2 at 1370ppmv	IPCC (2013)
4.5 (medium stabilization scenarios)	CO_2 at 650ppmv	IPCC (2013)

2.6.3 Observation data

Daily precipitation, minimum temperature, maximum temperature and discharge data series archived by the Nigeria Meteorological Agency (NiMet), Direction de la Meteorologie Nationale (DMN) of the Niger Republic and Diffa hydrological station are used for the study. The potential evapotranspiration is calculated using (Oudin et al. 2005) approach.

2.7 Experimental setup

2.7.1 Opening remarks

This section is designed to give the reader a broad overview of the recurring methodology in the experimental set up as well as the data used throughout the thesis. There are overlaps in the description of the methodology and the data used because the working chapters are similar to their submitted/published forms. This retains the uniqueness of each chapter in order to achieve the set objectives.

2.7.2 Conceptual framework and conclusion

The GCMs downscaled by the RCA is bias-corrected in order to project the climate extreme events in the basin. Furthermore, the impact of human activities and precipitation variability to changes in river discharge is examined at the historical time step. The observation time series is checked and corrected for homogeneity. Subsequently, the corrected data is used to drive the GR5J hydrological model. The results from the hydrological modelling account for the stream flow response to climate change. The detailed framework is presented below (Figure 5). The

conceptual framework shown below is adhered to in order to accomplish the objectives of the study.

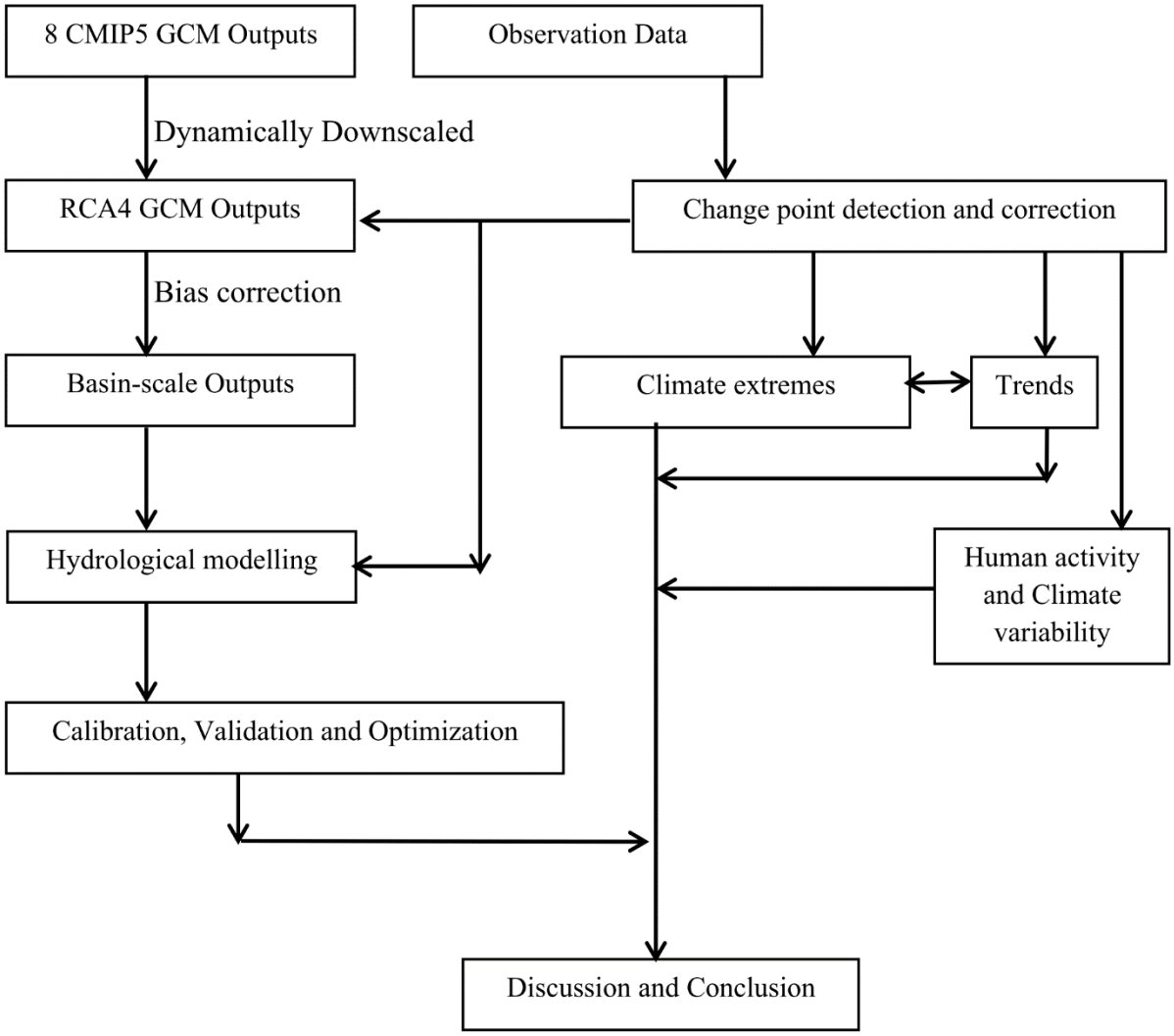

Figure 5: Conceptual framework of accomplishing the objectives of the study

CHAPTER 3: Spatio-temporal precipitation trend and homogeneity analysis (Paper One)

This chapter shows the result of the analysis of the spatial and temporal precipitation trend as well as the homogeneity analysis of precipitation in the Komadougu-Yobe basin, Lake Chad region as seen in section 3.4. This paper has been published in the Journal of Climatology and Weather Forecasting *(https://doi.org/10.4172/2332-2594.1000214)*.

Journal of Climatology & Weather Forecasting
ISSN: 2332-2594
Adeyeri et al., J Climatol Weather Forecasting 2017, 5:3
DOI: 10.4172/2332-2594.1000214
Research Article Open Access

Spatio-Temporal Precipitation Trend and Homogeneity Analysis in Komadugu-Yobe Basin, Lake Chad Region

Adeyeri OE[1,5*], Lamptey BL[2], Lawin AE[3] and Sanda IS[4]

[1]*Graduate Research Programme on Climate Change and Water Resources, West African Science Service Centre on Climate Change and Adapted Land Use, University of Abomey-Calavi, Benin*
[2]*African Centre of Meteorological Applications for Development, Niger*
[3]*Laboratory of Applied Hydrology, National Water Institute, University of Abomey-Calavi, Benin*
[4]*Centre Regional AGRHYMET, Niger*
[5]*Department of Meteorology and Climate Science, Federal University of Technology, Akure, Nigeria*

Abstract

This paper investigated the spatio-temporal trends and homogeneity analysis of rainfall over the Komadugu-Yobe basin using data from Nigerian Meteorological Agency (NiMet), Department of National Meteorology Niger (DMN) and a 10 km resolution gridded observation data from Princeton University (PGF) for the period 1979 and 2015. The data, analysed at the annual and seasonal (wet and dry seasons) timescales, were subjected to Mann-Kendal including modified Mann-Kendall trend test after testing for autocorrelation. Test for homogeneity was performed on the data using Pettitt's, Buishand's, Standard Normal Homogeneity Test and van Belle and Hughes' test. An overall homogenous trend of rainfall series was observed in the basin for all the seasons considered using van Belle and Hughes' homogeneity trend test. The global rainfall trend increases in the dry season and decreases in the annual and wet seasons for the period of study. Pettitt's homogeneity test for the annual and wet season rainfall series showed that change points were detected in the year 2005 for nine grids out of fifteen over the basin at 5% significant level. This study therefore, shows the importance of understanding the spatial and temporal distribution and trends in rainfall for effective planning and management of water resources in the basin

Keywords: Rainfall, Spatio-temporal trend, Homogeneity test, Komadougu-Yobe basin

3.1 Introduction

There has been increased concern about water resource management in river basins due to changes in climatic conditions combined with additional anthropogenic influences (Jones et al. 2015). Spatial and temporal patterns of water availability are also affected by precipitation (Lus et al. 2000). Therefore, knowledge of precipitation patterns is of crucial importance in hydrology, e.g. to derive precipitation-runoff relationships, flood/drought assessment and mitigation measures (Chattopadhyay and Edwards 2016). Different studies have investigated how changing precipitation patterns have affected the hydrological regimes of river basins. The results from these studies show that precipitation patterns in most cases dictates the hydrological regime of river basins. Other studies (e.g. (IPCC 2013) have observed variations in the long-term trend of precipitation patterns on both spatial and temporal scales. For example, (Xu et al. 2005) reported that in the 20th century, the mean annual land-surface precipitation increased by 7%-12% in the middle and high latitudes (30^{o}N-85^{o}N), but merely by 2% from 0o to 55^{o}S. However, between 1910 and 1996, there was a 10% increase in annual

precipitation across the United States (Karl and Knight 1998). (Philandras et al. 2011) found a generally negative trend in the long-term precipitation within the Mediterranean region over the period 1901-2009. In southern Italy, sub-regions of northern Africa and the western Iberian Peninsula, slightly positive trends were detected. (Abbaspour et al. 2009) studies in Iran noted an amplifying effect i.e. the wet regions would receive more precipitation in future, while dry regions would receive less. (Longobardi and Villani 2009) utilized 211 weather stations in the Campania region of southern Italy over the period 1918-1999. Negative trends in annual precipitation were observed in 27% and positive trends in 9% of the stations.

In Nigeria, (Fasona et al. 2011) stated that terrain, precipitation, and temperature are the major drivers of local climate variability in all seasons after using geographic information system and principal component analysis methods to investigate the influence of eco-geographic factors on local climate over the western Nigeria. (Oguntunde et al. 2011) examined the spatial and temporal patterns of monthly and annual precipitation between 1901 and 2000 and found a sharp difference in changing precipitation patterns between 1931-1960 and 1961-1990 and recorded that 1950s and 1980s are the wettest and driest decades. In northern Nigeria, (Ati et al. 2002) analysed precipitation data covering a period of 50 years (1953 to 2002) and reported an increase in annual trend of precipitation between 1993 and 2002. (Akinsanola and Ogunjobi 2017) analysed homogeneity and long-term spatiotemporal precipitation trends at the national scale in Nigeria using data from 18 stations and observed a significant increasing trend in the pre- and post-monsoon seasons. (Odunuga et al. 2011a) investigated the hydro-climatic variability of the Hadejia-Jama'are river systems in the Komadougu-Yobe Basin (KYB) and reported a decreasing trend of precipitation from the upstream (the south of the basin) to the downstream (northern part of the basin). KYB is currently facing a conflicting balance between effectively benefiting from the available water resources and a reduction in the damages caused by the developmental projects (Sobowale et al. 2010a). The Hadejia River sub-basin of the KYB which is a major contributor to the Lake Chad had been subjected to tremendous exploitation of its surface water resources through the construction of several dams and large-scale irrigation schemes without a prior knowledge of the trends in precipitation which regulates the water amount in the basin. This has led to the recession of Lake Chad out of Nigeria (Sobowale et al. 2010a). More also, there has been a decline in the occurrence of precipitation-dependent seasonal flooding which plays a vital role in maintaining and preserving the ecological system of the wetlands (Hadejia-Nguru Wetlands). This has negatively affected the practice of both flood and recession farming in the wetland region and over the entire basin (Odunuga et al. 2011b).

The earlier cited studies suggested that spatial variability in the long-term behaviour of precipitation is dependent on regional and local characteristics. Sequel to this, relatively small-

scale analyses and a check for inhomogeneity in order to avoid biases, spurious trends and erroneous interpretations from the data series used for such analyses, which is vital in practical applications of hydrology cannot be underemphasized. For this reason, this study focuses on investigating the homogeneity and trends in annual and seasonal precipitation series over the Komadougu-Yobe Basin (KYB) in the Lake Chad region between 1979 and 2015 to analyze whether or not there are significant changes in the precipitation trends as previous studies on this basin did not focus on this. This is necessary because of the enormous importance of the basin to sustaining the livelihood of the inhabitants and also its general water resources contribution to the drying Lake Chad.

3.2 Study Area

The study area is as described in chapter 2.

3.3 Data and Methods

The study utilizes data from Nigeria Meteorological Agency (NiMet), Niger Direction Meteorologie National (DMN) and a 10km resolution daily gridded dataset for West Africa (PGF) developed by Princeton University between 1979 and 2015 (Chaney et al. 2014). A method for assimilating station data into the gridded dataset which has been proven to improve the quality of gridded data set was developed and tested (Chaney et al. 2014; Funk et al. 2015). This method was applied to merge fifteen station data (Table 3) from NiMET and DMN into a full gridded dataset. In this study, a subset of fifteen grid cells of daily precipitation data over the KYB has been used for the period between 1979 and 2015 (Figure 6). An investigation of the annual and seasonal series and trend analysis was performed on each grid cells and for the entire basin. For the seasonal analysis, the monthly precipitation data was analysed over the dry season which is between November and April and the wet season which is between May and October. Additionally, after the evaluation and subsequent setting the most probable change point, the trend analysis was done on two partial sequences before and after the change point.

The following methods were used for the trend analysis;

3.3.1 Autocorrelation

Time-series data are often lacking serial independence. Positive serial correlation inflates the variance of the estimated time-series mean and, therefore, the time-series contains less information about the mean than a random series (Matalas and Langbein 1962). The serial correlation coefficient aids the validation of time-series independence.

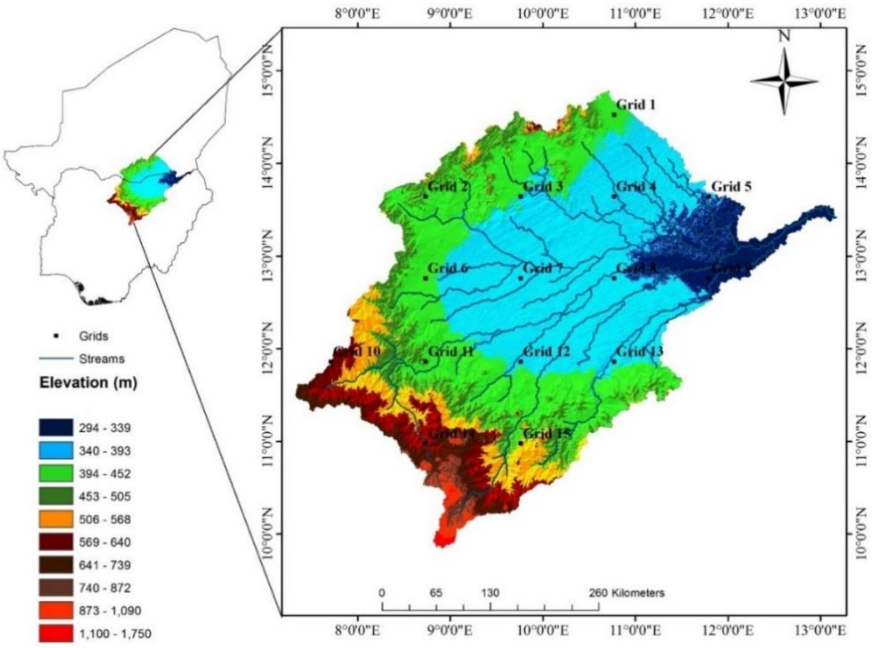

Figure 6: Location of the grids in the study area

Table 3: List of assimilated climatic stations

Country	Station	Lat	Long
Nigeria	Jos	9.92	8.9
Nigeria	Bauchi	10.286	9.7
Nigeria	Kaduna	10.52	7.44
Nigeria	Maiduguri	11.81	13.27
Nigeria	Potiskum	11.86	10.77
Nigeria	Kano	12	8.52
Nigeria	Nguru	12.88	10.45
Niger	Magaria	12.98	8.93
Nigeria	Katsina	13	7.53
Niger	Maine-Soroa	13.23	11.98
Niger	Diffa	13.314	12.612
Nigeria	Gombe	13.32	11.17
Niger	Zinder	13.75	8.98
Niger	Goure	13.98	10.3
Niger	Dole	14.76	10.69

The serial independence is tested using the student's 't' test (Yue et al. 2002) and it is given as;

$$t = \rho 1 \sqrt{\frac{n-2}{1-\rho_1^2}} \qquad \textit{Equation 1}$$

where the test statistic t has a Student's t-distribution with (n-2) degrees of freedom. If $|t| \geq t_{\alpha/2}$, the null hypothesis about serial independence is rejected at significance level α.

If serial correlation is found to be present in a time-series then the process of pre-whitening data may be performed. Pre-whitening a time-series removes a serial correlation component such as autoregressive process (red noise) prior to applying the trend detection test. Modified Mann–Kendall test (MMK) pre-whitening has been used to detect a trend in a time series in the presence of autocorrelation (Cunderlik and Burn 2004). Since pre-whitening may reduce the detection rate of significant trend in the Mann-Kendall (MK) test (Yue et al. 2003), the Modified Mann-Kendall (MMK) test (Hamed and Ramachandra Rao 1998) is employed for trend detection of an autocorrelated series. Only the significant values of ρk are used to calculate variance correction factor n /n*s, as the variance of S is underestimated when data are positively autocorrelated;

$$\frac{n}{n_s^*} = 1 + \frac{2}{n(n-1)(n-2)} \times \sum_{k=1}^{n-1}(n-k)(n-k-1)(n-k-2)\rho k \qquad \textit{Equation 2}$$

where n is the actual number of observations, n* s is considered as an 'effective' number of observations to account for autocorrelation in data, and ρk is the autocorrelation function of ranks of the observations.

The corrected variance is then computed as

$$V^*(S) = V(S) \times \frac{n}{n_s^*} \qquad \textit{Equation 3}$$

V(S) is described in Equations (5-8).

3.3.2 Trend test

The Mann-Kendall (MK) test (Mann 1945) is a rank-based nonparametric test, particularly suitable for censored, missing and non-Gaussian distributed variables, which searches for a trend in a time-series without stipulating whether the trend is linear or nonlinear (Lamptey 2008; Maidment 1993). Many studies have used the Mann-Kendall test to detect trends in climatological and hydrological time-series (Taxak et al. 2014; Yue and Hashino 2003), and this particular non-parametric test has been shown to be more powerful than some parametric tests, particularly when dealing with skewed data (Onoz and Bayazit 2003). The Mann-Kendall test statistic (Taxak et al. 2014), S, is defined as

$$S = \sum_{k=1}^{n-1}\sum_{j=k+1}^{n} Sgn(x_j - x_k) \qquad \textit{Equation 4}$$

Where x_j and x_k are sequential data values for the time series data of length n. The test statistic represents the number of positive differences minus the number of negative differences for all the differences between adjacent points in the time-series considered and equates to the sum of the Sgn series, which is defined as

$$Sgn(x_j - x_k) = \begin{cases} 1 \; if \; x_j > x_k \\ 0 \; if \; x_j = x_k \\ -1 \; if \; x_j < x_k \end{cases} \qquad \textit{Equation 5}$$

The mean and variance of S, E(S) and V(S) respectively, under the null hypothesis, Ho, of randomness, given the possibility that there may be ties in the x values is given as;

$$E(S) = 0 \qquad \textit{Equation 6}$$

$$V(S) = \frac{1}{18}\{n(n-1)(2n+5) - \sum_{i=1}^{n} t_i[(t_i - 1)(2t_i + 5)]\} \qquad \textit{Equation 7}$$

where t is the extent of any given tie. Σti denotes the summation over all ties and is only used if the data series contain tied values. The standard normal variate Z is calculated by

$$Z = \begin{cases} \frac{S-1}{\sqrt{V(S)}} \; if \; S > 0 \\ 0 \; if \; S = 0 \\ \frac{S+1}{\sqrt{V(S)}} \; if \; S < 0 \end{cases} \qquad \textit{Equation 8}$$

Positive values of Z indicate an upward trend and negative values indicate a downward trend.

3.3.3 Slope Test

Theil-Sen's estimator estimates the slope of n pairs of data points (Sen 1968; Theil 1950) in order to assess the magnitude of the trend and this is calculated as;

$$QS_i = \frac{(x_j - x_k)}{(j-k)} \textit{ for } i=1, \ldots\ldots N \qquad \textit{Equation 9}$$

where x_j and x_k are values at times j and k respectively. Note, j>k. QS_i is Sen's estimator of slope which is the median of these N values. If only one data in present in each time period, then

$$N = n(n-2)/2 \qquad \textit{Equation 10}$$

where n is the number of time periods. The N values of QS_i are ranked by $QS_1 \leq QS_2 \leq \cdots \leq QS_{N-1} \leq QS_N$ and

$$Sen's \; estimator = \begin{cases} QS_{(N+1)/2} & if \; N \; is \; odd \\ (1/2) * \left(QS_{N/2} + QS_{(N+2)/2}\right) & if \; N \; is \; even \end{cases} \qquad \textit{Equation 11}$$

3.3.4 Magnitude of Percentage Change

The percentage change in seasonal and annual precipitation series is computed by approximating it with a linear trend (Yue and Hashino 2003).

$$Percentage\ change(\%) = \frac{m \times l}{n} \times 100 \qquad \textit{Equation 12}$$

where m is the median slope, l is the length of year and n is the mean

3.3.5 Homogeneity test

A climatic series is said to be homogeneous, if the observed variation is resulting from fluctuations in weather and climate exclusively (Domonkos and Coll 2017). It is important to carry out different homogeneity tests. For example, standard normal homogeneity test (SNHT) is sensitive to change point towards the beginning and end of the data series while Buishand's and Pettitt's tests are sensitive to changes in the middle of a series.

Van Belle and Hughes' homogeneity of trend test

To obtain a single global trend, this test combines data from several stations after using the Mann–Kendall statistic for each station (van Belle and Hughes 1984; Helsel and Hirsch 2002). Testing for the homogeneity of a global trend requires the homogeneity $\chi 2$ statistic ($\chi 2$homog) which is calculated as;

$$x^2_{homog} = x^2_{total} - x^2_{trend} = \sum_{j=1}^{p} Z_j^2 - pZ^2 \qquad \textit{Equation 13}$$

Where Z_{Sj} is the test statistic, p is the total number of stations and Z_S for the j_{th} station obtained as;

$$z = \frac{1}{p}\sum_{j=1}^{p} Z_{sj} \qquad \textit{Equation 14}$$

Pettitt's and Alexandersson's SNHT test

Pettitt test is a rank-based test for detecting significant changes in the mean of time series data when the exact time of change is unknown (Pettitt 1979). The test is considered robust to changes in the distributional form of time series and relatively powerful compared to Wilcoxon-Mann-Whitney test, cumulative sum and cumulative deviations. Furthermore, Pettitt test has been widely adopted to detect changes in climatic and hydrological time series data (Zhang and Lu 2009).

The standard normal homogeneity test (SNHT) (Alexandersson 1986) uses series of ratios that compare the observations of a measuring station with the average of several stations. The ratios are then standardized. The standardized ratios are the series of X_i. The null and alternative hypotheses are given as;

Ho: The T variables Xi follow an N (0, 1) distribution.

Ha: Between times 1 and n, the variables follow an N(μ1,1) distribution, and between n+1 and T they follow an N(μ2,1) distribution.

The Pettitt's statistic is defined by;

$$T_0 = \max_{1 \le t \le T} [v z_1^2 + (n - v) z_1^2] \qquad \textit{Equation 15}$$

With

$$\begin{cases} z_1 = \frac{1}{v} \sum_{i=1}^{v} x_t \\ z_2 = \frac{1}{n-v} \sum_{t=v+1}^{T} x_i \end{cases} \qquad \textit{Equation 16}$$

By comparing the likelihood of the two alternative models, the T_0 statistic is derived. The model analogous to Ha indicates that i_1 and i_2 are estimated while defining the n parameter which maximizes the likelihood.

Buishand's test

Buishand's test is suitable for variables following any form of distribution whose properties have been mainly studied for the normal case (Buishand 1982). For this study, Buishand focuses on the case of the two-tailed test and the Q statistic. For Q statistic, the null and alternative hypotheses are given by;

$S_0^* = 0, S_k^* = z_1 = \sum_{i=1}^{k} (x_i - u), k = 1,2, \ldots . T$

And

$$S_0^* = {S_k^*}/{\sigma} \qquad \textit{Equation 17}$$

The Buishand's Q statistics follows;

$$Q = \max_{1 \le t \le T} |S_k^{**}| \qquad \textit{Equation 18}$$

These methods have been used previously for analysing climate data and also to investigate hydro-climatological signals of climate change and variability (Taxak et al. 2014; Ziegler et al. 2003).

3.3.6 Interpolation

The spatial precipitation pattern was explored using the Inverse Distance Weighted (IDW) interpolation technique. In IDW, weighted average of observation values is taken after which the neighbourhood about the interpolated points have been identified. The weights are a decreasing function of distance of which the simplest weighting function is inverse power of the distance between points (Shepard 1968);

$$w(d) = 1/d_p,\ p>0 \qquad \textit{Equation 19}$$

where d is the distance between points, p is the number of points, w is the weighting function.

The fusion of the IDW interpolated points and the Digital elevation map was carried out using the overlay function of ArcGIS.

3.4 Results and Discussion

3.4.1 Mean Climatology

Results from the initial analysis of precipitation show that mean annual precipitation ranges from 240 mm in the northern part (Grid 1) and 1060mm in the southern part (Grid 14). This is in agreement with (Thompson and Polet 2000) who established that the southern part of the basin experiences more precipitation due to the southward shifts of the average isohyets. The coefficient of variation (CV) ranges from 41.49% (Grid 5) to 13.47% (Grid 11) with an average CV of 25.06% in the whole basin. This is in line with (Odunuga et al. 2011a), who reported such CV over the Hadeija-Jama'are basin which is a sub-basin of the KYB. However, more variations in precipitation values are established in areas with lower precipitation. This result agrees with (Taxak et al. 2014) who reported that zones with least variations are located on heavy precipitation zones. Figure 7 (a-c) represents the mean, spatially represented for the annual, wet and dry seasons respectively while Figure 7d shows the fusion of the elevation and the annual mean over the KYB. In all the seasons, precipitation increases from the north to the south due to the African monsoon which brings humidity from the Atlantic Ocean (IUCN 2011; USGS 2012). Figure 7d explains the relationship between elevation and precipitation. This explains that in KYB, the mean annual values of precipitation increases as the elevation increases, that is, from north to south (Chu 2012).

3.4.2 Experimental data analysis at different time scales

To identify the precipitation pattern at different time scales, the time series of annual, dry and wet season precipitation data was used. It is observed that the running mean is not resistant to local fluctuations; hence, it is pertinent to reduce the local fluctuations by fitting the time series with locally weighted scatterplot smoothing (LOWESS) regression curves (Cleveland 1979, 1984). Figure 8 shows the LOWESS regression curve indicating an increasing pattern of precipitation from 1979 to 2001 before the trend started decreasing for the wet and annual timescale. This could be attributed to the partial recovery of precipitation during the 1990s in the region as a result of warming of the northern Atlantic Ocean (Hoerling et al. 2006; Nicholson 2001). The increased temperature over this period as a result of the warming of the northern Atlantic Ocean draws rains during the wet season further north, therefore, increasing precipitation in the region (USGS 2012). However, for the dry season (Figure 8), there was a gradual increase in the trend of precipitation during the study period. The set back of the LOWESS regression curve is that the statistically significant trends in the time series were not accounted for (Akinsanola and Ogunjobi 2017).

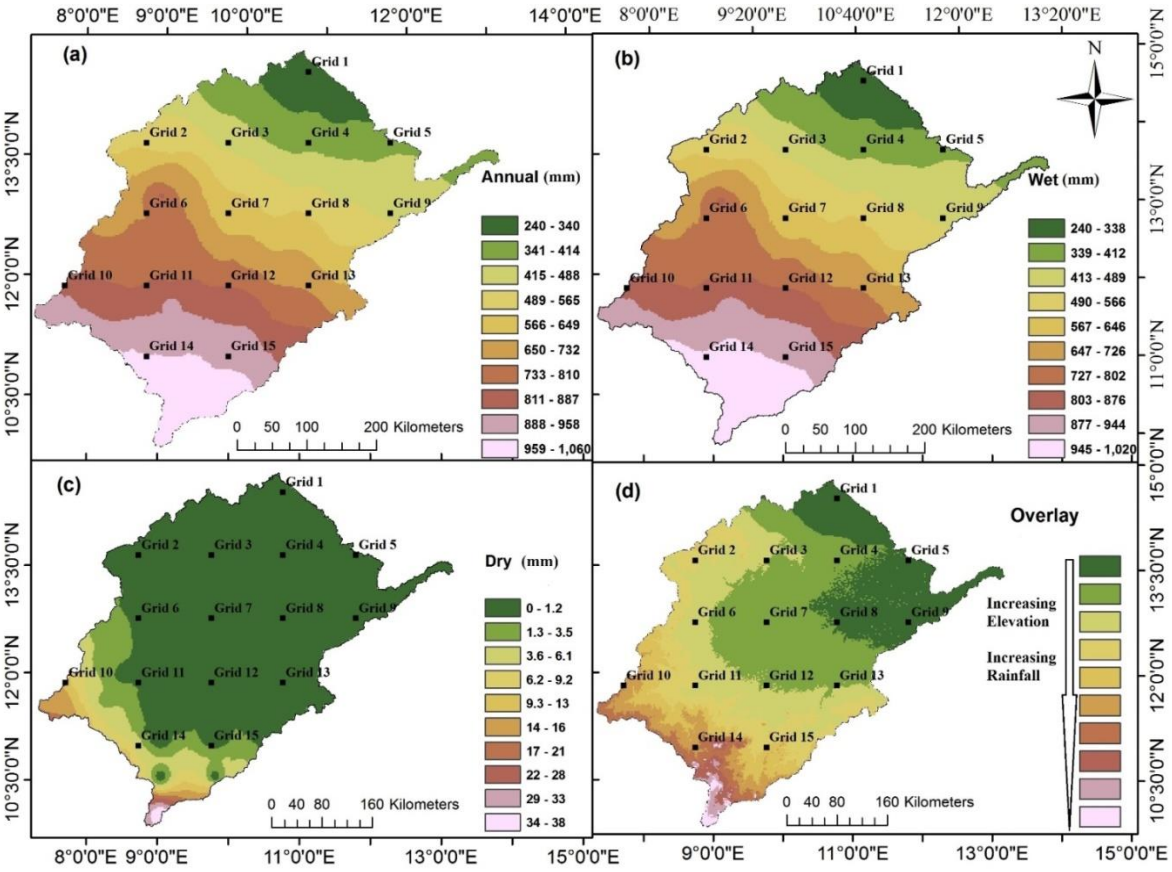

Figure 7: Precipitation map in Komadougu-Yobe Basin (a) Annual (b) Wet season (c) Dry season (d) Fusion of elevation and annual precipitation

3.4.3 Explanatory precipitation trends at different time scales

Table 4 presents the results of the autocorrelation analysis, Z statistic and MK/MMK test for the time series between1979 and 2015 at different time scales. On the annual scale, three grids (Grids 6, 7 and 10) were statistically autocorrelated. Grids 2, 3, 6, 7 and 14 were statistically autocorrelated during the wet season and only Grid 1 was statistically autocorrelated during the dry season, all at 5% significant level. On annual time series, 5 out of 7 grid points exhibited statistically significant decreasing trend while the other two grid points (Grids 14 and 15) exhibited statistically significant increasing trend. During the wet season, 4 out of 6 grids exhibited significant decreasing trend while the other two grids (Grids 14 and 15) showed a significant increasing trend. The dry season exhibited only two grid points (Grids 1 and 4) having a significant increasing trend.

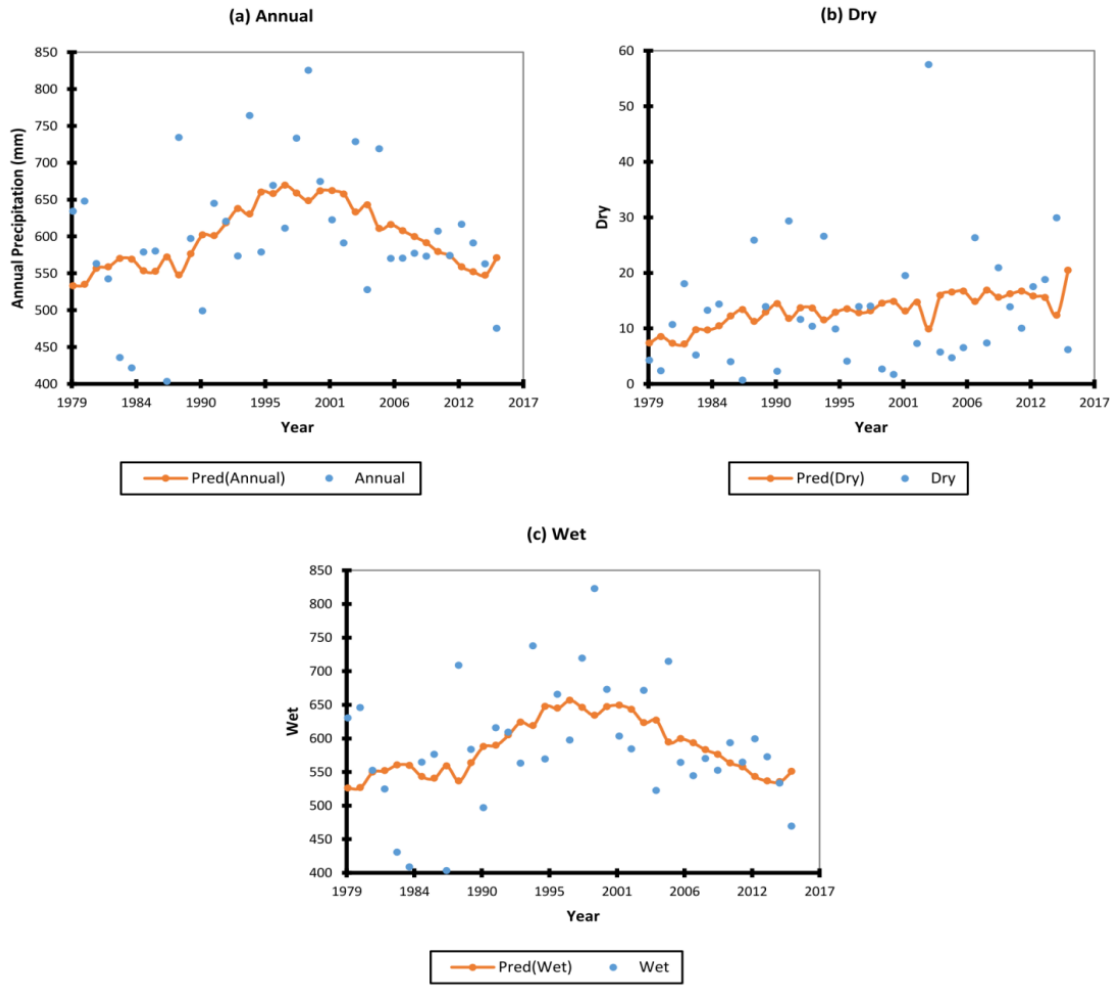

Figure 8: LOWESS regression line for precipitation in the basin for (a) annual, (b) dry and (c) wet seasons. "Pred is prediction"

Table 4 further explains the percentage changes in mean values for the annual, wet and dry seasons. It was observed that all the grids recorded changes in precipitation for all the seasons. Sen's slope estimator determines the magnitude of statistically significant trends. Statistically significant magnitude of change was observed in the annual series (Grid 13), Wet season (Grid 4) and Dry season (Grids 2,3,5,6 and 7). Figure 9 (a-c) shows that for the three-time scales considered, grids 14 and 1 were consistent in having the highest rising and lowest falling trends respectively at 5% significant level. It is worthy to note that PGF which is a high-resolution gridded dataset clearly reveals that the percentage of change of precipitation increases to the south of the basin. This phenomenon has not been recorded by larger scale regional studies (Giannini et al. 2003; Klutse et al. 2016). This ascertained the usefulness of the PGF for regional studies. However, Figure 9d shows a positive percentage magnitude of change of precipitation at higher elevation and a negative percentage magnitude of change of precipitation at lower elevation.

3.4.4 Change point analysis across grids and magnitude of trend slope in precipitation series

The change point probability and detection of homogeneity of the data series using Pettitt's test, SNHT test and Buishand's test are discussed in this section. Pettitt's homogeneity test for the annual precipitation series (Table 5) shows that most grids were heterogeneous and particularly, change points were detected in the year 2005 for nine grids, signifying a significant change in the mean before and after the identified change point. Most of the grids are homogenous in the dry season (Table 6) while the wet season follows the same trend as the annual series (Table 7). To find change point towards the beginning and end of the series, SNHT is applied while Buishand's and Pettitt's tests are sensitive to find the changes in the middle of a series. Change year in annual precipitation series is shown in Figure 10; (a) Grid 1 (b) Grid 2 (c) Grid 5 (d) Grid 9 (e) Grid 14 (f) Grid 15. Five of these six grids show a change point in 2005 while grid 15 is the only grid showing a change point in 1995. The change points recorded may be attributed to changes in instruments, observing practices, station location, station environment, satellite sensors, and network configuration and density (Klein Tank et al. 2009; Peterson et al. 1998; Reeves et al. 2007). Grids located at the southern part of the basin (grids 14 and 15) recorded an increased annual precipitation after the change points while the grids located in the north of the basin recorded a decreased annual precipitation after the change point. In general, human activities (Adeyeri et al. 2017b; Charney et al. 1977), build-up of atmospheric dust and frequent sand storm (Ekpoh and Nsa 2011), regional and global scale pattern of sea surface temperature (SST) (Adeniyi and Oladiran 2000), reduction in forest cover (Adeyeri et al. 2017d; Nair 2003), anthropogenic activities (Sarkar and Kafatos 2004) global climate shift (Baines and Folland 2007), or weakening global monsoon circulation (Pant 2003) may be the probable causes of the changes in precipitation.

3.4.5 Analysis of homogeneity of trends for the entire basin

To obtain a single global trend for the entire basin, van Belle and Hughes' homogeneity trend test was applied to the precipitation time series data from the several grids considered during the annual, wet and dry seasons.

Table 8 shows that at 95% confidence level, there exist an overall homogenous trend of precipitation series in the KYB for all the seasons considered. The values of x^2homogenous are 0.11, 0.28 and 0.06 for annual, dry and wet seasons respectively. There was also a statistically non-significant decreasing trend of precipitation in Annual and wet seasons while the increasing trend in dry season is statistically non-significant. In the entire basin, the wet season and annual precipitation decreased by 0.11% and 0.03% respectively while there was an increase of 46.22% in the dry season for the period of study.

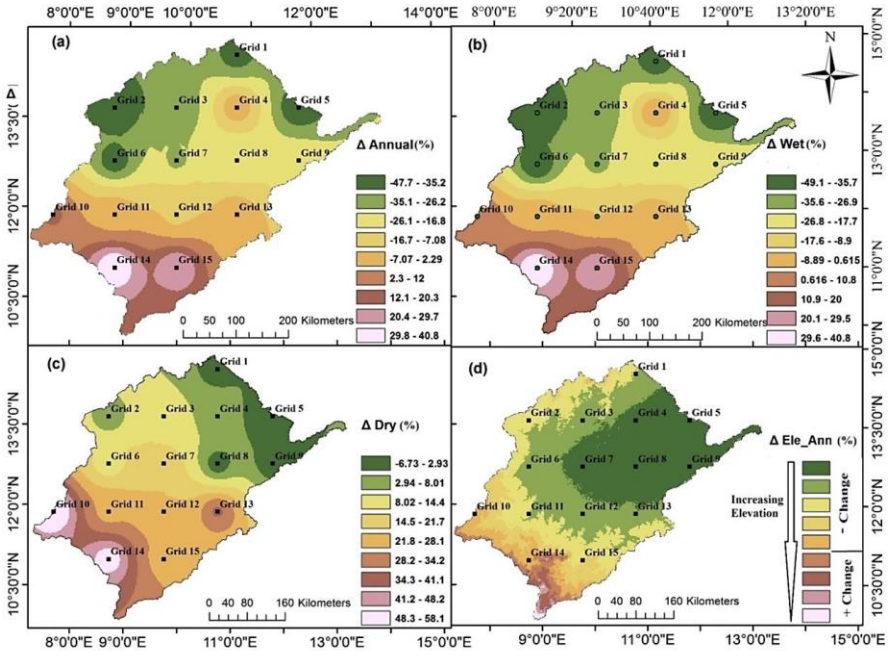

Figure 9: Spatial distribution of the percentage of change (a) Annual (b) Wet season (c) Dry season (d) Fusion of elevation and annual precipitation

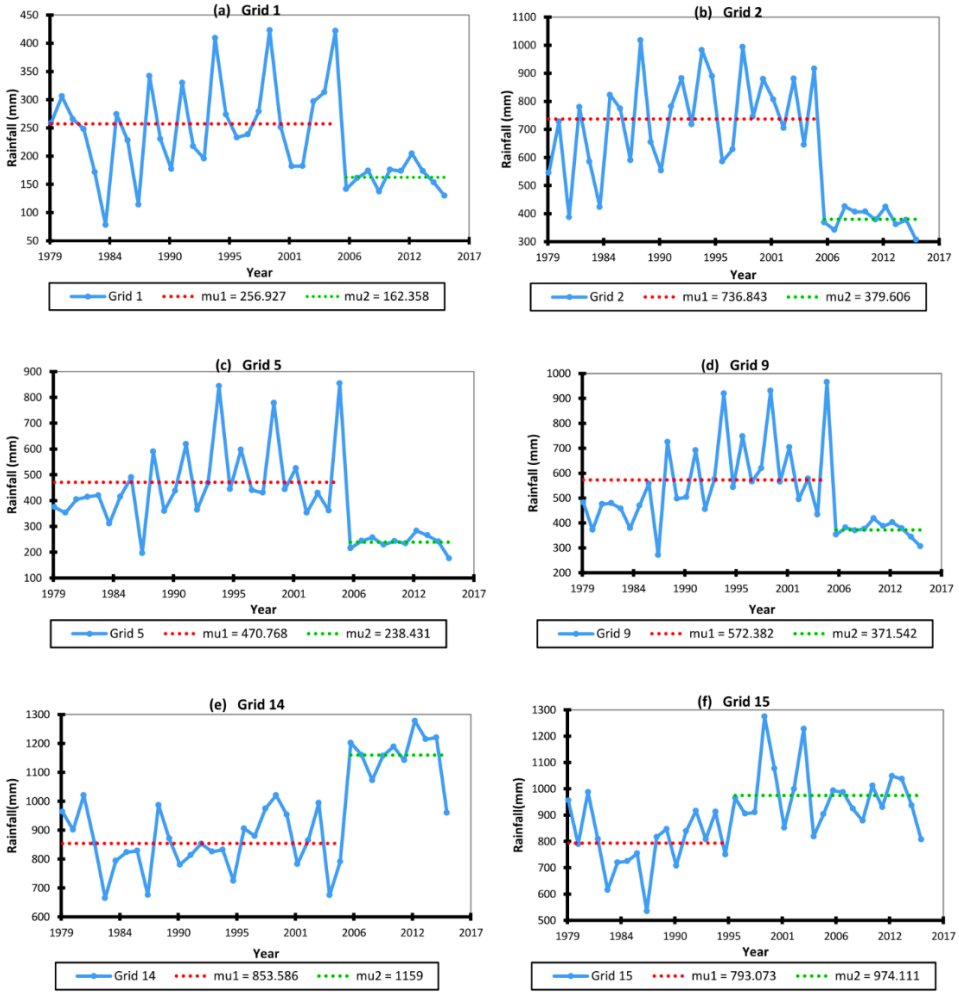

Figure 10: Change year in annual precipitation series (a) Grid 1 (b) Grid 2 (c) Grid 5 (c) Grid 9 (d) Grid 14 (f) Grid 15. mu1 and mu2 are the first and second means respectively

Table 4: Mann-Kendall (Modified MK) test (at 5% significant level) and percentage change with autocorrelation

Grids	Seasons								
	Annual			Wet			Dry		
	Z-value	Sen's Slope	% change	Z-value	Sen's Slope	% change	Z-value	Sen's Slope	% change
1	-0.23	-2.48	-39.63	-0.22	-2.53	-40.54	**0.38***	0	0
2	-0.25*	-8.26	-47.71	**-0.26***	-8.39	-49.1	0.15	0.01s	4.37
3	-0.23*	-4.35	-34.5	**-0.23***	-4.35	-34.65	0.17	0.01s	10.61
4	0.02	0.11	1.11	0.01	0.07s	0.73	0.25*	0.002	6.46
5	-0.23*	-4.88	-44.22	-0.21	-4.89	-44.76	-0.2	-0.01s	-6.73
6	**-0.26***	-8.77	-41.43	**-0.26***	-9.47	-45.49	0.13	0.04s	10.04
7	**-0.18**	-4.25	-27.58	**-0.19**	-4.45	-29.15	0.16	0.03s	18.91
8	-0.25*	-2.71	-24.5	-0.25*	-2.64	-24.09	0.04	0	0
9	-0.15	-2.96	-21.11	-0.13	-3	-21.68	-0.02	0	0
10	**0.13**	3.14	13.53	**0.1**	2.38	10.55	0.17	0.36	58.08
11	-0.03	-0.33	-1.69	-0.04	-0.49	-2.55	0.13	0.09	26.46
12	-0.15	-1.52	-9.01	-0.14	-1.49	-8.98	0.15	0.06	23.58
13	0.01	0.01s	0.06	-0.02	-0.34	-2.34	0.21	0.07	35.18
14	0.40*	10.34	40.85	**0.37***	9.89	40.82	0.17	0.58	53.36
15	0.37*	7.14	29.67	0.38*	6.87	29.43	0.06	0.19	25.98

Bold values represent autocorrelation in precipitation series, * means significant trend, positive/negative Z means increasing/decreasing trend, s means statistically significant magnitude of change

Table 5: Change year (t) by Pettitt's, SNHT and Buishand's tests for the Annual season

Grids	Pettitt's Test				(SNHT)				Buishand Test			
	K	t	P-value	Trend	To	t	P-value	Trend	Q	t	P-value	Trend
1	212	2005	0.0045	Ha	9.25	2005	0.0271	Ha	8.33	2005	0.0225	Ha
2	258	2005	0.0001	Ha	20.08	2005	<0.0001	Ha	12.27	2005	<0.0001	Ha
3	240	2005	0.0005	Ha	14.95	2005	0.0004	Ha	10.59	2005	0.0014	Ha
5	252	2005	0.0003	Ha	13.75	2005	0.0058	Ha	10.15	2005	0.0014	Ha
6	270	2005	<0.0001	Ha	19.6	2005	<0.0001	Ha	12.12	2005	<0.0001	Ha
7	224	2005	0.0016	Ha	13.53	2005	0.0008	Ha	10.07	2005	0.0026	Ha
8	174	2005	0.0323	Ha								
9	230	2005	0.0011	Ha	9.98	2005	0.0251	Ha	8.65	2005	0.0138	Ha
10	180	1990	0.0259	Ha								
14	258	2005	<0.0001	Ha	23.9	2005	<0.0001	Ha	13.39	2005	<0.0001	Ha
15	254	1995	<0.0001	Ha	13.68	1995	0.0005	Ha	11.37	1995	<0.0001	Ha

Ha denotes Heterogeneous series, t denotes year of change.

Table 6: Change year(t) by Pettitt's, SNHT and Buishand's tests for the Dry season

Grids	Pettitt's Test				SNHT				Buishand's Test			
	K	t	P-value	Trend	T0	t	P-value	Trend	Q	t	P-value	Trend
1	212	2005	0.0001	Ha	16.05	2005	0.0154	Ha	10.97	2005	0.0004	Ha

Ha denotes Heterogeneous series, t denotes year of change.

Table 7: Change year(t) by Pettitt's, SNHT and Buishand's tests for the Wet season

Grids	Pettitt's Test				SNHT				Buishand's Test			
	K	t	P-value	Trend	T0	t	P-value	Trend	Q	t	P-value	Trend
1	212	2005	0.0028	Ha	9.34	2005	0.0261	Ha	8.37	2005	0.0214	Ha
2	262	2005	0.0001	Ha	20.35	2005	<0.0001	Ha	12.35	2005	<0.0001	Ha
3	240	2005	0.0005	Ha	14.08	2005	0.0007	Ha	10.64	2005	0.0013	Ha
5	252	2005	0.0002	Ha	13.64	2005	0.0059	Ha	10.11	2005	0.0015	Ha
6	268	2005	0.0001	Ha	20.19	2005	<0.0001	Ha	12.31	2005	0.0002	Ha
7	224	2005	0.0013	Ha	13.98	2005	0.0006	Ha	10.24	2005	0.0021	Ha
8	174	2005	0.0313	Ha	5.64	2005	0.1662	Ho	6.51	2005	0.1299	Ho
9	228	2005	0.001	Ha	9.76	2005	0.0282	Ha	8.56	2005	0.0158	Ha
10	174	1990	0.0333	Ha	6.25	1990	0.2133	Ho	7.22	1990	0.0719	Ho
14	260	2005	0.0003	Ha	23.47	2005	<0.0001	Ha	13.27	2005	<0.0001	Ha
15	260	1995	<0.0001	Ha	14.16	1995	0.0001	Ha	11.56	1995	<0.0001	Ha

Ha denotes Heterogeneous series, t denotes year of change.

Table 8: Homogeneity trends, MK (MMK) test, Thiel and Sen's slope and % change over the Komadougu-Yobe Basin

Seasons	x^2homogenous	Trend	Mean	MK(MMK)	Sen's slope	% change
Annual	0.11	Ho	601	-0.003	-0.005	-0.03
Dry	0.28	Ho	13	0.17	0.166	46.22
Wet	0.06	Ho	588	-0.003	-0.018	-0.11

Ho indicates significant homogenous trends in precipitation over the entire basin

3.5 Conclusion

The study investigated trends and homogeneity of trends in precipitation time series for annual, wet and dry season over Komadougu-Yobe basin between 1979 and 2015. The analysis shows that the annual precipitation increases from the northern to the southern part of the basin. The Mann-Kendall statistic shows that there is a decreasing trend of precipitation in most grids over the basin for both annual and wet season while dry season exhibited an increasing trend indicating a shift in seasonal precipitation (Sobowale et al. 2010a). This trend was also established in the entire basin for the period of study. As a result of this, precipitation-dependent seasonal flooding phenomenon in the basin could be subdued and this will greatly reduce fishing and agricultural activities in the basin's wetlands (Muhammad et al. 2015). (Odunuga et al. 2011b) already investigated the declining agricultural activities in the Hadejia sub-basin of the KYB and this was attributed principally to the decreasing precipitation, although, they pointed out other human activities like the dam construction at the upstream of the sub-basin. This could lead to communal clashes among the inhabitants (Fasona and Omojola 2005). However, care must be taken no to run to incorrect conclusions as the observed patterns may be a swing in the 200-year cycle of the region (Giannini et al. 2003). The rising and falling trends of precipitation are observed at higher elevation and at lower elevation respectively. Furthermore, the result shows that precipitation series vary at both temporal and spatial scales. The variations at both scales will have a major impact on water resources management, agricultural practices and the socio-economic activity of the basin. Additionally, in attaining greater efficiency in the consumption of valuable fresh water resources in the face of drought and climate change, there is a need for adequate preparation in terms of storage, distribution and environmental services which are necessary for optimizing the fresh water resource. Further studies are required to verify and quantify the precipitation variations presented in statistical tests by ascertaining the physical mechanisms behind the changes.

CHAPTER 4: Analysis of hydrometeorological variables (Paper Two)

In the previous chapter, the spatial and temporal precipitation trend as well as the homogeneity analysis of precipitation in the study area was analysed using data from Nigeria Meteorological Agency (NiMet), Niger Direction Meteorologie National (DMN) and a 10km resolution daily gridded dataset for West Africa (PGF) developed by Princeton University between 1979 and 2015. However, due to low density of station data, the station data were assimilated into the gridded dataset. This was done to improve the quality of the gridded dataset for good representation of climatic features of locations with data paucity. In the analysis, abrupt change points were detected by the different homogeneity tests at different periods and location but these change points were not corrected. This, coupled with the overall quality of the gridded dataset inadvertently affected the quality of the results. This setback birthed the second paper in this chapter. This chapter focuses on the analysis of hydrometeorological variables in the study area. The data used were limited to observed station data. The abrupt change points were corrected using a recently developed methodology for change point correction in climate time series. Hence, a new homogenized data was generated. Furthermore, the relationship between hydrometeorological variables was established. This ascertains the robustness of the homogenization methodology. Hence, the quality of the results of this chapter is an improvement over the previous chapter as presented in section 4.4. This manuscript has been published in the Journal of Water and Climate Change (https://doi.org/10.2166/wcc.2019.283).

Analysis of hydrometeorological variables over the transboundary Komadugu-Yobe basin, West Africa

O. E. Adeyeri, P. Laux, A. E. Lawin, S. O. Ige and H. Kunstmann

ABSTRACT

Spatiotemporal trends in daily observed precipitation, river discharge, maximum and minimum temperature data were investigated between 1971 and 2013 in the Komadugu-Yobe basin. Significant change points in time series are corrected using Adapted Caussinus-Mestre Algorithm for homogenizing Networks of Temperature series algorithm. Mann–Kendall test and Sen's slope are used to estimate the trend and its magnitude at dry, wet and annual season time scales, respectively. Preliminary results show an increasing trend of the observed variables. There is a latitudinal increase (decrease) in the basin temperature (precipitation) from lower to higher latitudes. The minimum temperature (0.05 °C/year) increases faster than the maximum temperature (0.03 °C/year). Overall, the percentage changes in minimum temperature range between 3 and 10% while that of maximum temperature ranges between 1 and 3%. Due to precipitation dependence on regional characteristics, the highest percentage change was recorded in precipitation with values between −5 and 97%. In all time scales, river discharge and precipitation have strong positive correlations while the correlation between river discharge and temperature is negative. It is imperative to advocate and support positive developmental practices as well as establishing necessary mitigation measures to cope with the effects of climate in the basin.

Key words | homogeneity tests in hydrometeorological variables, Komadugu-Yobe basin, Lake Chad region, return period, trends in hydrometeorological variables, wavelet

O. E. Adeyeri (corresponding author)
West African Science Service Centre on Climate Change and Adapted Land Use,
University of Abomey-Calavi,
Cotonou,
Benin
E-mail: *cyndyfem@gmail.com*

O. E. Adeyeri
P. Laux
H. Kunstmann
Institute for Meteorology and Climate Research Atmospheric Environmental Research,
Karlsruhe Institute of Technology, Campus Alpine,
Garmisch-Partenkirchen,
Germany

A. E. Lawin
Laboratory of Applied Hydrology,
National Water Institute,
University of Abomey-Calavi,
Cotonou,
Benin

S. O. Ige
Nigerian Meteorological Agency,
National Weather Forecasting and Climate Research Centre,
Lagos,
Nigeria

4.1 Introduction

The effects of global warming and climate change on the environment cannot be underemphasized. This has generated considerable interest amongst scientists and has resulted in various studies in climate trend detection at regional (Khatiwada et al. 2016) and global scales (Trenberth and Shea 2005). Global climate warming is principally attributed to the significant rise in air temperature (IPCC 2013). As a result of increasing temperature, the intensity and frequency of extreme climate events such as drought and flood are likely to increase (IPCC 2013). This could induce extreme hydrological events such as extreme river discharge, thereby affecting the hydrological cycle. For the California drought (2012-2014), (Mao et al. 2015) reported that warmer temperatures greatly influence river discharge while (Williams et al. 2015) stated that increasing temperature escalates drought conditions. Over the Colorado Basin, (Vano et al. 2012) reported that warmer temperatures reduce the discharge from Colorado River. Conversely, (Reynolds et al. 2015) reported that the drying frequencies of intermittent streams in that basin are caused by changes occurring in both temperature and precipitation. At a regional scale, significant correlations have been observed between monthly mean temperature and precipitation in Europe and North America (Madden and Williams 1978). This relationship has been extended on a global scale which establishes that high maximum temperatures are accompanied by dry conditions (Trenberth and

Shea 2005). Results from (Trenberth and Shea 2005) showed a positive correlation between lower temperatures and higher precipitation over the continents in warm seasons. (Rusticucci and Penalba 2000) established a positive correlation between warm summers and low precipitation in the north-eastern and central-western parts of Argentina, Paraguay and southern Chile. They further emphasized that cold seasons (June, July & August) exhibit a weak correlation between the variables. Furthermore, they reported a significant and positive correlation between precipitation and temperature in the coastal parts of Chile especially between May and September as a result of high sea surface temperature which favours convection. (Nicholls 2004) reported increased potential evaporation as a result of higher mean values of maximum and minimum temperatures, thereby enhancing the severity of the 2002 Australian drought. The effect of changes in the basin's precipitation and temperature can often be related to river discharge. However, uncertainties in the trends of hydro-meteorological variables as a result of data's temporal limitations, gaps in spatial coverage, change points in the dataset, regional differences and forcing cannot be down-sized (Huntington 2006). For example, after the 1976-1977 climate shift caused by the El-Nino southern oscillation (ENSO), major African rivers have experienced lower river discharges (IPCC 2013). Attogouinon et al. (2017) attributed the increase in the frequency of flood events in many African countries to climate change. Likewise, (Adeyeri et al. 2019a) noted a significant positive trend in annual total precipitation, number of consecutive dry days, warm spell duration, warm day-, and warm night frequencies over the Komadougu-Yobe Basin (KYB). They also projected more frequent extreme precipitation and temperature events in the future. (Adeyeri et al. 2019b) observed an increasing trend in annual precipitation and river discharge over the KYB between 1971 and 2013. (Oyebande 2001) attributed the disruption of the Jama'are and Hadejia river flow of the KYB between 1979-1989 to human activities, droughts and evapotranspiration losses while (Adeyeri et al. 2019b) showed that approximately 50% precipitation variability and 50% human activities caused an increase in discharge between 1971 and 2013. However, the spatiotemporal behaviour of precipitation, river discharge, minimum and maximum temperature depend on the regional and local forcing. In order to proffer solutions to the problems associated with water resources management within the KYB, there is a need to understand the relationship between these variables at the basin's scale. Therefore, this study seeks to improve the understanding of the relationships in the observed trends of precipitation, maximum air temperature, minimum air temperature and river discharge over the KYB between 1971 and 2013. Our approaches include the detection and correction of inhomogeneity in the hydrometeorological

variables, trend analyses at both temporal (monthly, seasonal and annual) and spatial scales, correlation and wavelet analyses among the variables.

4.2 Study Area and Data Used

The study area is as described in Chapter 2. Daily precipitation, river discharge, minimum and maximum temperature data series archived by the Nigeria Meteorological Agency (NiMet), Direction de la Meteorologie Nationale (DMN) of the Niger Republic and Diffa hydrological station are used for the analysis in this study (Fig. 4). The period of analysis for this study is between 1971 and 2013.

4.3 Methods

The daily climatological time series are quality controlled using the Rclimdex package (Zhang and Yang 2004). During quality control, outliers and negative precipitation values and days with minimum temperature greater than maximum temperature are checked. Missing values from one station's data series (candidate series) are filled by calculating the weighted average of the other network data series' anomalies (partner series) which are later adjusted to the candidate series' climatic mean (Domonkos and Coll 2017). There are no missing data after quality control. For a reliable and consistent climate variability and climate impact study, observational data should be checked and corrected for inhomogeneity (Acquaotta and Fratianni 2014). The Adapted Caussinus-Mestre Algorithm for homogenising Networks of Temperature series (ACMANT) is used to check and correct the inhomogeneities in the quality-controlled time series. A full description of ACMANT set up can be found in (Domonkos and Coll 2017). Several studies (e.g. (Adeyeri et al. 2019a; Domonkos and Coll 2017) have effectively used ACMANT in homogenising series. The result evaluation from these studies showed good performances of homogenising climate series with ACMANT. The Mann-Kendall (MK) trend test (Khatiwada et al. 2016) and wavelet spectral methods (Veleda et al. 2012) are used in detecting the trend in the time series. The magnitude of the trend is estimated using the Theil and Sen's slope estimator. The spatial trend is represented using the Inverse Distance Weighted (IDW) interpolation technique.

4.3.1 Change points detection, step function fitting and homogenization of data series

The Caussinus Lyazrhi criterion (Caussinus and Lyazrhi 1997) and the optimal step function fitting (Domonkos and Coll 2017) are used in ACMANT to optimize break numbers in data series while the break detection incorporates the weighted reference data. The optimal step function minimizes the variance of internal distances and maximizing the variance of external distances.

To identify the shifts in annual mean,

$$\min_{[j_1, j_2, \ldots j_k]} \left\{ \sum_{k=0}^{k} \sum_{i=j_k+1}^{j_{k+1}} \left(d(U_1)_{k,i}^2 + c\left(d(U)_{k,i}\right)^2 \right) \right\} \quad \textit{Equation 20}$$

The internal distance (d) is given as;

$$d(U)_i = U_{(q)i} - \overline{U_{(q)k}} \; where \; i \in K$$

Equation 21

Where,

U is the operator for generating of time averages, K is the total number of breaks, j_1 and j_2 is the starting and ending year, k is the serial number of break/steps, q is the relative time series, i is the time point, j is the year, c is the empirical constant = 0.2.

To correct the inhomogeneity in data series;

$$HY_{s,j} = \begin{Bmatrix} \min & if \; sign\left(t_{s,j,x}\right) = g \; for \; every \; x \\ x = \left\{1, N'_{s,j}\right\}^{|t_{s,j,x}|} & \\ 0 & if \; sign\left(t_{s,j,x}\right) \neq g \; for \; any \; x \in \left\{1, N'_{s,j}\right\} \end{Bmatrix}$$

Equation 22

$$g = 1 \; or \; g = -1$$

where;

HY is the adjustment term, s is the reference series serial number, x is an ensemble homogenisation serial number, N′ is the total number of usable reference series at a particular step, j is the year, g is a parameter. The details of this method are documented in (Domonkos and Coll 2017). The homogenised data series is subjected to Mann-Kendall trend test to investigate the trend. The Mann-Kendall trend test, slope test, the magnitude of percentage of change as well as the interpolation method methods are same as presented in sections 3.3.2, 3.3.3, 3.3.4 and 3.3.6 respectively.

4.4 Results

4.4.1 Change point detection

Table 9, 10 and 11 show the significant change points in precipitation, maximum and minimum temperature respectively. In Table 9, significant change points are located in precipitation series of Goure in 1999 and Potiskum station in 1994 and 1998. The other stations have homogenous data series. The maximum temperature time series (Table 10) for all stations are inhomogeneous while thirteen stations (except Diffa) are inhomogeneous for minimum temperature time series (Table 11). These change points may be a result of changes in instruments, changes in station

location and environment, station network density and structure as well as observation methods (Klein Tank et al. 2009). Other factors may include anthropogenic activities, deforestation and urbanization (Adeyeri et al. 2017c; Ige et al. 2017). However, for robust analysis, these change points are corrected using the ACMANT algorithm before further analyses.

Table 9: Change points in daily precipitation time series

s/n	Stations	Year	Month	Day	Change in Mean
1	**Goure**	1999	2	31	1.2
2	**Potiskum**	1994	5	12	0.9
3		1998	10	16	1.6

Table 10: Change points in daily maximum temperature time series

s/n	Stations	Year	Month	Day	Change in Mean
1	**Bauchi**	1984	10	31	0.4
2		2012	12	1	-1.4
3	**Diffa**	1990	7	31	1.2
4	**Gombe**	1985	3	31	0.4
5		1994	7	31	0.6
6		2011	3	31	-0.7
7	**Goure**	2005	11	30	-1.0
8	**Jos**	2005	11	30	-2.2
9		2006	4	30	1.9
10	**Kaduna**	1976	12	31	0.5
11	**Kano**	1983	11	30	-0.2
12	**Katsina**	1976	9	30	-0.3
13	**Maiduguri**	2006	7	31	0.9
14		2007	8	31	-1.1
15	**Maine-Soroa**	1978	3	31	0.5
16		1982	6	30	-0.4
17		1999	9	30	0.5
19		2010	12	29	-2.6
20	**Nguru**	2011	2	28	-0.6
21	**Potiskum**	2000	4	9	-2.3
22		2005	10	31	0.7
23	**Zinder**	1989	4	30	0.2
24		2004	3	31	-2.1
25		2007	9	30	0.7

Table 11: Change points in minimum temperature time series

s/n	Stations	Year	Month	Day	Change in Mean
1	**Bauchi**	1978	1	31	0.3
2		2003	4	30	1.0
3		2007	1	31	-1.6
4		2007	11	30	1.4
5	**Gombe**	2000	12	31	2.6
6		2009	3	31	-0.6
7	**Goure**	1992	12	31	-1.0
8		1994	6	30	1.0
9	**Jos**	1978	2	28	-1.1
10		1984	3	31	-0.8
11	**Kaduna**	1984	3	6	-1.5
12		1984	11	23	1.5
13	**Kano**	1988	5	31	-0.7
14		1992	6	30	0.4
15		2010	10	31	-0.6
16	**Katsina**	1978	4	30	0.5
17		1990	12	31	-0.6
18		1993	3	17	-1.8
19		1996	12	31	1.4
20		2001	3	31	0.4
21	**Magaria**	1996	4	30	0.7
22		2000	11	30	-0.8
23		2005	12	31	1.8
24	**Maiduguri**	1982	3	31	-0.4
25		1986	3	31	-0.8
26		1989	6	30	0.5
27		2006	9	30	0.5
28	**Maine-Soroa**	1976	12	31	-0.5
29		1981	12	31	0.3
30		1997	7	31	0.6
31		2010	3	31	0.5
32	**Nguru**	1981	6	30	-0.5
33		1986	12	31	0.5
34		1998	3	31	-0.4
35		2013	6	30	-1.0
36	**Potiskum**	2008	3	31	-0.2
37	**Zinder**	2002	5	31	-1.2
38		2008	2	29	0.5

4.4.2 Mean Climatology

The monthly analysis of temperature variables (Figure 11) shows the monthly range of maximum and minimum temperature varies from 24 to 41 ^{o}C and 11 to 27 ^{o}C respectively. The highest values of maximum temperature are seen from March to June. These months precede the rain months and months with high river discharge as shown in (Adeyeri et al. 2019b). This may be attributed to the intensification of convective precipitation at high temperatures (Berg et al. 2013) especially in conditions where the ocean drives the atmosphere. For minimum temperature, the highest values are seen from March to October while the lowest values are seen from December to February. Higher values of minimum temperature may be attributed to the formation of stratiform cloud in the mornings (Janiga and Thorncroft 2014). There is also a positive trend in both annual maximum and minimum temperature for the period of study (Figure 12). However, the rate of increase in minimum temperature (0.05 ^{o}C/year) is higher than the rate of increase maximum temperature (0.03 ^{o}C/year). This is a pointer to more extreme hot temperature events with potential impacts on crop growth and yield (Hatfield and Prueger 2015). For example, minimum temperature affects the respiration rates of plants during the night also, high minimum temperature decreases crop yield and also enhances plants deterioration with age (Hatfield and Prueger 2015).

4.4.3 Temporal and Spatial trends

Table 12 presents the result of the temporal trends in temperature, discharge and precipitation time series. The monthly trend shows a non-significant decrease in the trend of discharge for all months except the months of June, July, August and September with Z values of 0.18, 0.12, 0.12 and 0.21 respectively. This was confirmed by (Adeyeri et al. 2019b) that the river discharge in these months is between 20 to 100 mm/month while the other months have fewer discharges. The highest positive percentage of change (40%) occurs in September while the highest negative percentage of change (-16%) occurs in the month of March. However, for the seasonal trends, there are significantly increasing trends of discharge in both wet and annual seasons with Z values of 0.2 and 0.1 respectively. The dry season has a non-significant decreasing Z value of -0.07. For the precipitation time series, there is a non-significant decreasing trend in May, June and July. However, the highest positive percentage change of 163% is recorded in October while the highest negative percentage change of -53% is recorded in July. The seasonal analysis shows an increasing trend of precipitation for all seasons. There are increasing trends in both minimum and maximum temperature time series for all months and seasons. Nonetheless, the highest trend increase in maximum temperature is seen on the annual scale and in April and with Z values of 0.5 and 0.4

respectively. Furthermore, the highest percentage of change (6%) is seen in May. For minimum temperature, the highest increase is seen at the annual scale and in July with Z values of 0.7 and 0.6 respectively. The highest percentage of change (15%) is seen in the month of November. The results for the Mann-Kendall test in the basin show increasing trends for all variables in all stations in the KYB except Jos and Kaduna with a decreasing precipitation trend of -0.1 and -0.05 respectively (Table 13).

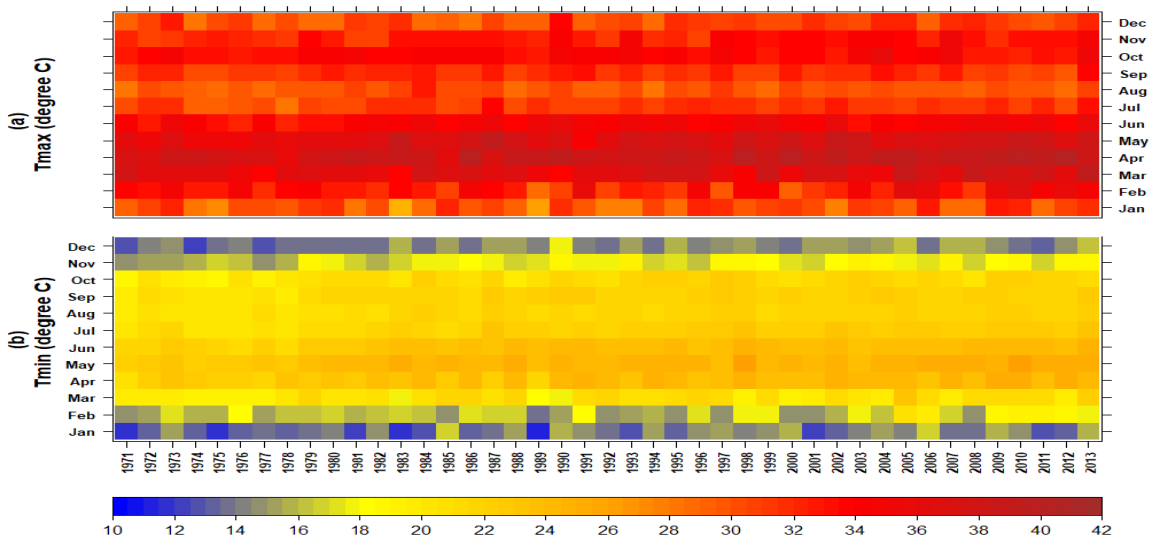

Figure 11: Temporal distributions of temperature variables over the KYB (a) Maximum Temperature (^oC), (b) Minimum Temperature (^oC)

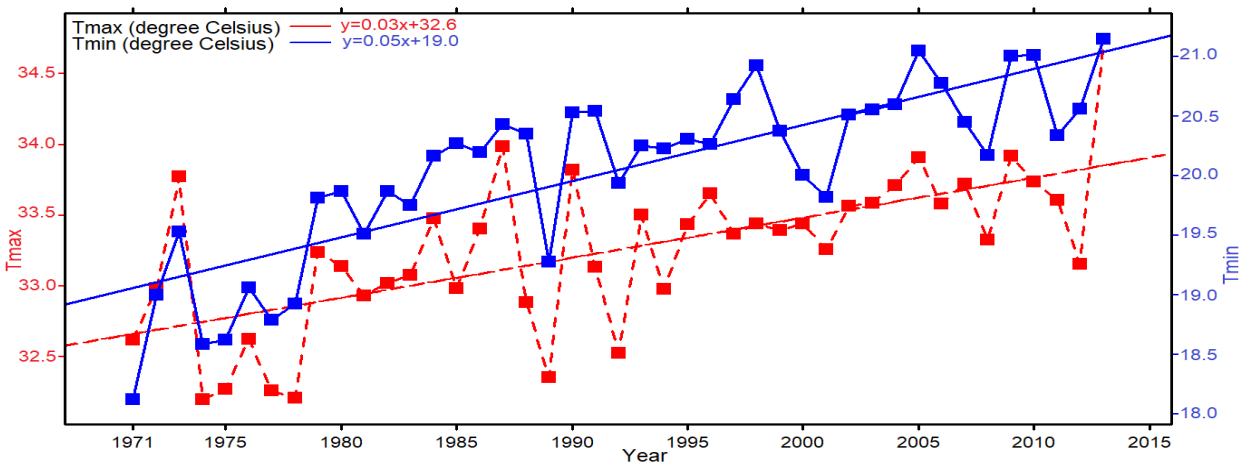

Figure 12: Annual trend of maximum and minimum temperature over the KYB between 1971 and 2013

These findings agree with (USGS 2012) who reported an increasing trend of temperature in the Sahel as a consequence of the warming of the northern Atlantic Ocean and the Mediterranean,

thereby, increasing the meridional convergence of external moisture at of low-levels. This eventually increases the precipitation in the region and creating a partial precipitation recovery especially in the 1990s. Consequently, yearly variations in precipitation are greatly influenced by local moisture recycling rate which is controlled by planetary flow configurations linked with the El Niño-Southern Oscillation (Sheen et al. 2017). Highest precipitation is seen to increase towards the south-western part of the basin (Figure 13a). The range of precipitation in the basin is between 400 and 750 mm in the northern part to between 750 to 1300 mm in the southern part of the basin. There is an overall latitudinal increase (decrease) of temperature (precipitation) i.e. from lower to higher latitudes (USGS 2012). The results of the spatial distribution of the percentage changes in precipitation are presented in Figure 13b. The highest percentage changes in precipitation are seen in Potiskum, Kano and Goure with values between 85% to almost 100% while the lowest percentage changes are seen in Gombe and Nguru with values between -5% to 21% (Figure 13b). Furthermore, the result of the periodicity in the properties of the observed variables shows different variations across different time scales (Figure 15). For example, there is an evident 3-4 years periodicity of high flow signal (≥4) in the maximum temperature wavelet between 1971 and 1995 and between 2009 and 2013. This same high flow signal is present in minimum temperature wavelet between 1971 and 1979, 1987 and 1995, and between 2007 and 2013. A periodicity of 8-11 year of low flow signals (≤ 0.3) manifested in the minimum temperature series throughout the period of study whilst this is only present between 1978 and 1991 and between 1996 and 2013 for maximum temperature. However, for precipitation, there is a regular 6 years periodicity of high flow signal (≥ 3) between 1988 and 2013 while for discharge; this same signal is captured between 1993 and 2000. Although, there are some resemblances in the properties of the periodic trends of all variables which show associated trends, however, the dissimilarities in the pattern of trends show that the properties of the variables are being modified by non-climatic influences. The spatial trend of the annual mean values of temperature variables in the KYB (Figure 14) shows the range of between 34 and 35^{o}C in the northern part to 28 and 34 ^{o}C in the southern part for maximum temperature. The range is between 20 and 22 ^{o}C in the northern part and between 16 and 20 ^{o}C in the southern part for minimum temperature. This agrees with (Funk et al. 2015) who observed coolest air temperatures at the southern edges of the Sahel. The results of the spatial distribution of the percentage changes in temperature for maximum temperature, the highest percentage change (4%) is observed in Magaria while the lowest is observed in Zinder and Maine-Soroa (<2%). The highest percentage change in minimum temperature is observed in Jos (10%) while the lowest is observed in Goure, Magaria and Diffa (between 3% and 4%).

Table 12: Trend in discharge, precipitation and temperature for monthly, dry, wet and annual seasons

	Discharge		Precipitation		Tmax		Tmin	
	Z	**%change**	**Z**	**%change**	**Z**	**%change**	**Z**	**%change**
Monthly								
Jan	-0.08	-14	0.00	0	0.13	4	**0.23**	12
Feb	-0.10	-15	0.22	0	0.11	4	**0.23**	13
Mar	-0.10	-16	**0.30**	0	**0.24**	5	**0.24**	8
Apr	-0.08	-10	0.13	0	**0.44**	5	**0.50**	11
May	-0.01	-2	-0.03	0	**0.40**	6	**0.59**	11
Jun	0.18	38	-0.01	0	**0.30**	5	**0.58**	9
Jul	0.12	26	-0.15	-53	**0.31**	4	**0.61**	10
Aug	0.12	20	0.15	36	0.04	0	**0.54**	8
Sep	0.21	40	**0.40**	133	0.00	0	**0.45**	8
Oct	-0.01	-1	**0.44**	163	0.03	1	**0.45**	10
Nov	0.01	1	**0.41**	0	**0.32**	5	**0.40**	15
Dec	-0.01	-3	**0.28**	0	**0.22**	6	**0.32**	12
Seasonal								
Dry	-0.07	-11	0.37	0	0.02	4	**0.37**	10
Wet	**0.15**	26	**0.26**	47	0.21	3	**0.60**	8
Annual	**0.10**	19	**0.30**	54	**0.48**	4	**0.65**	10

Bold values represent significant trends

4.4.4 The relationship between precipitation, temperature and river discharge

In an attempt to further understand the relationship between precipitation, river discharge, minimum and maximum temperature, the correlation plot among these variables are examined. For the dry season (Figure 16a), there exists a positive correlation between precipitation, minimum temperature, maximum temperature and years. Furthermore, river discharge in the dry season shows a negative correlation with the temperature variables and a decrease with years.

For the wet season (Figure 16b), there is a negative correlation between river discharge and the two temperature variables i.e. -0.5 for maximum temperature and -0.1 for minimum temperature while the correlation between precipitation and the maximum temperature is also seen to be negative (-0.3). These agree with (Trenberth and Shea 2005) and (Berg et al. 2013) who reported separately that over land in the dry season, there is a positive correlation between precipitation and temperature due to the low moisture holding capacity of the atmosphere. (Trenberth and Shea

2005) further reported that wet summers are cool, thereby creating a negative relationship between wet season maximum temperature and precipitation. In the warm season, precipitation intensity is influenced by moisture availability rather than the atmospherics' moisture storage capacity (Berg et al. 2013). In the same vein, the local mechanism of moisture transport may also lower the supply of moisture during the wet season. (Berg et al. 2013) confirmed that the process of drying soil in the wet seasons may also increase the temperatures. However, this contributory relationship is reversed in the dry months. For the annual season (Figure 16c), all variables show positive correlations except for the correlation between discharge and maximum temperature which is -0.1 while there is no correlation between discharge and minimum temperature. In all seasons, the river discharge and precipitation have strong positive correlations. This may be attributed to discharge increase as a result of the precipitation recovery after the droughts episodes (Guo et al. 2014). According to (Berg et al. 2013), heavy precipitation intensity is enhanced by increasing temperature through increased atmospheric moisture which drives the precipitation event through moisture convergence at low levels. As a consequence of the heavy precipitation intensity and discharge, there have been flooding events in the basin.

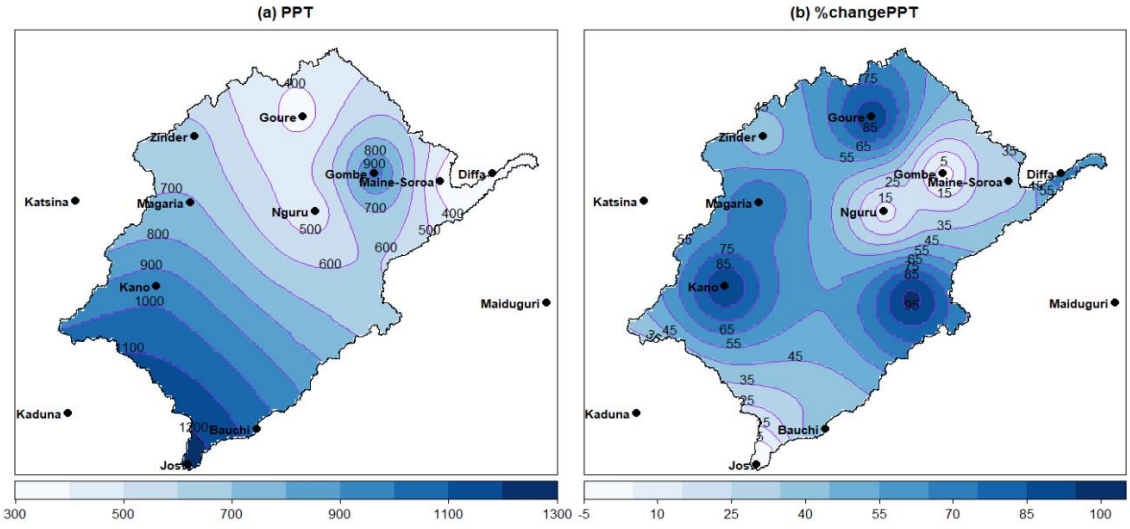

Figure 13: Spatial distribution of (a) Annual Precipitation (mm), (b) percentage change in Annual Precipitation (%)

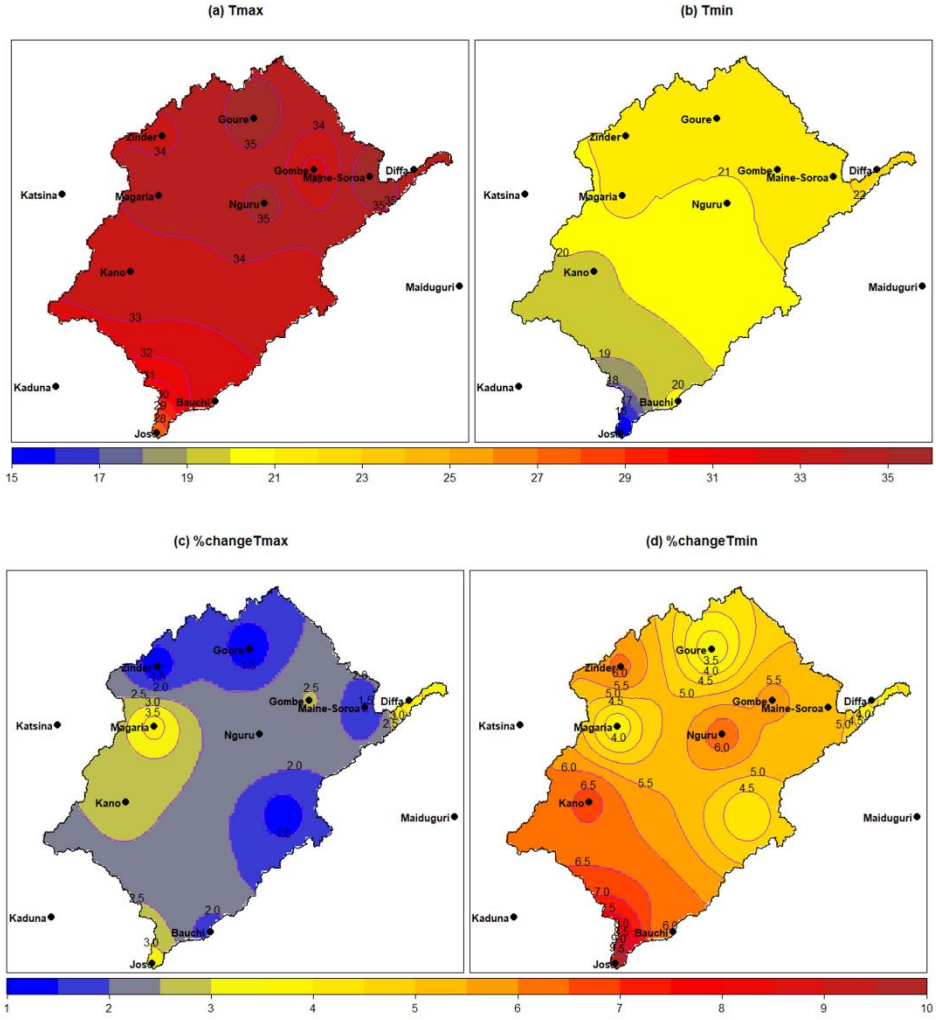

Figure 14: Annual Temperature of the Komadougu-Yobe Basin (a) Maximum Air Temperature (^{0}C), (b) Minimum Air Temperature (^{0}C) (c) Percentage change in Annual Maximum Air Temperature (%), (d) Percentage change in Annual Minimum Air Temperature (%)

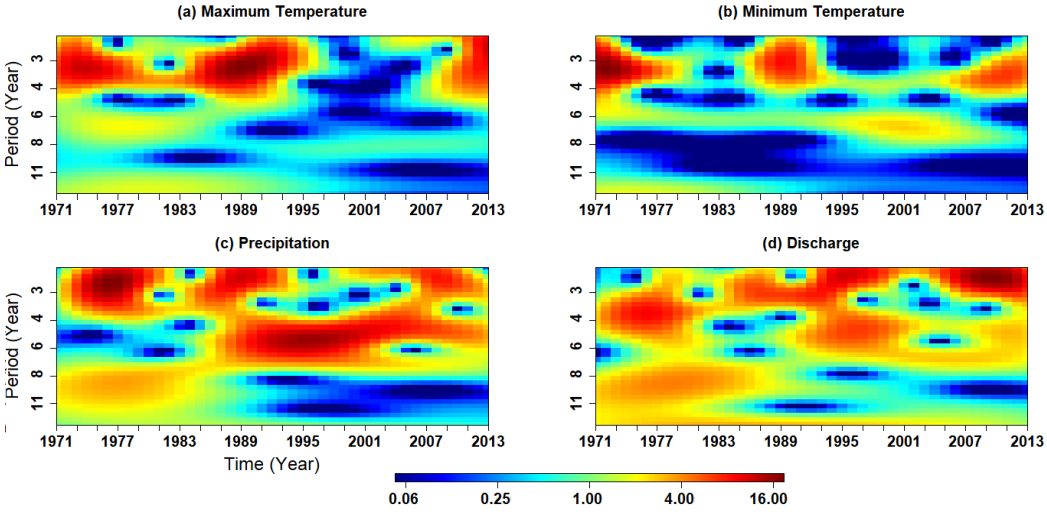

Figure 15: Periodicities in (a) Maximum Temperature (^{0}C), (b) Minimum Temperature (^{0}C), (c) Precipitation (mm), and (d) Discharge (mm)

Table 13: Mann–Kendall test (at 5% significant level) and percentage change. Bold value means significant trend, positive Z means increasing trend.

	Maximum Temperature (Tmax)			Minimum Temperature (Tmin)			Precipitation		
Stations	Z-value	Sen's Slope	% change	Z-value	Sen's Slope	% change	Z-value	Sen's Slope	% change
Bauchi	**0.23**	0.014	2	**0.44**	0.028	6	**0.3**	9.5	38.2
Diffa	**0.26**	0.03	4	0.24	0.018	4	**0.38**	4.82	68.28
Gombe	**0.36**	0.019	3	**0.42**	0.028	6	0.03	0.52	2.33
Goure	0.2	0.01	1	**0.25**	0.016	3	**0.47**	7.46	91.15
Jos	**0.44**	0.02	3	**0.54**	0.035	10	-0.1	-1.36	-4.63
Kaduna	**0.35**	0.016	2	**0.52**	0.029	7	**-0.05**	-1.26	-4.47
Kano	**0.4**	0.02	3	**0.5**	0.03	7	**0.51**	20.8	92.45
Katsina	**0.29**	0.02	3	**0.4**	0.029	6	0.17	3.63	27.29
Magaria	**0.34**	0.03	4	**0.23**	0.018	4	0.18	12.28	73.93
Maiduguri	**0.25**	0.014	2	**0.44**	0.028	6	**0.29**	5.59	42.16
Maine-Soroa	0.2	0.012	2	**0.46**	0.028	6	0.2	2.32	29.21
Nguru	**0.33**	0.02	3	**0.5**	0.029	6	0.07	1.18	12.12
Potiskum	0.19	0.01	1	**0.37**	0.02	4	0.58	14.69	97.32
Zinder	**0.22**	0.01	1	**0.53**	0.03	6	**0.23**	6.09	40.96

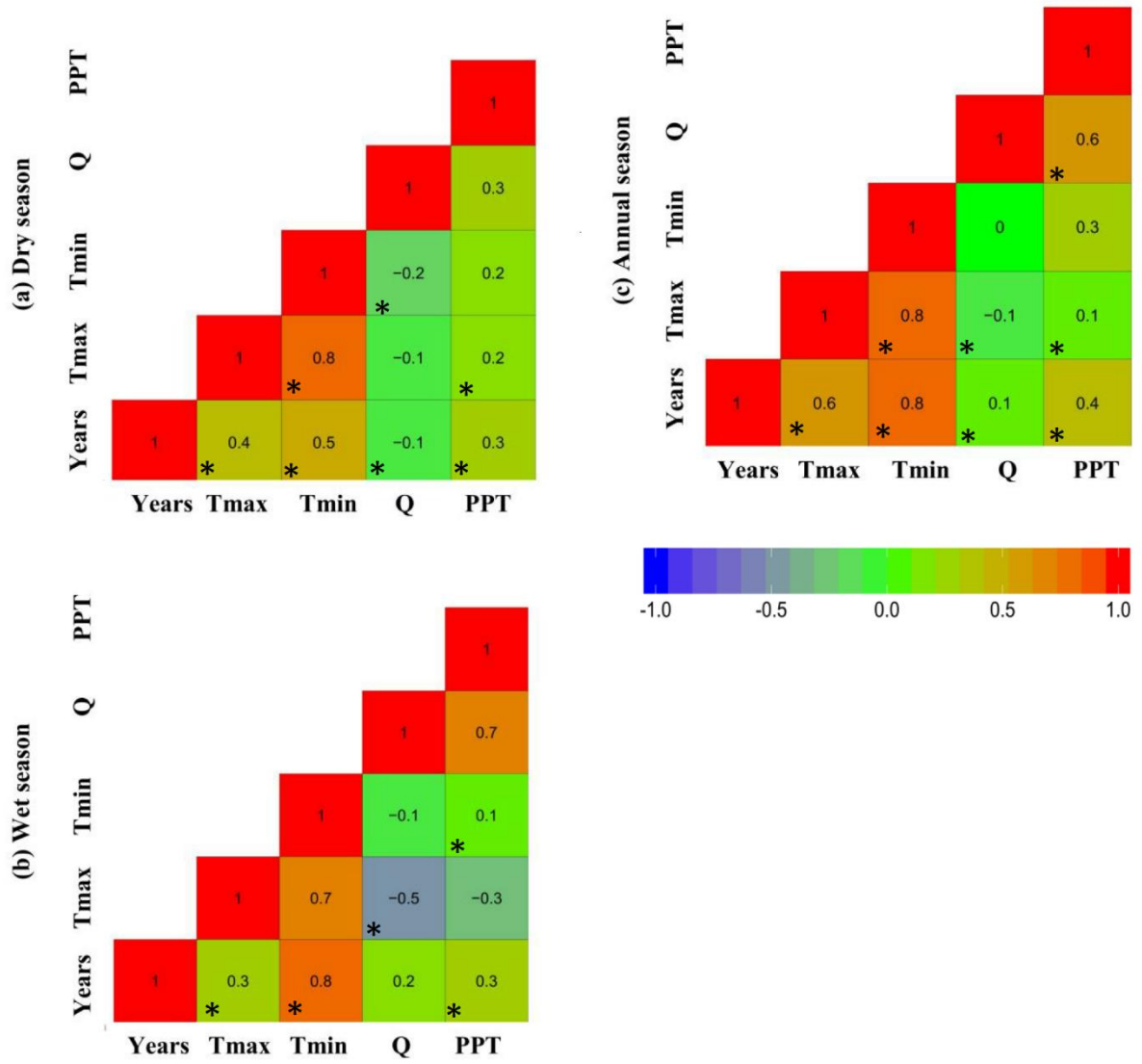

Figure 16: Correlation plot of hydro-meteorological variables during; (a) Dry season, (b) Wet season, and (c) Annual

Q is the river discharge, Tmax is the maximum temperature, Tmin is the minimum temperature, and PPT is the precipitation. * represents significant trend.

4.5 Conclusion

The study investigated the inhomogeneity and analysed the spatiotemporal trends as well as the relationship between precipitation, river discharge, maximum and minimum temperature over the Komadougu-Yobe basin, Lake Chad region between 1971 and 2013. Significant change points in

the time series were detected and corrected using ACMANT. This correction provides a more robust time series for climate impact studies in the basin. Initial results show a latitudinal increase (decrease) in the basin temperature (precipitation) from lower to higher latitudes. There are overall increasing temperature, precipitation and river discharge in the basin. On the other hand, increasing precipitation as a result of the Sahelian precipitation recovery could revive the wetlands in the basin thereby maintaining the food chain balance and preserving the ecosystem. However, excess water from heavy precipitation intensity as a result of increasing temperature as well as increasing river discharge could lead to flooding, thus, farmlands, farm produce and properties could be affected. This could have significant impacts on water management and the socio-economic activity in the basin. Furthermore, the impacts of drought on water demand and supply by natural systems and humans could be aggravated by the warming climate (Cook et al. 2015). Adequate measures and relevant developmental practices should be put in place to mitigate the warming trend as well as flooding that could arise as a result of the increased precipitation and discharge.

There should be a coordinated effort from all stakeholders in participatory dialogue in understanding and tackling climate and environmental issues in the basin. This will promote a harmonised management of climate extreme events, flood, land, water and associated resources without compromising the sustainability of dynamic ecosystems in the basin. Established transboundary cooperation should establish effective linkages between various sectors for the development of integrated water planning and management to eliminate confrontational cross-border impacts in the management of the basin. However, in an attempt to secure the basin resources from climate extreme events, feasibility studies and environmental impact assessment should be prioritised before embarking on relevant developmental projects. Nevertheless, limited hydrological and climatic data of sufficient quality have hindered sound research and in-depth investigations of the basin's hydrology. Future works should seek include more recent data.

CHAPTER 5: Assessing the impact of human activities and rainfall variability on the river discharge (Paper Three)

The previous chapter focuses on the analysis of hydrometeorological variables in the study area using observed station data. The abrupt change points were corrected, thereby creating a newly homogenized data which was used for the analysis. The trends in the meteorological variables were established. With the use of the homogenized data, this chapter therefore assesses and quantifies the impact of human activities and precipitation variability on the river discharge of the basin. This gives more information on how the trend observed in the previous chapter affects the river discharge in the basin as described in section 5.4. This manuscript is submitted to the Journal of Environmental Earth Sciences.

Abstract

The impact of human activities and precipitation variability on river discharge is of main concern for policymakers in the Komadougu-Yobe Basin (KYB), Lake Chad area. The KYB is of strategic importance because its rivers contribute significantly to the recharge of Lake Chad whose shrinkage has been of concern to policy makers and the international society. This study investigates the variations in river discharge as a result of the contributory effects of precipitation variability and human influences using daily precipitation and discharge data between 1971 and 2013. The land-use land-cover (LULC) analysis shows that an increase in bare surface, plantation, settlements and water bodies occurred in the KYB from 1975 to 2013, in association with a decrease in the forest, and grassland coverage. In order to partition the impacts of precipitation variability and human activities on river discharge, breakpoints related to abrupt environmental changes caused by human activities are identified using the Pettitt's test, the Generalized Variance (GV), Double Mass Curve (DMC) and the wavelet spectral methods. Breakpoints are found in 1974 and 1993, which corresponds to times when major dams in the basin became operational. These breakpoints may also be related to LULC changes. Overall, the mean discharge between the pre-break and post-break periods has increased by 24%. This increment in discharge was caused by approximately 50% precipitation variability and 50% human activities. Hence, the effects of human activities appear to be as important as the effect of natural precipitation variability on the river discharge changes in the KYB.

Keywords: precipitation variability, river discharge, land-use land-cover, trends, wavelet analysis, Double Mass Curve

5.1 Introduction

Annual variation of surface river discharge from a basin is primarily affected by the variability of precipitation and potential evaporation (Chien et al. 2013). Human activities such as land-

use land-cover (LULC) change, dam constructions and operations, groundwater and surface water extractions, irrigation canals and mining have led to alterations in river discharges (Destouni et al. 2013). Further findings confirmed that precipitation variability and human activities affect basins' discharge (Buma et al. 2016; Qiu et al. 2015).

The relationship between LULC changes and river discharge depends on the basin's size and location, elevation, land management and LULC types (Li et al. 2001). For example, (Sriwongsitanon and Taesombat 2011) argued that in dense forests, the discharge coefficient is increased during severe flooding in dense forests but decreases during moderate flooding. (Hao et al. 2004)concluded that discharge increases with increasing forest cover over the Naoli Basin of China. Contrariwise, (Jia et al. 2009)established a decreasing river discharge when the forest cover increases over Beijing, China. Furthermore, (Legesse et al. 2003) showed that LULC change from plantation to forest in the Ketar Basin, North Africa, resulted in decreasing discharge. They further argued that a decreasing precipitation in the Ketar Basin also contributed to the decreasing discharge. (Awotwi et al. 2017) investigated the effect of precipitation variability and LULC changes on the water balance components of the White Volta Basin, West Africa. The findings showed that the conversion of grassland and savannah to plantation reduced the amount of available blue water (i.e. water in freshwater lakes, rivers and aquifers) while the green water (i.e. water used by plants derived from soil moisture after precipitation) increased significantly. They further stated that increasing precipitation and temperature in the White Volta Basin increased the surface runoff, evapotranspiration and base flow. (Hundecha and Bárdossy 2004) also reported that afforestation decreases discharge peaks while urbanization increases them. In order to partition the impact of climate variability and human activities on river discharge, many studies have used statistical approaches (Tang et al. 2014; Zhang et al. 2012). By analysing the historical hydrometeorological dataset, these studies established the relationship between climatic factors and river discharge (Donders et al. 2005; Gao et al. 2011). Others combined the statistical approach with breaking point detection methods in order to detect the alteration of discharge caused by human activity, such as e.g. dam construction (Bian et al. 2017). These studies showed that the contribution of human activity to annual discharge variation can be remarkably larger than the contribution of precipitation variability in several regions of the world. In the case of West Africa, (Awotwi et al. 2017) found that the contribution of human activities to annual discharge change in the Lower Pra river of Ghana was about 83%.

Over the years, Lake Chad Basin (LCB) has witnessed changes in LULC coupled with poor water management practices such as the diversion of river channels, construction of large-scale dams and irrigation projects (Li et al. 2007). The combined effects of climate variability, LULC

changes and unsustainable water management practices have led to a significant alteration in the water balance of the Lake Chad Basin. This has contributed to the lake's shrinkage from 25,000 km^2 in the 1960s to 1350 km^2 in year 2000 (Coe and Foley 2001). Several studies argued that climate variability and environmental degradation have influenced the fluctuating lake levels over the past decades (Buma et al. 2016; Coe and Foley 2001).

The Komadougu-Yobe Basin (KYB) is a sub-basin of the larger Lake Chad Basin. The basin is drained by Hadejia river and Jama'are river located in the Komadougu Yobe and the Komadougu Gana river sub-systems. The basin contains significant wetlands. Before the 1970s and 1980s droughts, Lake Chad had received a considerable volume of water from this basin. However, there have been significant modifications to the environment since the drought episodes, which also led to the reduced agricultural activities. This poses a severe threat to the socio-economic well-being of people living in the basin (Tafida and Galtima 2016). In the last decades, the Komadougu-Yobe Basin (KYB) has witnessed different watershed developmental projects which were aimed at poverty alleviation and environmental sustainability (IUCN 2011). This led to the fast development at the upper reaches of the basin, nonetheless, the environment was severely degraded (Tafida and Galtima 2016). (Odunuga et al. 2011a) attributed the flow disruption at the Hadejia River and Jama'are river of KYB between 1964-1973 and 1979-1989 to the construction of the dams (Tiga and Challawa), large-scale irrigation, LULC changes, evapotranspiration losses and droughts. (IUCN 2011) reported that the construction of Tiga Dam in 1974, its lack of good management by the authorities coupled with uncoordinated irrigation practices had led to the destruction of river flow as well as over-abstraction in the basin. These practices have subsequently affected the river discharge and the stream flow into Lake Chad, causing alterations to the KYB ecosystem and delta.

Some studies have also explored the changes in the hydrological components of the KYB as a result of precipitation variability (Adeyeri et al. 2017c; Tafida and Galtima 2016). For example, (Odunuga et al. 2011a) and (Adeyeri et al. 2017c) found out that there is a precipitation gradient from the upstream (the south of the basin) to the downstream northern part of the basin. However, the categorisation of changes in river discharge in the KYB due to both precipitation variability and human activities has not been documented in detail yet.

With the increasing rate of water resources scarcity, it is important to quantify and separate the effects of human activities and precipitation variability on river discharge for better decision making on water resources management and land-use planning. A more efficient water resources management, land use planning and policy-making have the potential to cushion the effect of the freshwater resources in the KYB.

This study seeks to improve the understanding of the stream flow response in the KYB basin to both precipitation variability and human activities by (1) detecting both, the trends and change point using the available hydro-meteorological datasets (2) assessing the change points related to human activities (3) analysing and quantifying the contributions of precipitation variability and human activities to alterations in river discharge.

5.2 Study Area

The study area is same as described in section 4.2

5.3 Method

5.3.1 Observational datasets

The data used is as presented in chapter 2; however, daily discharge data from the Diffa hydrological station was included for this study. This study focuses on the analysis between 1971 and 2013. The LULC map was obtained from the West Africa Landuse Landcover Dynamics (Cotillon 2017).

5.3.2 Discharge change point detection

To identify the change points where the discharge was affected by human activities, the Generalized Variance (GV) Method (Doğu and Kocakoç 2011) and the Double Mass Curve (DMC) method (Searcy and Hardison 1960) was adopted.

The GV method analyses the combined process variability of several correlated variables. In a GV plot, if the red points are above the upper control limit, there exists a non-common-cause variation in the correlated variables. If the alterations in the relation between the variables considered are of common cause (in-control), the points fall below the upper control limit.

The upper control limit is given as;

$$\begin{cases} UCL = |\Sigma|\left(b_1 + 3\sqrt{b_2}\right) \\ b_1 = \frac{1}{(n-1)^p}\prod_{i=1}^{p}(n-i) \\ b_2 = \frac{1}{(n-1)^{2p}}\prod_{i=1}^{p}(n-i)\left(\prod_{j=1}^{p}(n-j+2) - \prod_{j=1}^{p} n-j\right) \end{cases}$$

Equation 23

where the determinant of the in-control covariance matrix of the variables is represented as $|\Sigma|$, b_1 and b_2 are the coefficients, p is the number of variables and n is the number of observations.

The DMC on the other hand is a plot of the cumulative data of one variable against the cumulative data of a correlated variable for a simultaneous period (Searcy and Hardison 1960). Breaks in the variables' DMC are caused by alterations in the relation between the variables

considered. Furthermore, the Pettitt's test (Pettitt 1979) is used to confirm the change points result of discharge from the GV and DMC methods.

5.3.3 Quantification of precipitation variability and human activity on discharge

The GV and DMC are used to identify the break periods in order to assess the variability in the post-break and pre-break periods for quantifying the effects of precipitation variability and human influences on the discharge. Hence, the total discharge variation is given as (Awotwi et al. 2017);

$$\Delta D_{total} = \Delta D_{rainfall} + \Delta D_{human} \qquad \textit{Equation 24}$$

Where ΔD_{total} is the total discharge variation, $\Delta D_{rainfall}$ is the discharge variation due to precipitation variability, ΔD_{human} is the discharge variation as a result of human influences.

Furthermore, the effect of changes in precipitation (i.e. changes between pre-break and post-break periods) on discharge is calculated as;

$$\Delta D_{rainfall} = \frac{D_{calculated} - D_{prebreak}}{(D_{calculated} - D_{prebreak}) - (D_{postbreak} - D_{calculated})} * 100 \qquad \textit{Equation 25}$$

Where $\Delta D_{rainfall}$ is the influence of precipitation variability on discharge variation, $D_{prebreak}$ is the pre-break period mean of the observed annual discharge, $D_{postbreak}$ is the post-break period mean of the observed discharge, $D_{calculated}$ is the mean of the calculated discharge. The calculated discharges in each post-break period are calculated by substituting the precipitation value in these periods to the pre-break period regression equation.

The global regression equation is given as;

$$Discharge = slope * rainfall + intercept \qquad \textit{Equation 26}$$

Hence, the variation in discharge due to human influence based on the assumption that removing the effect of precipitation variability leaves behind the effect of human activity. This is given as;

$$\Delta D_{human} = 1 - \Delta D_{rainfall} \qquad \textit{Equation 27}$$

5.4 Results

5.4.1 Changes in LULC

To understand the effect of LULC changes on the discharge in the basin, LULC was analysed for 1975, 2000 and 2013 (Figure 17a). The LULC classification reveals some level of alterations in the LULC classes from 1975 to 2013. Figure 17b shows the rate of relative change in the distribution of LULC classes for three periods i.e. 1975-2000, 2000-2013 and 1975-2013. Between 1975 and 2000, there is an increase in all LULC classes except forest and grassland with relative changes of -10% and -20% respectively. Grassland has the highest loss of -20%

while plantation has the highest gain of 22%. Between 2000 and 2013, forest and grassland continue to decrease. However, there is a decrease in irrigated agriculture (-10%). This is a deviation from the positive relative change of 17.6% recorded between 1975 and 2000. Settlements have the highest gain of 20% while grassland has the highest loss of -23%. For the entire period, i.e. from 1975 to 2013, there is a continuous decrease in forest and grassland while there are gains in other LULC classes. Overall, plantation has the highest gain of 41% while grassland has the highest loss of 38%. The LULC transition matrix (Table 14) shows the different transformations among LULC classes. For example, from 1975 to 2000, 19% of grassland was transformed into vegetation while over 7% of plantation was transformed into settlements. Between 2000 and 2013, over 16% of plantation was transformed into settlements while between 1975 and 2013, over 36% of grassland has been transformed into bare surface. Throughout the entire period, the gains in settlement are mainly from plantation and grassland while the gains in bare surface are majorly from grassland. However, gains in plantation are principally from grassland.

Results from other studies (Hundecha and Bárdossy 2004) have shown that the transformations in basin's LULC classes have significant effects on the river discharge. The effects of these LULC transformations will be furthered explored using the GV and DMC in the subsequent sections.

Table 14: LULC transition matrix (%)

Periods	LULC	Plantation	Bare Surface	Forest	Irrigated	Grassland	Settlement	Water Body
	Plantation	80.26	0.00	0.00	0.65	1.59	7.18	2.61
	Bare Surface	0.01	96.44	0.00	0.00	0.01	0.27	0.11
	Forest	0.40	0.00	99.42	0.00	0.14	0.00	0.28
1975-2000	Irrigated Agriculture	0.00	0.00	0.00	86.36	0.00	0.00	0.00
	Grassland	19.00	2.81	0.46	12.99	98.20	7.71	2.89
	Settlement	0.00	0.00	0.00	0.00	0.00	84.84	0.00
	Water Body	0.33	0.75	0.12	0.00	0.07	0.00	94.11
	Plantation	98.15	1.87	0.00	1.95	1.46	16.22	4.56
	Bare Surface	0.22	81.84	0.00	0.00	0.35	0.80	0.00
	Forest	0.11	0.00	96.88	0.00	0.01	0.00	0.17
2000-2013	Irrigated Agriculture	0.00	0.00	0.00	86.36	0.01	0.00	1.06
	Grassland	16.74	34.64	0.23	0.65	75.20	6.38	4.06
	Settlement	0.10	0.00	0.00	0.00	0.00	94.41	0.00
	Water Body	0.30	0.00	0.00	2.60	0.09	1.60	95.28
	Plantation	79.47	2.43	0.00	1.95	1.73	21.28	6.61
	Bare Surface	0.23	78.84	0.00	0.00	0.34	0.80	0.11
	Forest	0.52	0.00	96.30	0.00	0.12	0.27	0.44
1975-2013	Irrigated Agriculture	0.00	0.00	0.00	72.73	0.01	0.00	1.06
	Grassland	34.70	36.52	0.69	14.29	74.79	15.43	7.11
	Settlement	0.09	0.00	0.00	0.00	0.00	80.05	0.00
	Water Body	0.62	0.56	0.12	2.60	0.14	1.60	89.78

5.4.2 Precipitation and Discharge variability

The temporal precipitation variability in the KYB from 1971 to 2013 (Figure 18a) shows that the rainy season generally started in May and ended in October during the entire period. The wettest month was August, with a maximum precipitation amount of 300 mm in 1999. The dry months were from November till April, although there were some rain events in the dry months of 2012 and 2013. The monthly distribution of mean discharge (Figure 18b) shows that the maximum discharge occurred for the wettest month of August. Although the rain season generally started in May, a significant amount of discharge was generally only recorded from June. Nevertheless, 1979 and 1980 had a significant amount of discharge throughout the whole year. There was also an increasing trend in both variables in the basin with slopes of 1.9 mm/year and 3.0 mm/year for discharge and precipitation respectively (Figure 19).

5.4.3 Change point detection

Using the GV, if the modifications in the relationship between discharge and precipitation are of common cause (in-control), the red points should fall below the upper control limit (UCL) while in DMC, the relationship between discharge and precipitation should exhibit a straight line without breakages, provided that there are no external influences. The GV result (Figure 20) shows two points

in 1974 and 1993 which are above the UCL. This is an indication of non-common-cause variation in the discharge and precipitation. On the other hand, the DMC results (Figure 21) confirmed these two major breakpoints in 1974 and 1993, suggesting that the changes in discharge were not only from precipitation variability but also from human influences. These change points correspond to the years when the different dams and the large-scale irrigation schemes became fully operational.

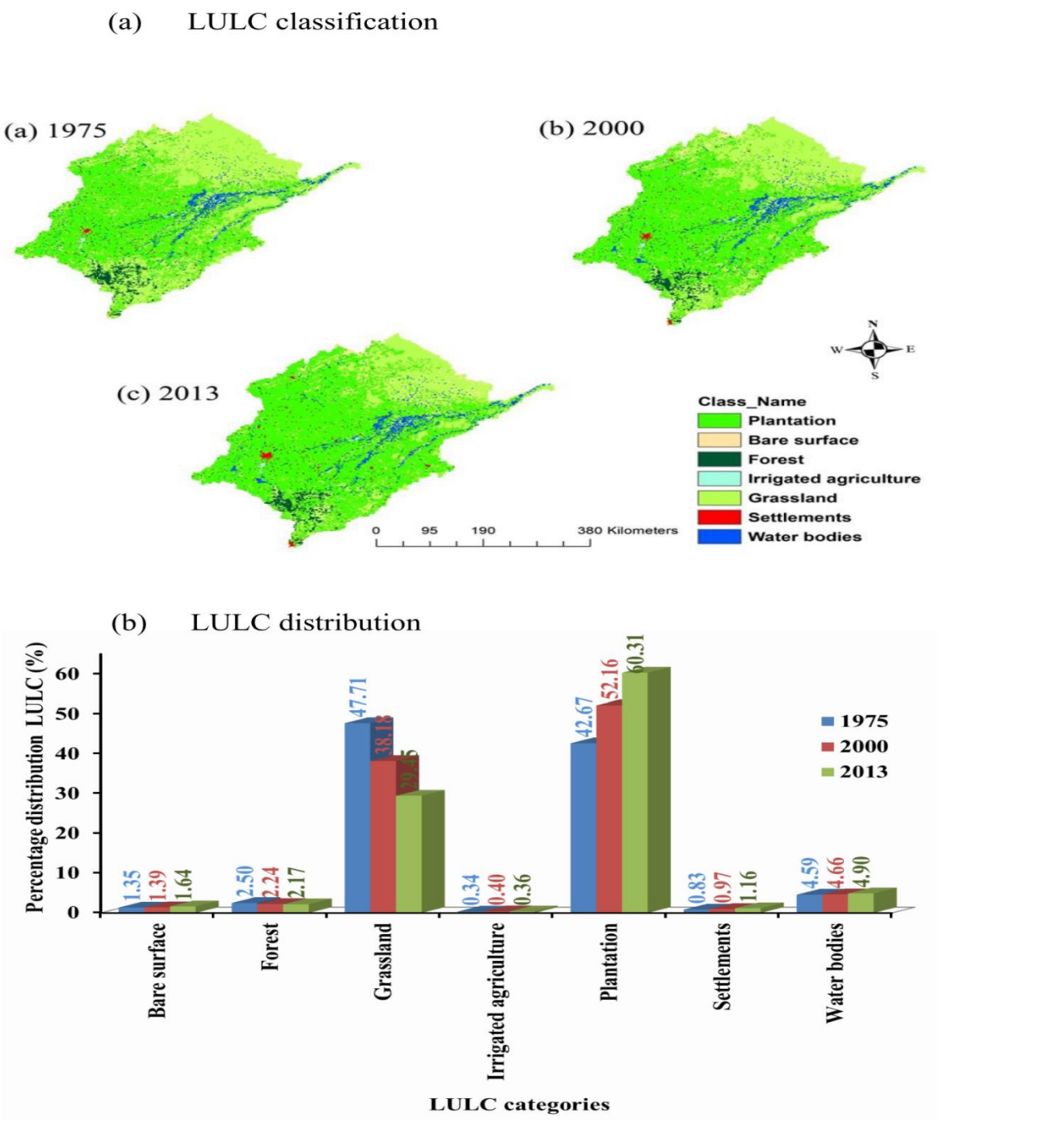

Figure 17: KYB LULC (a) classification for 1975, 2000 and 2013 (b) distribution (%) for 1975, 2000 and 2013

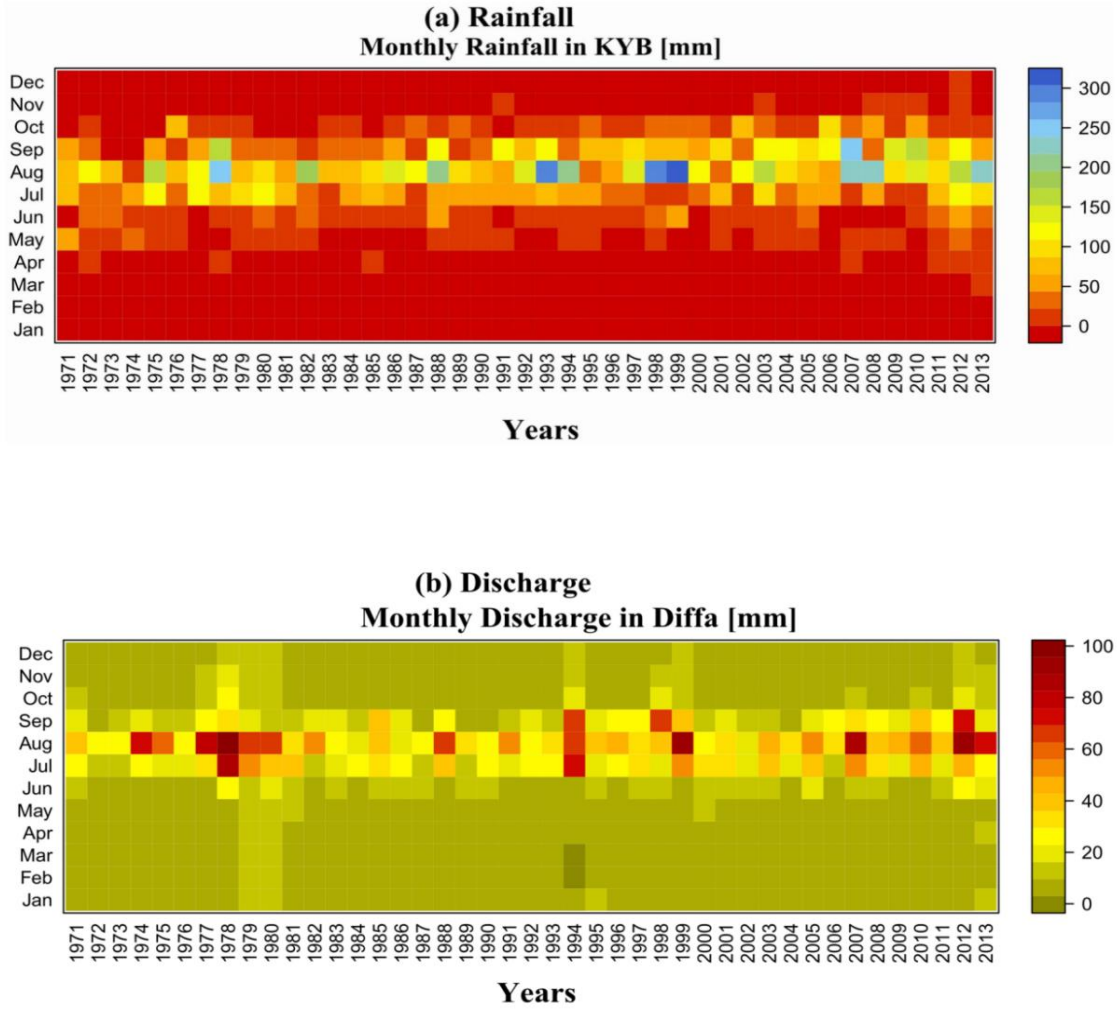

Figure 18: Temporal distribution of Hydro-meteorological variables at KYB (a) Precipitation (b) Discharge

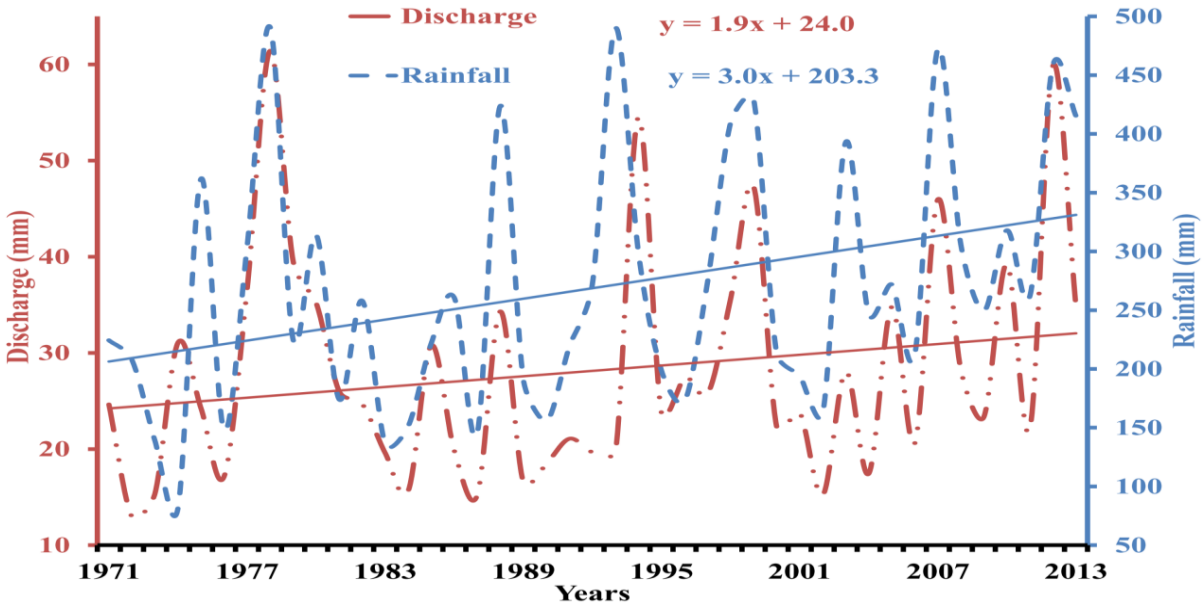

Figure 19: Trend of precipitation and discharge in KYB between 1971 and 2013

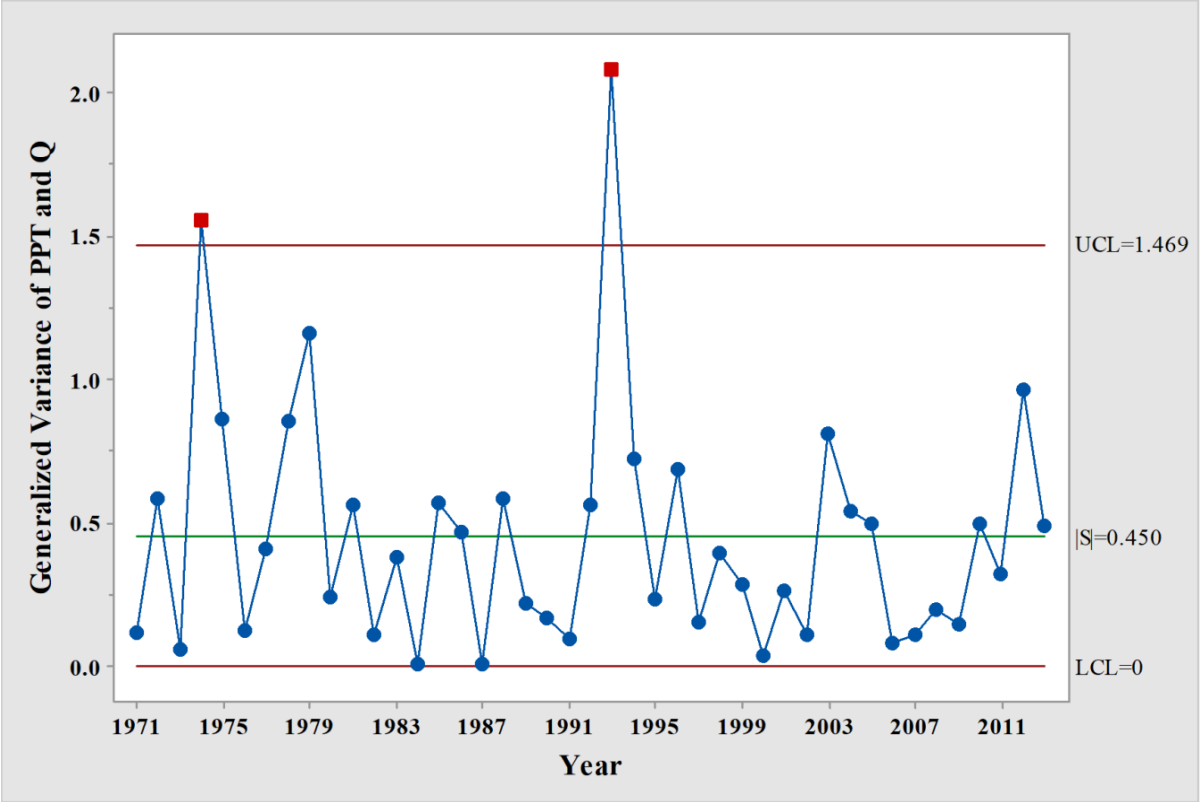

Figure 20: Generalised variance of precipitation and discharge

UCL is the upper control limit, LCL is the lower control limit and |S| is the generalized variance.

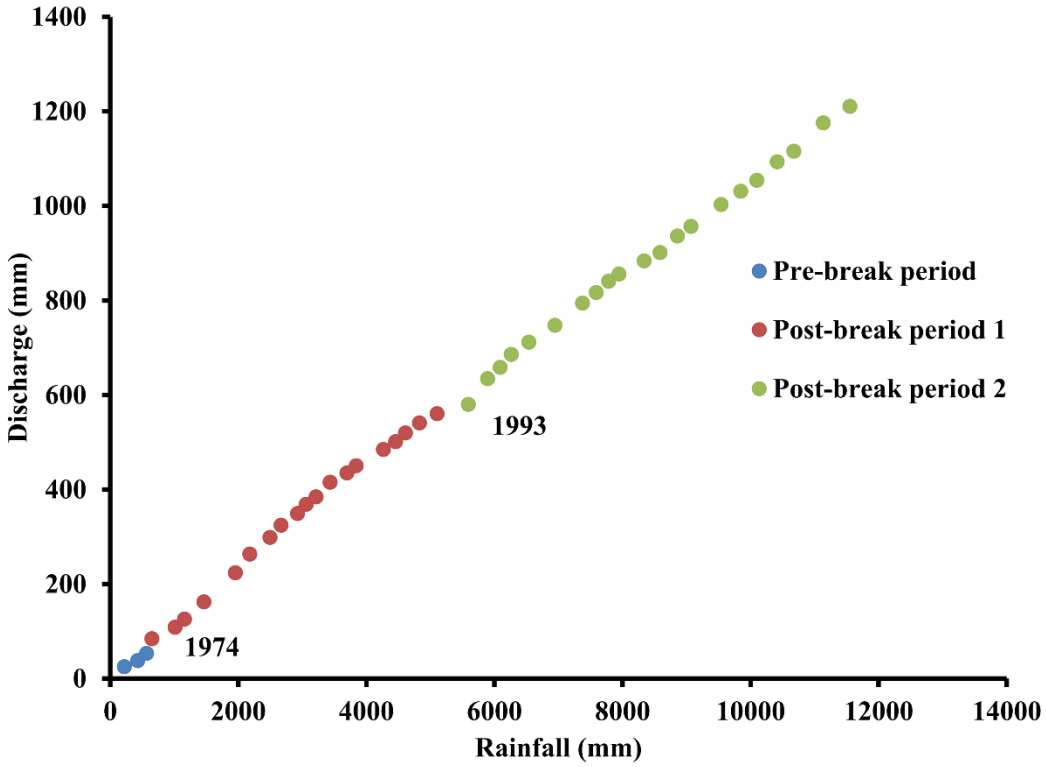

Figure 21: DCC between discharge and precipitation between 1971 and 2013

5.4.4 Quantification of discharge response to precipitation and human activities

The study period from 1971 to 2013 is divided according to the breaks identified by the GV and DMC methods. The years between 1971 and 1973 are considered as the reference period (pre-break period) when discharge was not influenced by human activities. Period 1 is between 1974 and 1992; period 2 is between 1993 and 2013, while the last period, period 3, is the entire post-break period of between 1974 and 2013. For more understanding about the changes in discharge, the linear regression equations between discharge and precipitation were established for the GV-DMC-based change points considering the non-monotonic property of discharge (Figure 22). The line of fit for the reference period lies below the line of fit for the other periods. This is a confirmation of the role of human activities on discharge increment after 1973. A test of the regression equations (Table 15) shows relatively low standard error values which demonstrate high precision of the regression equation. The low P values and significance F values established the reliability of the regression results (Murtaugh 2014).

Table 16 shows the quantification of the discharge changes in response to precipitation variability and human activities. The result reveals that the periods after the dams were built had more discharges than the pre-dam period. This may be attributed to the ability of the dams to retain excess water in the wet season and release it evenly to the downstream. Other factors include the LULC transformations as a result of human activities that have taken place in the basin. Furthermore, the increasing precipitation trend as a result of the precipitation recovery after the droughts episodes also increases river discharge.

The contribution of precipitation variability and human activities to changes in discharge was based on the linear fits (Figure 22) of the pre-break period (Table 15). In period 1, changes in discharge were caused majorly by human activities (64%). In period 2, the contribution of human activities to the variation in discharge has reduced to 42%. However, in period 3, which is the overall post-break period, the increment in discharge was caused by 50% human activities. Hence, the contribution of human activities to changes in river discharge cannot be under-emphasized in the KYB. Human activities can be considered to be a major driver to river discharge changes in KYB. Likewise, the time series analysis of the observed and calculated discharges (Figure 23) shows an alteration in the cyclic pattern of the observed discharge at the downstream station over the years. Similarly, the increased discharge peaks in the observed discharge are very evident. The discharge peaks are more in the observed discharge compared to the calculated discharge. This is a direct consequence of increased urbanization in the basin. Discharge peaks can be increased as a result of increased urbanization and deforestation.

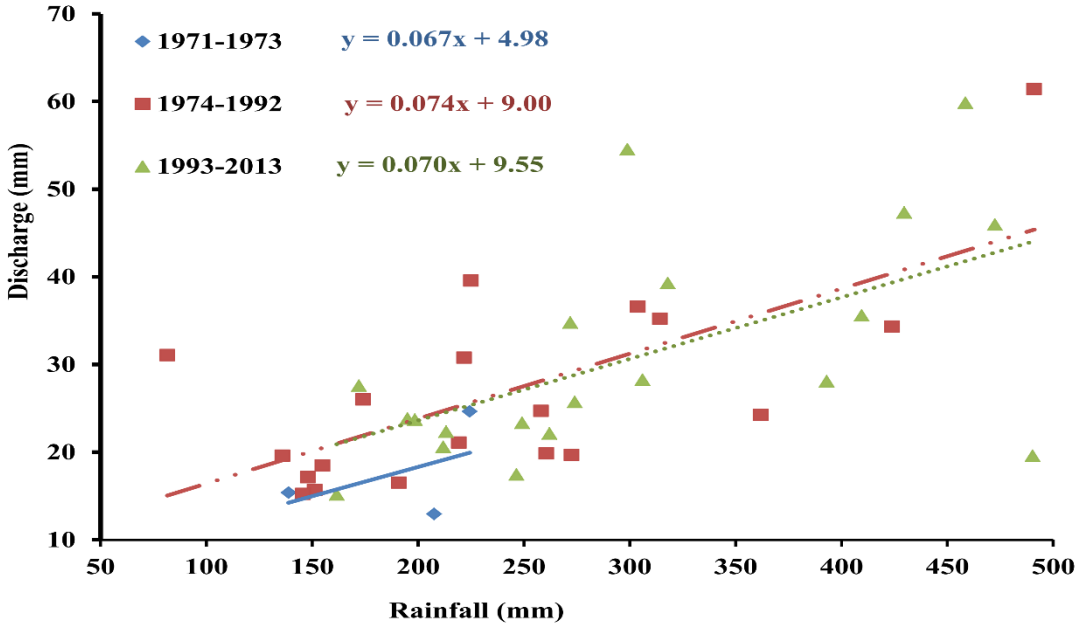

Figure 22: Best-fitted lines of linear regression between discharge and precipitation

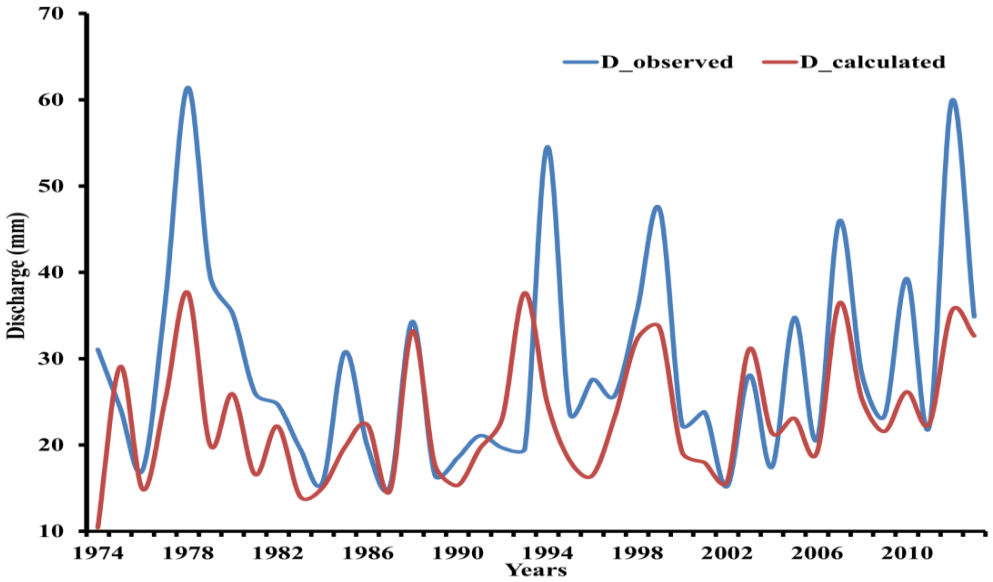

Figure 23: Time series of the whole post-break period when affected (D-observed) and not affected by human activities (D_calculated)

Table 15: Analysis of regression equation

(a) Regression coefficients

Dependent period	Slope	Intercept
Dpre-break period	0.067	4.98
Dpost-break period1	0.074	9.00
Dpost-break period2	0.070	9.55
Dpre-break period	0.067	4.98

(b) Test of regression equation

Slopes	Post-break Period 1	Post-break Period 2
P value	0.04	0.02
Standard Error	4.8	6.2
t Stat	-2.0	0.7
F statistic	4.0	0.5
Significance F	0.05	0.01

Table 16: Quantification of the discharge changes in response to precipitation variability and human activities

Year	Observed Discharge (mm)	Calculated Discharge (mm)	Impact of Precipitation (%)	Impact of Human activities (%)
1971-1973	17.7	17.7		
1974-1992	26.7	20.9	35.6	64.4
1993-2013	31.0	25.4	58.5	41.5
1974-2013	28.9	23.3	49.8	50.2

5.5 Discussion and Conclusion

In this study, the impact of human activities and precipitation variability on the river discharge of Komadougu-Yobe Basin, Lake Chad Area was analysed. We found an increasing trend of precipitation, which may be attributed to the warming of the Atlantic Ocean which pulls the ITCZ further north during the wet season, thereby, creating a precipitation partial recovery in the region (Nicholson 2001; USGS 2012). The river discharge also had an increasing trend, which might be related to the ability of the constructed dams to retain water in the wet season and later release it evenly throughout the year. This is in agreement with the findings of (Adams 1993). Furthermore, the increasing precipitation trend as a result of the precipitation recovery after the droughts episodes can also lead to an increase in discharge (Guo et al. 2014).

The constructed dams and reservoirs in the basin have effects on the water discharge in the basin. The main dam constructions are in the Hadejia river sub-system. The Tiga Dam which was the first dam was completed in 1974 while other dams were completed in 1992 and started operations in 1993 (Oyebande 2001). These years were confirmed by the breakpoint analyses. The breakpoint in 2003 may be attributed to Typha grass infestation along the Nguru Lake and Marma channel caused by the short-term measures taken by the farmers to avert flooding as a result of increasing river discharge in previous years (Muhammad et al. 2015; Umar and Ankidawa 2016). However, densely populated Typha grass is capable of impeding the flow through drainage channels at the point of infestation,

thereby increasing the overall flow of water downstream as a result of flooding (Parsons and Cuthbertson 1992). The assessment of LULC reveals that the period with the highest discharge means coincides with the periods of reduced irrigated agriculture, forest and grassland. This means that a reduced irrigated agriculture, forest and grassland potentially reduced the rate of evapotranspiration and infiltration as well as interception loss, hence, making more water available for discharge downstream, as also suggested by e.g. (Jia et al. 2009) and (Spracklen et al. 2012). Additionally, our result is in line with several studies reporting that basin's discharge significantly increased after deforestation while it decreases with afforestation (Legesse et al. 2003; Tuteja et al. 2007), as an increase in waterbodies increases the discharge coefficient, despite a higher evaporation rate caused by the LULC change (Li and Shi 2015). As reported by (Wang and Hejazi 2011), climate variability and human activities are generally seen as the main forces causing an alteration in river discharge. However, in this study, the impact of human activities and precipitation variability on river discharge was seen to be equally shared. Hence, hypothesis one is confirmed. A better knowledge of the driving factors affecting discharge variability in the KYB will help in better decision making and plan concerning water management and security in the region. However, this study is limited by short span of data series. Further works should seek the use of longer data series.

Chapter 6: Analysis of climate extreme indices: Past and future occurrences (Paper Four)

The previous chapter assessed and quantified the impact of human activities and precipitation variability on the river discharge of the basin using the newly generated homogenised data series. However, in an attempt to further understand the susceptibility of KYB to climate change, especially how the extreme conditions affect precipitation and temperature variation from historical to future projections at two climate scenarios, the climate extreme indices were analysed using homogenized observed stations' data for past climate extremes' characteristics and an ensemble mean of 8 bias-corrected CORDEX climate models for future projection of climate extremes under two RCP scenarios. This present chapter, therefore, presents the results of the analysis of climate extreme indices over the Komadougu-Yobe basin as described in section 6.4. This also gives an indication to precipitation related events which are capable of influencing the volume of stream flow under different climate scenarios for the future. This research is published in the Journal of Weather and Climate Extremes (https://doi.org/10.1016/j.wace.2019.100194).

Weather and Climate Extremes 23 (2019) 100194

Contents lists available at ScienceDirect

Weather and Climate Extremes

journal homepage: www.elsevier.com/locate/wace

Analysis of climate extreme indices over the Komadugu-Yobe basin, Lake Chad region: Past and future occurrences

O.E. Adeyeri[a,c,*], A.E. Lawin[b], P. Laux[c], K.A. Ishola[d], S.O. Ige[e]

[a] Graduate Research Programme on Climate Change and Water Resources, West African Science Service Centre on Climate Change and Adapted Land Use, University of Abomey-Calavi, Benin
[b] Laboratory of Applied Hydrology, National Water Institute, University of Abomey-Calavi, Benin
[c] Institute for Meteorology and Climate Research Atmospheric Environmental Research, Karlsruhe Institute of Technology, Germany
[d] Department of Geography, National University of Ireland, Maynooth, Ireland
[e] Nigerian Meteorological Agency, National Weather Forecasting and Climate Research Centre, Nigeria

ARTICLE INFO

Keywords:
Homogeneity
Climate extreme indices
Linear trends
Bias correction
Komadugu-Yobe basin
Lake Chad region

ABSTRACT

This study investigates trends of climate extreme indices in the Komadugu-Yobe Basin (KYB) based on observed data of the period 1971–2017 as well as regional climate model (RCM) simulations for the historical period (1979–2005), the near future (2020–2050), and the far future (2060–2090). In order to correct change points in the time historical series, the Adapted Caussinus Mestre Algorithm for homogenising Networks of Temperature series homogeneity test is used. The magnitude of the linear trends is estimated using the Sen's slope estimator and Mann-Kendall's test is performed to check the statistical significance of the trends. Future trends are assessed using the ensemble mean of eight regional climate model data under two emission scenarios, provided by the Coordinated Regional Climate Downscaling Experiment (CORDEX). Therefore, the projected rainfall and temperature have been corrected for biases by using empirical Quantile Mapping. In the observations, warm spell duration, warm day-, and warm night frequencies exhibit statistically significant positive trends. Although there is a positive trend in the annual total rainfall, the number of consecutive wet (dry) days decreases (increases). The future climate also shows a continuing positive trend in the temperature extreme indices as well as more frequent extreme rainfall events. Therefore, it is pertinent for decision-makers to develop suitable adaptation and mitigating measures to combat climate change in the Basin.

6.1 Introduction

In recent decades, there has been an increase in the frequency, intensity and extent of the impact of natural disasters on the environment which is a concern to many nations. This has been attributed to climate change and environmental degradation (Lyon and DeWitt 2012). (Mouhamed et al. 2013)

argued that climate variability is mainly associated with increasing concentration of anthropogenic greenhouse gases in the atmosphere. This has resulted in global warming. Over the Sudanian, Sahelian and Sahelo-Saharan ecological zones of West Africa, there has been an increasing trend of both maximum and minimum temperatures with minimum temperatures increasing more rapidly (Mouhamed et al. 2013). (Abatan et al. 2018a) examined the trend in absolute indices of temperature extremes over Nigeria linking it with the Northern Atlantic Oscillation (NAO) for the period 1971-2012 using weather stations. They found out that warming is most pronounced in the southern part of the country with a significant increasing trend. (Abatan et al. 2018b) investigated the trends in mean and extreme temperatures over Ibadan, Southwest Nigeria between 1971-2012 using ERA-20C reanalysis data and reported increasing annual and seasonal mean minimum temperatures with a non-significant decrease in the annual mean maximum temperature. The coldest night also shows greater warming trend than on the coldest day.

In many West African countries, the frequency of flood events has increased which had led to the loss of human lives and properties (Attogouinon et al. 2017). This has been connected to the adverse effects of climate change (Adeyeri et al. 2017a). (Abiodun et al. 2017) examined the impacts of climate change on characteristics of extreme precipitation events over four African coastal cities under two future climate scenarios (RCP4.5 and RCP8.5) and reported an increase in dry spells and a decrease in wet days over the four cities in the future for the two climate scenarios. Results from other studies (Mason and Joubert 1997; Shongwe et al. 2010) showed that the modifications in extreme weather and climate events in Africa can be attributed to climate change. For example, (Mason and Joubert 1997) projected an increasing intensity of extreme precipitation over South Africa using an ensemble of global circulation models (GCMs). (Shongwe et al. 2010) also projected an increasing intensity of dry extremes over South-western Africa in summer months for the years of 2046-2065 and 2081-2100, respectively. As a result of the coarse spatial resolution of the GCM simulations and projections used in the studies, it is difficult to account for the influence and effect of the continent's complex topography on the synoptic-scale features and mesoscale atmospheric systems that favour extreme precipitation. To bridge this gap, studies over the continent (Engelbrecht et al. 2009) have downscaled GCM projections with regional climate models (RCMs). Although many studies have utilized an RCM to investigate the changes in the long-term means of temperature and precipitation over Africa, just a few have examined the influence of climate change on climate extremes. It is also worthy to note that many studies have explored the suitability of a single RCM in downscaling GCM simulations (e.g. (Dosio and Panitz 2016). The Coordinated Regional Climate Downscaling Experiment (CORDEX) (Nikulin et al. 2012), initiated international efforts in regional climate downscaling and made the data accessible publicly. Regardless of this development, only a few studies have utilised the CORDEX dataset in providing multi-RCM future projections in Africa e.g. on precipitation extremes over Southern Africa (Pinto et al. 2016). It is worthy to note that studies

from other parts of the world (Pinto et al. 2016; Zhang et al. 2006) have evaluated the trend in future projections of climate extremes using RCMs. However, biases in temperature and precipitation simulations as a result of discretization and spatial averaging within grid cells hinder the direct use of climate simulations for impact studies (Teutschbein and Seibert 2013). Hence, it is important to bias-correct model output before using it for impact studies. Furthermore, the use of extreme indices for climate extremes analysis is based on the exceeding threshold or probability of occurrence of a given variable. Results from various studies in Africa (Abatan et al. 2018a; Mouhamed et al. 2013) showed no uniform pattern in the trend of annual precipitation as it depends on the locality. A faster increase in minimum temperature over maximum temperature is seen as a contributing factor to a smaller diurnal temperature range (Mouhamed et al. 2013). Overall, the different patterns of the above results encourage continuing analysing the climate extremes for several spatial scales (e.g. regional, local, watersheds). Therefore, the present paper aims at assessing the trends in extreme precipitation and temperature indices in the Komadougu-Yobe Basin (KYB) of the Lake Chad Basin over the observed historical period (1971-2017), validation period (1979-2005), regional climate model simulated historical period (1979-2005), near future (2020-2050) and far future (2060-2090) simulations. To this regard, six temperature indices (Table 17), namely cool day frequency (tx10p), warm day frequency (tx90p), cool night frequency (tn10p), warm night frequency (tn90p), warm spell duration indicator (wsdi), diurnal temperature range (dtr), as well as six precipitation indices, namely maximum 5-days precipitation (rx5day), consecutive dry days (cdd), consecutive wet days (cwd), very wet days (r95p), extremely wet days (r99p), and annual total precipitation (prctot) were analysed for these periods. This study will provide information as regards the overall understanding of past and future climate extreme events in the basin which could trigger relevant adaptation as well as mitigation strategies suitable for the basin.

6.2 Study Area

The study area is as described in chapter 2.

6.3 Data and Methods

The data used is as described in section 2.6, 4.2 and 4.3. However, in this section, the analysis period was extended to 2017. An ensemble of CORDEX data comprising of eight GCMs (Table 2) dynamically downscaled by one RCM RCA4 (Swedish Meteorological and Hydrological Institute-Rossby Centre Atmosphere model version 4) which has a resolution of 0.44° × 0.44° was used for the projection between near future (2020-2050) and far future (2060-2090) under two representative concentration pathways (RCP 4.5 and RCP 8.5) while the simulated historical was between 1979 and 2005.

Table 17: Definitions of indices used in this study

Indices	Name	Definition	Unit
		Precipitation Indices	
rx5day	Maximum 5-days precipitation	Maximum 5-days precipitation	mm
cdd	Consecutive dry days	Maximum number of consecutive days with RR < 1 mm	Days
cwd	Consecutive wet days	Maximum number of consecutive days with RR ≥ 1 mm	Days
r95p	Very wet days	Annual total precipitation when RR > 95 percentiles	mm
r99p	Extremely wet days	Annual total precipitation when RR > 99 percentiles	mm
prctot	Annual Total Precipitation	Annual total precipitation in wet day (RR > 1 mm)	mm
		Temperature Indices	
dtr	Diurnal temperature range	Annual mean difference between tx and tn	^{o}C
tx10p	Cool day frequency	Percentage of days with tx <10th percentile	%
tx90p	Warm day frequency	Percentage of days with tx > 90th percentile	%
tn10p	Cool night frequency	Percentage of days with tn < 10th percentile	%
tn90p	Warm night frequency	Percentage of days with tn > 90th percentile	%
wsdi	Warm spells duration indicator	Annual count of days with at least 6 consecutive days with tx > 90th percentile	Days

tn and tx are the daily minimum and maximum temperatures respectively, RR is daily precipitation amount

RCA4 uses the Flake lake model which is capable of predicting the mixing conditions and vertical temperature structure and in various lakes' depth at different timescales (Mironov 2008). It uses the Bechtold Kain-Fritsch convection scheme which separates the shallow and deep convection

processes. Its convective available potential energy (CAPE) convection closure is more suitable for high-resolution simulations (Bechtold et al. 2001). The soil carbon in RCA4 improves the simulated diurnal temperature range and reduces the soil-heat transfer. Further description of the physical parameterizations can be found in (Samuelsson et al. 2011). This RCM is chosen due to its performance over West Africa and particularly its ability to adequately reproduce West Africa precipitation regimes (Akinsanola et al. 2018; Alamou et al. 2017). The station point data for both historical CORDEX (1979-2005) and projection phase (2020-2050, 2060-2090) were extracted from the CORDEX grid of the CORDEX data. The climate extreme indices of the homogenised validation period (1979-2005), CORDEX simulated historical period (1979-2005), near future (2020-2050) and far future (2060-2090), as well as the homogenised data series for the observed historical period were calculated using the Rclimdex package.

6.3.1 Detecting breakpoints, step function fitting and homogenization of climate data series

Quality climate data series especially long-term are necessary for observing and studying climate variability and change. To obtain a high quality and reliable climate data series free errors and inhomogeneities, the climate data series must be homogenized (Acquaotta and Fratianni 2014; Aguilar 2003). Inhomogeneity in climate data can be caused by instrument repositioning, changes in reading instruments' time, station relocations etc. (Acquaotta et al. 2016). The most frequent form of climate data series inhomogeneity is the change or break point which occurs as a result of the sudden shift of the means (Domonkos and Coll 2017). A detail of the homogeneity correction is presented in section 4.3.

6.3.2 Analysis of Climate extreme trends

In analysing the climate extreme trend, the Mann-Kendall statistic was performed on the homogenous climatic time series while the magnitude of the trend was calculated using the Sen's slope estimator (Sen 1968). The details of this method are as presented as in section 3.3.

6.3.3 Bias correction of Precipitation and Temperature time series

The Quantile Mapping (QM) bias correction method (Teutschbein and Seibert 2013), which is recognized to efficiently correct precipitation and temperature output of RCMs, was used to correct the daily time series data over the basin in order to project the future changes in climate extremes under two Representative Concentration Pathways (RCP 4.5 and RCP 8.5) in the basin. The RCP is the pathway of the cumulative greenhouse gases emission by humans from all sources in part per million volumes (ppmv). RCP 45 is the medium stabilization scenario when carbondioxide emission is at 650 ppmv while RCP 85 is the very high baseline emission scenario when carbondioxide emission is at 1370 ppmv. The data series is divided into calibrating and validating set which aims to

adjust the distribution of daily CORDEX time series data with the distribution of daily stations' observed time series using a transfer function (k).

The transformation can be formulated as below (Gudmundsson et al. 2012):

$$Observed = k(CORDEX) \qquad \textit{Equation 28}$$

If the series has a known distribution, the transformation is defined as:

$$Observed = F_O^{-1}(F_s(CORDEX)) \qquad \textit{Equation 29}$$

where F_s is the Cumulative Distribution Function (CDF) of CORDEX and F_O^{-1} is the inverse CDF of Observed.

The bias-corrected CORDEX data was divided into two parts; the historical phase (1979-2005) as well as the projection phase - the near future (2020-2050) and far future (2060-2090) under two Representative Concentration Pathways (RCP 4.5 and RCP 8.5). These data were used to generate future changes in climate extremes by applying the Mann-Kendall test to these future time series data.

6.3.4 Validation of RCM

To test the ability of the RCM output to reproduce the climate extreme characteristics, both the raw CORDEX output and the bias-corrected CORDEX output were used to analyse the temperature and precipitation indices over the basin between 1979 and 2005. The results were compared with the temperature and precipitation indices output from the homogenised station-controlled climate data series for the period from 1979 to 2005. Furthermore, results of the indices trends for both bias-corrected CORDEX and station-controlled outputs were analysed and compared spatially to verify the robustness of the bias-corrected CORDEX in reproducing the extreme indices.

6.4 Results

6.4.1 Temperature Indices

In Table 18, an overall positive trend is observed in warm day frequency, warm night frequency and warm spell duration while the cold night frequency has an overall negative trend over the entire stations for the observed historical period (1971-2017). The cool day frequency in most stations shows statistically significant negative slope with two stations having statistically significant positive slopes. The cool night frequency has statistically significant negative trends for all stations except Kano and Jos with a not-significant negative trend. Warm day and warm night frequencies have statistically significant positive trends for all stations. Warm spells trend increases significantly in all stations. The diurnal temperature range trend varies between -0.08 and 0.09 ^{0}C/year with most stations having significant negative trends which indicates an increase in both maximum and minimum temperature with the minimum temperature having a greater rate of warming. Figure 24 shows the spatial trends in station-controlled historical temperature indices between 1979 and 2005. The result

shows a decreasing trend of cool night frequency, cool day frequency and diurnal temperature range in most parts of the basin. The warm day frequency, warm night frequency and warm spells indicator, all having increasing trends (Figure 24). To test the ability of the bias-corrected CORDEX data to reproduce the spatial trends of the temperature indices, the spatial trend of the bias-corrected CORDEX data is analysed between 1979 and 2005 (Figure 25). The result shows a similar trend with the station-controlled historical temperature indices, however, with different magnitudes. For example, Figure 24a and Figure 25a show that the trend for cool day frequency for the validation period and bias-corrected CORDEX varies from -0.22 to 0.27 %/year and from 0.35 to 0.32 %/year respectively. The spatial patterns for both figures also show the negative trends (-0.35 to 0.00 %/year) being recorded at the north-eastern and south-western parts of the basin. In Table 19a, the number of stations with significant and non-significant trend in temperature indices is analysed. This shows that five, ten and seven stations observed significant negative trends in cool day frequency, cool night frequency and diurnal temperature range respectively while fourteen, twelve and fourteen stations observed significant positive trends in warm day frequency, warm night frequency and warm spells duration respectively.

6.4.2 Precipitation Indices

Unlike temperature, the variations in the trend of precipitation are dependent on local and regional characteristics. There is a mixed trend in the 5-day cumulate precipitation (Table 18) with significant increasing trend in five stations and significant decreasing trend in one station (Table 19b). There are increasing trends in the number of consecutive dry days except for Jos, Potiskum and Zinder with negative trends (Table 18; Table 19b). The consecutive wet days also have a decreasing trend in seven stations and an increasing trend in the other seven stations. There are mixed trends in the frequency of very wet days and extremely wet days. The spatial patterns of the trends validation period and bias-corrected CORDEX data between 1979 and 2005 (Figure 26 and Figure 27) show an increasing trend of maximum 5-days precipitation, consecutive dry days, very wet days and annual total precipitation while the consecutive wet days and extremely wet days had decreasing trends in most parts of the basin.

Table 20 presents the validation results of the bias-corrected CORDEX and raw CORDEX for the entire basin. The bias-corrected CORDEX performed better than the raw CORDEX in reproducing the trends of the climate indices for the station controlled historical period between 1979 and 2005. It was also able to capture the significant observed direction and magnitude in the indices.

Table 18: Mann-Kendall (Modified MK) test (at 5% significant level) for observed historical period (1971-2017). Bold values represent significant change in trend

	Temperature Indices						**Precipitation Indices**					
Stations	tx10p	tx90p	tn10p	tn90p	wsdi	dtr	rx5day	cdd	cwd	r95p	r99p	prctot
Bauchi	**-0.102**	**0.332**	**-0.310**	**0.389**	**0.446**	**-0.021**	**1.489**	0.176	-0.03	**8.283**	**5.223**	**9.908**
Diffa	**-0.318**	**0.916**	**-0.145**	**0.409**	**2.383**	**0.087**	0.028	**1.415**	**0.047**	-0.989	-0.607	**4.054**
Gombe	**-0.054**	**0.144**	**-0.433**	**0.599**	**0.286**	**-0.084**	**1.159**	0.336	-0.055	**4.006**	**2.215**	2.188
Goure	0.179	**0.595**	**-0.303**	**0.207**	**1.417**	-0.005	**0.846**	0.054	-0.025	**3.806**	0.814	**5.365**
Jos	**-0.116**	**0.646**	-0.043	**0.845**	**1.949**	0.008	**-0.634**	-0.036	-0.023	-1.847	-0.994	-0.394
Kaduna	-0.05	**0.36**	**-0.23**	**0.426**	**0.498**	**-0.009**	-0.047	0.629	-0.008	-0.352	0.046	-0.616
Kano	**-0.101**	**0.514**	-0.025	**0.39**	**1.237**	0.014	**2.952**	0.259	0.000	**9.656**	**3.833**	**19.394**
Katsina	**-0.117**	**0.542**	**-0.066**	**0.549**	**1.228**	0.003	-0.342	0.097	0.014	1.582	0.256	4.01
Magaria	0.127	**0.344**	**-0.491**	**0.644**	**0.631**	**-0.077**	-1.019	**1.23**	-0.025	-2.517	-1.534	**-8.281**
Maiduguri	-0.021	**0.118**	**-0.059**	**0.278**	**0.175**	**-0.015**	**1.296**	0.146	**0.038**	**2.848**	1.648	**6.122**
Maine-Soroa	-0.061	**0.359**	**-0.388**	**0.555**	**0.556**	**-0.029**	0.091	0.078	0.015	-0.227	-0.315	**2.413**
Nguru	**-0.094**	**0.381**	**-0.195**	**0.220**	**0.625**	0.002	-0.032	0.476	-0.018	-0.27	-0.345	1.507
Potiskum	**0.269**	**0.337**	**-0.335**	**0.016**	**0.858**	**-0.029**	0.579	**-1.566**	0.037	**4.148**	0.33	**13.584**
Zinder	**0.170**	**0.331**	**-0.098**	**0.100**	**0.594**	-0.004	-0.078	-0.386	0.004	-0.843	-0.489	4.524

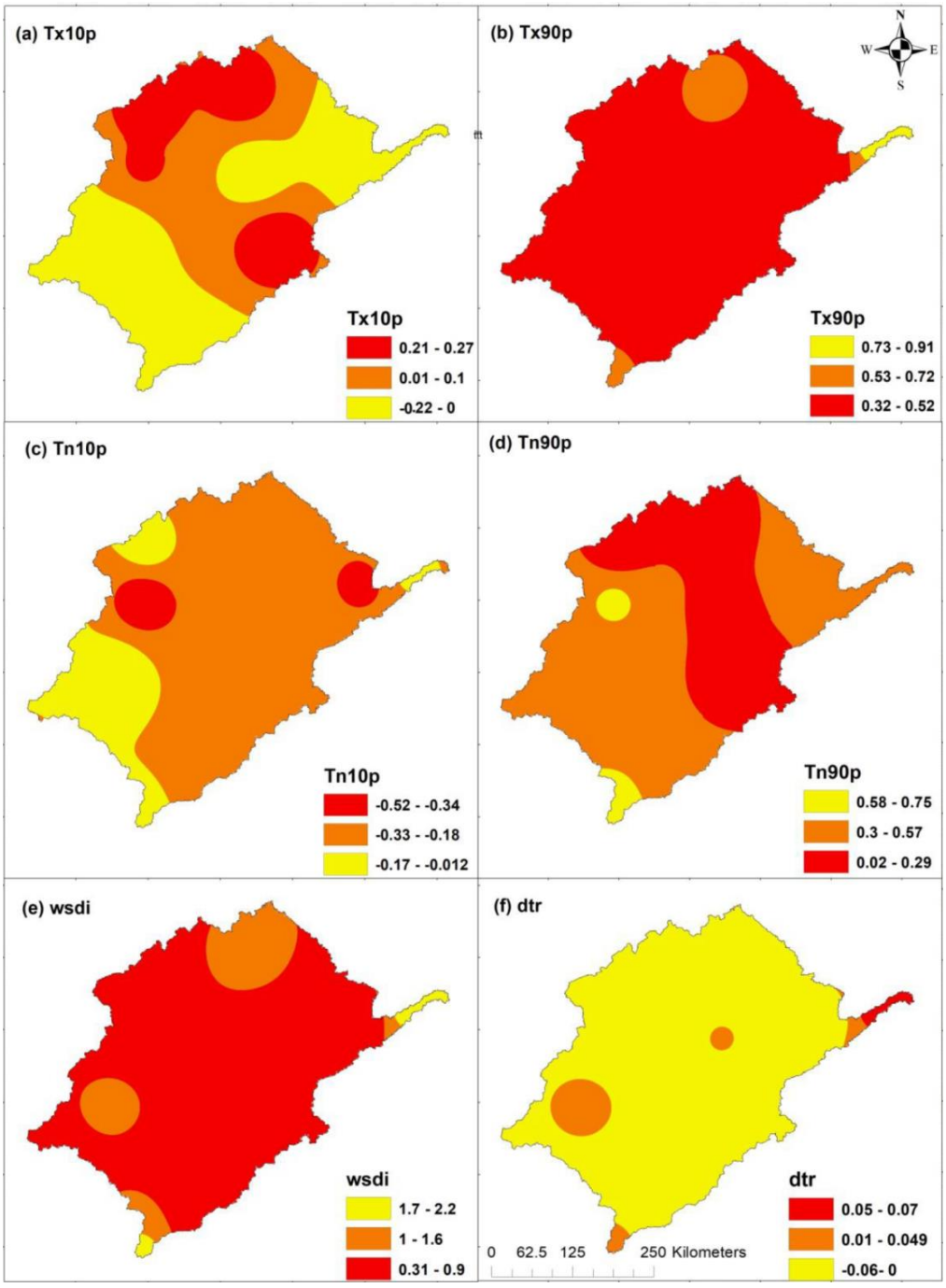

Figure 24: Spatial trends in temperature indices for the validation period between 1979 and 2005 of: (a) Cool day frequency (%/year), (b) Warm day frequency (%/year), (c) Cool night frequency (%/year), (d) Warm night frequency (%/year), (e) Warm spells duration

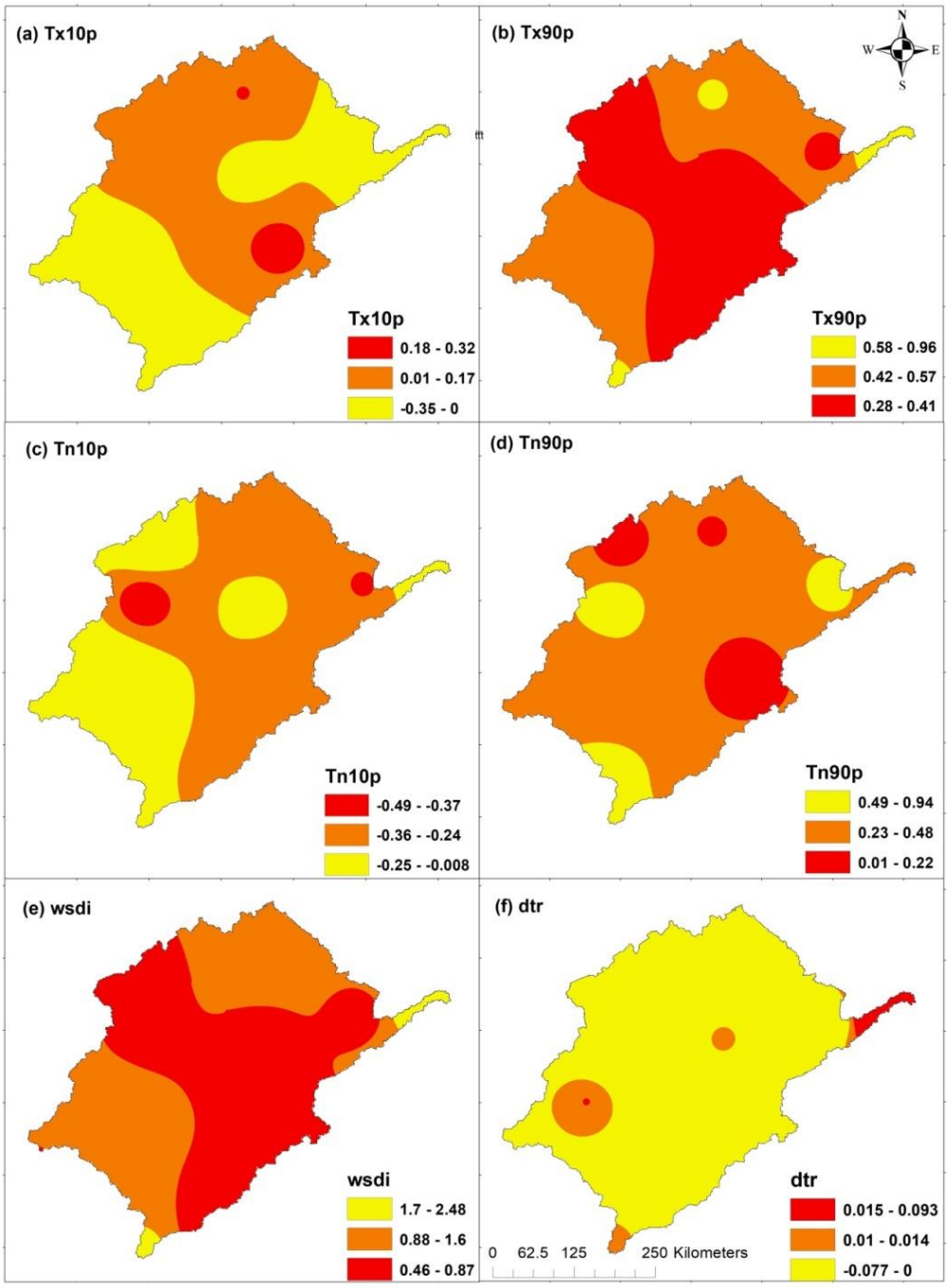

Figure 25: Spatial trends in temperature indices for bias corrected CORDEX historical period between 1979 and 2005 of: (a) Cool day frequency (%/year), (b) Warm day frequency (%/year), (c) Cool night frequency (%/year), (d) Warm night frequency (%/year), (e) Warm spells duration

Table 19: Number of stations with significant and non-significant trends for observed historical period (1971-2017)

(a) Temperature indices			(b) Precipitation indices		
Indices	**Significant positive Trend**	**Significant negative Trend**	**Indices**	**Significant positive Trend**	**Non-significant negative Trend**
tx10p	2	7	rx5day	5	3
tx90p	14	0	cdd	2	0
tn10p	0	10	cwd	2	4
tn90p	12	0	r95p	6	0
wsdi	14	0	r99p	3	0
dtr	1	7	prctot	7	2

Table 20: Basin-scale trend of indices for validation period from observed data, bias-corrected CORDEX and raw CORDEX between 1979 and 2005. Bold values represent significant change in trend

	Temperature Indices						**Precipitation Indices**					
	tx10p	**tx90p**	**tn10p**	**tn90p**	**wsdi**	**dtr**	**rx5day**	**cdd**	**cwd**	**r95p**	**r99p**	**prctot**
Validation period												
Slope	**-0.30**	**0.35**	**-0.72**	**0.40**	0.18	0.01	**0.60**	0.34	**0.85**	**4.94**	1.27	**11.00**
Bias-Corrected CORDEX												
Slope	**-0.32**	**0.21**	**-0.73**	**0.37**	0.26	0.01	**0.5**	0.42	**0.66**	**3.44**	1.02	**10.24**
SD	0.01	0.10	0.01	0.02	0.06	0.00	0.07	0.06	0.13	1.06	0.18	0.54
RMSE	0.02	0.14	0.01	0.03	0.08	0.00	0.10	0.08	0.19	1.50	0.25	0.76
MSE	0.00	0.02	0.00	0.00	0.01	0.00	0.01	0.01	0.04	2.25	0.06	0.58
PBIAS	6.7	-40.00	1.40	-7.50	44.40	0.00	-16.70	23.50	-22.40	-30.40	-19.70	-6.90
Raw CORDEX												
Slope	**-0.41**	**0.60**	**-0.74**	**1.13**	**1.25**	**-0.01**	-0.01	**1.77**	0.02	1.41	0.10	**1.67**
SD	0.08	0.18	0.02	0.51	0.76	0.01	0.43	1.01	0.58	2.49	0.83	6.60
RMSE	0.11	0.25	0.02	0.73	1.07	0.02	0.61	1.43	0.83	3.53	1.17	9.33
MSE	0.01	0.06	0.00	0.53	1.15	0.00	0.37	2.05	0.69	12.46	1.37	87.05
PBIAS	36.70	71.40	2.80	182.50	594.4	-200.00	-101.70	420.6	-97.60	-71.50	-92.10	-84.80

SD is the standard deviation, RMSE is the root mean square error and PBIAS is the percentage bias.

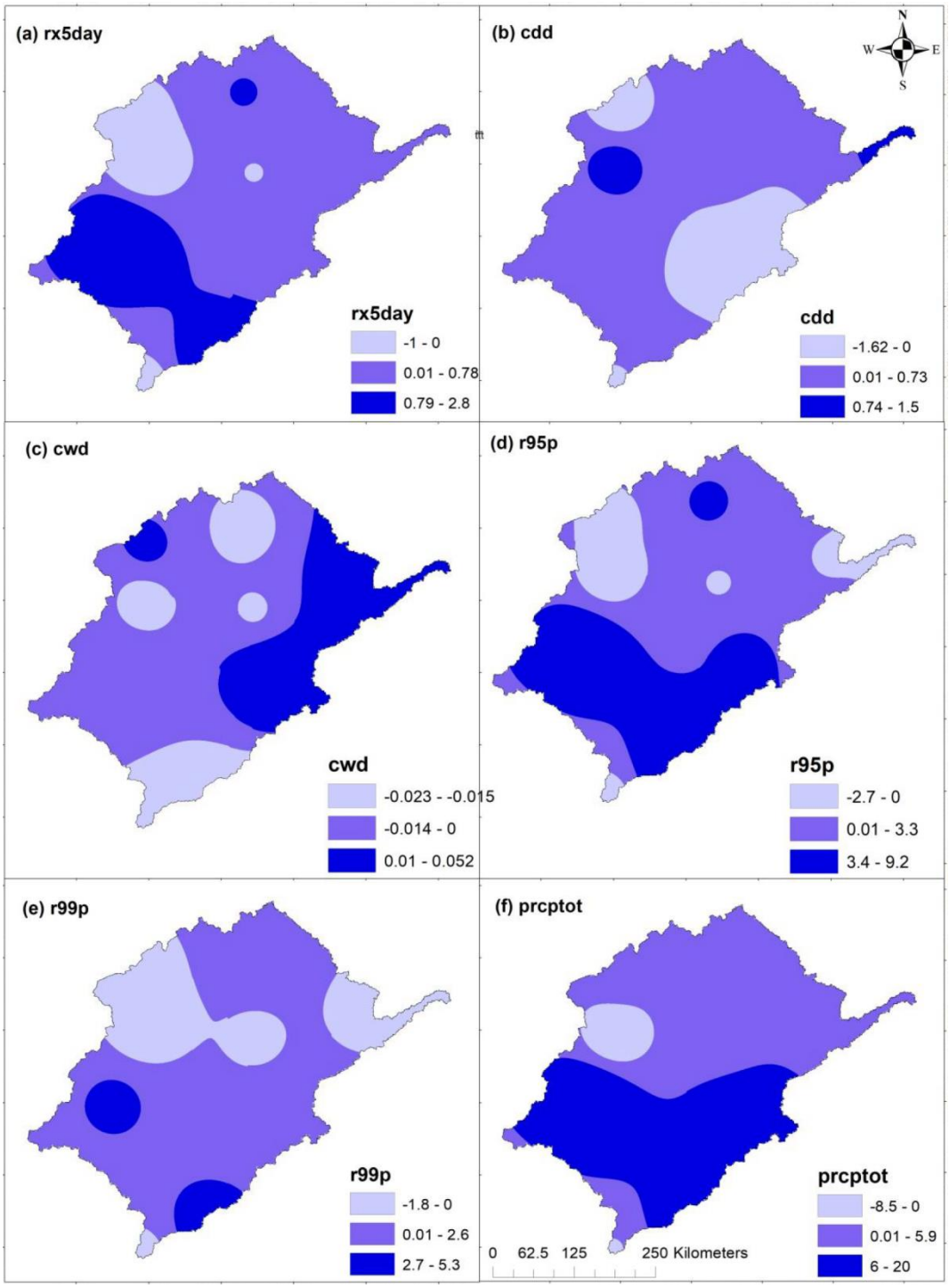

Figure 26: Spatial trends in precipitation indices for the validation period between 1979 and 2005 of: (a) Maximum 5-day precipitation (mm/year), (b) Consecutive dry days (days/year), (c) Consecutive wet days (days/year), (d) Very wet days (mm//year), (e) Extreme wet days (mm/year), and (f) Annual total precipitation (mm/year)

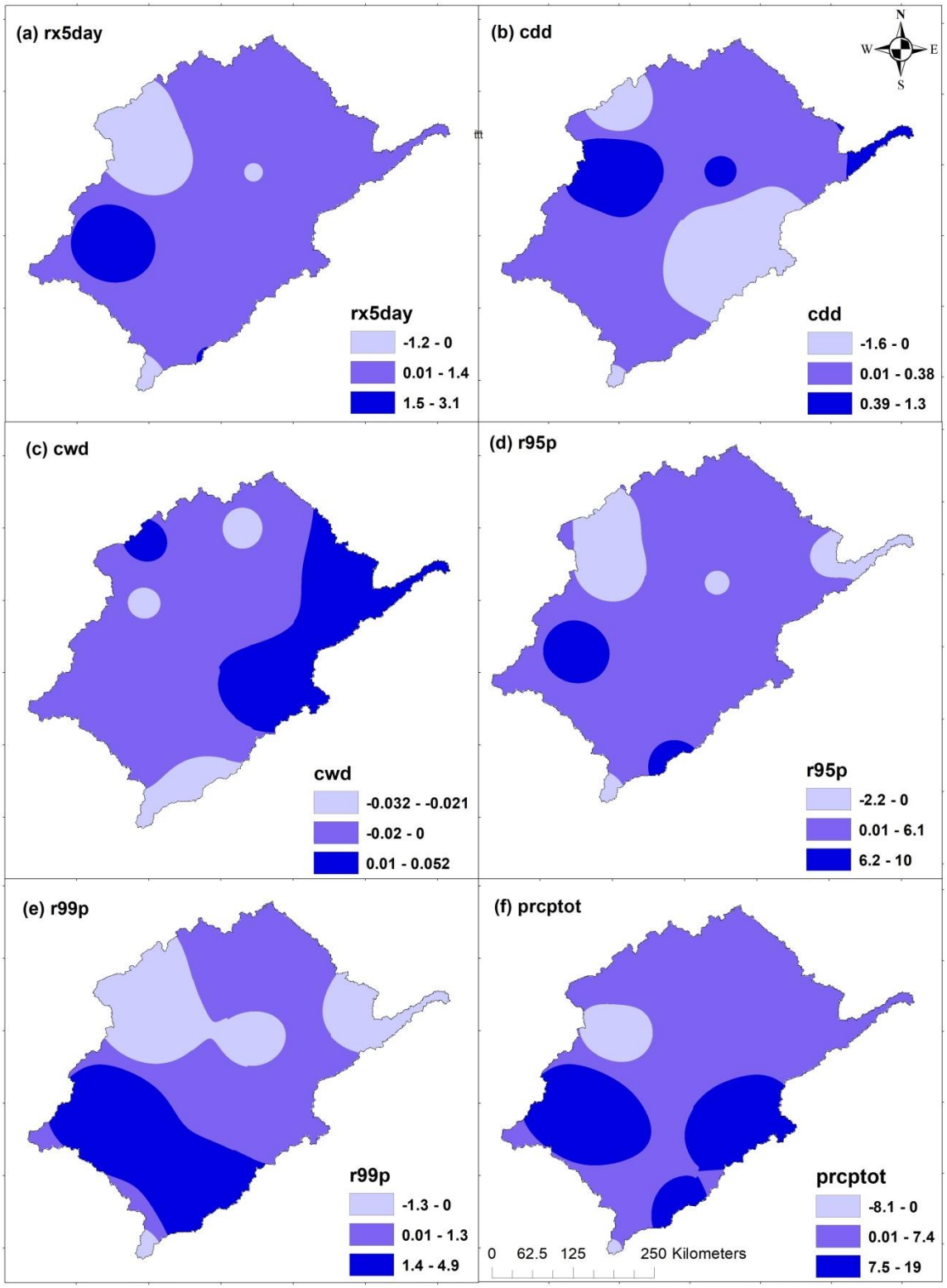

Figure 27: Spatial trends in precipitation indices for bias corrected CORDEX historical period between 1979 and 2005 of: (a) Maximum 5-day precipitation (mm/year), (b) Consecutive dry days (days/year), (c) Consecutive wet days (days/year), (d) Very wet days (mm/year), (e) Extreme wet days (mm/year), and (f) Annual total precipitation (mm/year)

6.4.3 Projection

Table 21 presents the results of climate indices over the basin under two representative concentration pathways (RCP4.5 and RCP 8.5) projections for global warming for two-time slices.

Temperature Indices Trend under RCP 4.5

For the near future (Table 21 a), the trends in cool day frequency, cool night frequency and diurnal temperature range are seen to be significantly decreasing in all stations except for three stations with non-significant negative trend. The trend in warm day frequency, warm night frequency and warm spells duration are seen to be significantly positive in all stations except for two stations with non-significant positive trend in warm night frequency. The spatial trend pattern (Figure 28) shows a decreasing trend of cool day frequency, cool night frequency and diurnal temperature range for the entire basin while the warm day frequency, warm night frequency and warm spell duration exhibited increasing trends. High magnitudes of negative trends in cold night frequency decreases towards the south-western part of the basin.

Table 21: Trend in the projection of temperature and precipitation indices.

a. Near future analysis at RCP4.5 (2020-2050)

	Temperature Indices						**Precipitation Indices**					
Stations	tx10p	tx90p	tn10p	tn90p	wsdi	dtr	rx5day	cdd	cwd	r95p	r99p	prctot
Bauchi	**-0.33**	**0.58**	**-0.53**	**0.76**	**0.87**	**-0.02**	**-3.04**	0.68	**-0.19**	**-8.07**	**-5.31**	**-23.79**
Diffa	**-0.23**	**0.60**	**-0.56**	**0.65**	**1.30**	**-0.03**	-0.25	-0.10	-0.08	-2.10	-1.12	-5.82
Gombe	**-0.23**	**0.54**	**-0.56**	**0.74**	**0.70**	**-0.05**	**-2.47**	0.65	**-0.18**	**-9.36**	**-5.47**	**-19.37**
Goure	**-0.25**	**0.56**	**-0.62**	**0.68**	**1.26**	**-0.04**	-0.81	0.07	-0.13	-1.52	-0.68	-4.48
Jos	**-0.24**	**0.30**	**-0.37**	**0.61**	0.26	**-0.04**	**-4.80**	0.77	**-1.19**	**-19.40**	**-5.90**	-39.02
Kaduna	**-0.20**	**0.25**	**-0.36**	**0.49**	0.19	**-0.04**	**-3.11**	0.61	**-0.23**	**-9.83**	**-5.14**	-27.67
Kano	**-0.24**	**0.36**	**-0.37**	**0.53**	**0.46**	-0.02	-2.01	0.10	**-0.16**	**-8.83**	0.13	-22.91
Katsina	**-0.31**	**0.57**	**-0.55**	**0.60**	**1.21**	**-0.02**	-1.77	0.66	**-0.09**	-0.80	-1.38	-9.34
Magaria	**-0.29**	**0.58**	**-0.57**	**0.62**	**1.35**	-0.02	-2.34	-0.25	**-0.25**	-4.19	-2.33	-13.91
Maiduguri	**-0.16**	**0.40**	**-0.50**	**0.68**	**0.48**	**-0.03**	**-2.96**	0.71	-0.09	**-4.79**	-1.54	-11.62
Maine-Soroa	**-0.25**	**0.57**	**-0.58**	**0.61**	**1.37**	**-0.02**	-0.18	0.61	0.00	-1.58	-0.91	-4.60
Nguru	**-0.21**	**0.36**	**-0.56**	**0.56**	**0.52**	**-0.02**	-1.10	0.85	-0.02	-2.07	-0.39	**-6.06**
Potiskum	**-0.27**	**0.61**	**-0.59**	**0.64**	**1.31**	**-0.02**	-0.54	0.62	**-0.31**	-1.28	0.62	**-8.63**
Zinder	**-0.28**	**0.58**	**-0.59**	**0.62**	**1.37**	-0.02	-0.94	-0.78	-0.15	-1.99	-0.60	-5.17

b. Far future analysis at RCP4.5 (2060-2090)

Stations	tx10p	tx90p	tn10p	tn90p	wsdi	dtr	rx5day	cdd	cwd	r95p	r99p	prctot
Bauchi	**-0.33**	0.23	**-0.49**	**0.45**	0.49	0.00	**2.62**	-0.04	0.15	**9.85**	2.01	**23.56**
Diffa	**-0.29**	**0.28**	**-0.41**	**0.39**	0.34	-0.01	0.95	1.30	**-0.11**	0.90	1.02	0.98
Gombe	**-0.44**	**0.37**	**-0.47**	**0.41**	0.26	0.00	2.28	0.00	**0.11**	**7.98**	0.85	**13.32**
Goure	**-0.34**	**0.28**	**-0.47**	**0.37**	0.45	**-0.03**	-0.89	**1.91**	-0.06	-1.58	-0.35	-1.67
Jos	**-0.50**	**0.39**	**-0.37**	**0.42**	**0.33**	**-0.03**	**3.28**	0.01	**0.57**	**11.72**	**4.96**	**23.33**
Kaduna	**-0.45**	**0.38**	**-0.43**	**0.46**	**0.39**	-0.01	1.25	0.05	0.11	4.65	2.65	**10.05**
Kano	**-0.50**	**0.43**	**-0.38**	**0.35**	0.24	**-0.04**	-1.10	-0.12	0.04	-1.93	-0.17	3.99
Katsina	**-0.35**	**0.27**	**-0.41**	**0.38**	0.47	**-0.03**	-0.62	0.84	-0.03	-2.44	-0.72	-0.56
Magaria	**-0.37**	**0.31**	**-0.42**	**0.35**	0.46	**-0.02**	-0.08	**1.98**	-0.09	0.30	-0.18	1.23
Maiduguri	**-0.31**	**0.30**	**-0.44**	**0.36**	0.19	**-0.05**	1.64	0.50	0.00	3.45	1.62	4.33
Maine-Soroa	**-0.33**	**0.28**	**-0.46**	**0.43**	0.46	**-0.03**	-0.13	0.15	-0.02	1.31	-0.33	0.63
Nguru	**-0.31**	**0.27**	**-0.42**	**0.40**	**0.35**	**-0.05**	0.76	**1.89**	-0.02	-0.89	0.04	1.93
Potiskum	**-0.35**	**0.28**	**-0.43**	**0.33**	0.45	0.00	0.53	0.95	**0.16**	2.52	1.64	3.51
Zinder	**-0.33**	**0.29**	**-0.45**	**0.42**	0.33	0.00	**-3.61**	**2.27**	-0.01	**-6.76**	**-5.07**	-6.24

c. Near future analysis at RCP8.5 (2020-2050)

Stations	tx10p	tx90p	tn10p	tn90p	Wsdi	dtr	rx5day	cdd	cwd	r95p	r99p	prctot
Bauchi	**-0.64**	**0.77**	**-0.91**	**1.12**	**1.04**	**-0.03**	-1.60	0.31	**-0.40**	**-8.69**	-0.67	**-28.17**
Diffa	**-0.53**	**0.77**	**-0.87**	**0.98**	**1.51**	**-0.03**	-1.94	-0.97	-0.08	-6.67	**-3.02**	**-11.46**
Gombe	**-0.45**	**0.80**	**-0.79**	**1.24**	**1.01**	**-0.04**	-2.71	0.39	**-0.22**	-6.74	-3.30	**-22.67**
Goure	**-0.55**	**0.76**	**-0.87**	**0.98**	**1.36**	**-0.05**	-1.54	-1.22	-0.20	**-5.57**	-0.79	**-9.64**
Jos	**-0.53**	**0.47**	**-0.68**	**0.93**	**0.39**	**-0.06**	**-2.78**	0.50	-0.34	**-9.75**	**-5.27**	**-36.46**
Kaduna	**-0.46**	**0.45**	**-0.62**	**0.99**	**0.45**	**-0.06**	-0.97	0.63	-0.21	**-7.19**	-3.24	**-24.92**
Kano	**-0.56**	**0.66**	**-0.53**	**0.86**	**1.16**	**-0.03**	-1.93	0.66	-0.03	-5.32	**-5.78**	**-27.37**
Katsina	**-0.57**	**0.81**	**-0.80**	**0.96**	**1.51**	**-0.03**	**-2.34**	-0.17	-0.08	**-5.69**	-2.04	**-14.66**
Magaria	**-0.56**	**0.81**	**-0.81**	**0.93**	**1.59**	**-0.02**	-1.93	-1.13	**-0.34**	**-8.00**	-2.13	**-19.72**
Maiduguri	**-0.45**	**0.56**	**-0.86**	**1.00**	**0.74**	**-0.05**	-1.87	0.20	-0.03	**-7.18**	**-3.08**	**-15.67**
Maine-Soroa	**-0.57**	**0.75**	**-0.85**	**0.96**	**1.32**	**-0.03**	-1.00	0.92	-0.04	-1.58	-1.39	**-9.58**
Nguru	**-0.46**	**0.59**	**-0.84**	**0.93**	**0.89**	**-0.04**	-1.43	0.89	-0.07	-4.10	-1.95	**-12.65**
Potiskum	**-0.60**	**0.81**	**-0.86**	**1.01**	**1.34**	**-0.02**	**-3.44**	0.49	**-0.29**	**-8.56**	**-6.26**	**-18.87**
Zinder	**-0.53**	**0.79**	**-0.82**	**0.93**	**1.32**	-0.02	-2.65	-1.17	0.00	**-9.16**	-2.65	**-17.10**

d. Far future analysis at RCP8.5 (2060-2090)

Stations	tx10p	tx90p	tn10p	tn90p	wsdi	dtr	rx5day	cdd	cwd	r95p	r99p	prctot
Bauchi	**-0.81**	**0.87**	**-1.36**	**1.28**	**1.44**	0.00	**3.89**	0.61	**0.15**	**14.05**	**5.18**	**34.01**
Diffa	**-0.70**	**0.81**	**-1.16**	**1.15**	**1.58**	-0.01	1.23	1.85	0.11	4.99	1.69	**12.64**
Gombe	**-0.92**	**1.10**	**-1.31**	**1.34**	**1.62**	**-0.02**	**5.40**	0.61	**0.23**	**17.95**	**7.28**	**36.04**
Goure	**-0.70**	**0.79**	**-1.14**	**1.18**	**1.65**	**-0.02**	1.07	**1.93**	-0.06	**3.52**	1.67	**9.38**
Jos	**-0.75**	**1.12**	**-1.19**	**1.30**	**1.35**	**-0.02**	**4.27**	0.54	**0.87**	**20.76**	**7.56**	**48.35**
Kaduna	**-0.69**	**1.07**	**-1.12**	**1.34**	**1.13**	**-0.03**	**2.56**	0.65	0.14	11.07	3.93	**28.84**
Kano	**-0.80**	**1.05**	**-1.18**	**1.10**	**1.42**	**-0.03**	1.64	0.50	0.00	3.45	1.62	4.33
Katsina	**-0.77**	**0.80**	**-1.26**	**1.20**	**1.53**	**-0.03**	2.52	0.94	**0.23**	**5.41**	**2.69**	**18.06**
Magaria	**-0.87**	**0.83**	**-1.25**	**1.16**	**1.76**	**-0.02**	**4.07**	**2.22**	**0.32**	**12.71**	5.79	**27.18**
Maiduguri	**-0.66**	**0.88**	**-1.24**	**1.17**	**1.19**	**-0.05**	**3.46**	0.11	**0.14**	**8.82**	**2.92**	**17.43**
Maine-Soroa	**-0.71**	**0.79**	**-1.18**	**1.13**	**1.63**	**-0.03**	**2.07**	0.50	0.04	**5.44**	**2.09**	**13.87**
Nguru	**-0.63**	**0.72**	**-1.20**	**1.12**	**1.21**	**-0.04**	1.75	0.53	0.05	**6.97**	**4.16**	**14.99**
Potiskum	**-0.77**	**0.76**	**-1.27**	**1.16**	**1.53**	**0.02**	**4.06**	0.59	0.14	**14.69**	**4.96**	**26.08**
Zinder	**-0.69**	**0.78**	**-1.19**	**1.13**	**1.59**	**0.02**	2.92	**3.10**	**0.33**	**8.96**	4.65	**21.24**

Bold values represent significant changes

The consistency rate of the eight bias corrected models and the ensemble mean (nine models altogether) shows 100% consistent rate for all temperature indices except for diurnal temperature range with model consistency between 78% and 100%. For far future (Table 21 b), cool day frequency and cool night frequency still exhibits significant negative trend in for all stations in the basin. However, diurnal temperature range both significant and non-significant negative trend although with some stations like Bauchi, Gombe, Potiskum and Zinder having no trend. Positive trend in warm day and warm night frequencies is evident in all stations. The spatial trends (Figure 29) reveals that the highest negative trend in cool night frequency (-0.44 to -0.48%/year) while the lowest negative trend in cool night frequency (-0.37 to -0.41%/year) is also seen at the south-western side of the basin. The highest positive trend for warm night frequency (0.41 to 0.45% per year) is also seen at the southern and north-eastern part of the basin. The warm spell duration possesses high trend values (0.42 to 0.49 days/year) in most parts of the basin. This warm spell duration trend gradually decreases towards the south-western part of the basin. The model consistency varies between 78% and 100% for diurnal temperature range while it maintains 100% consistent rate for other temperature indices.

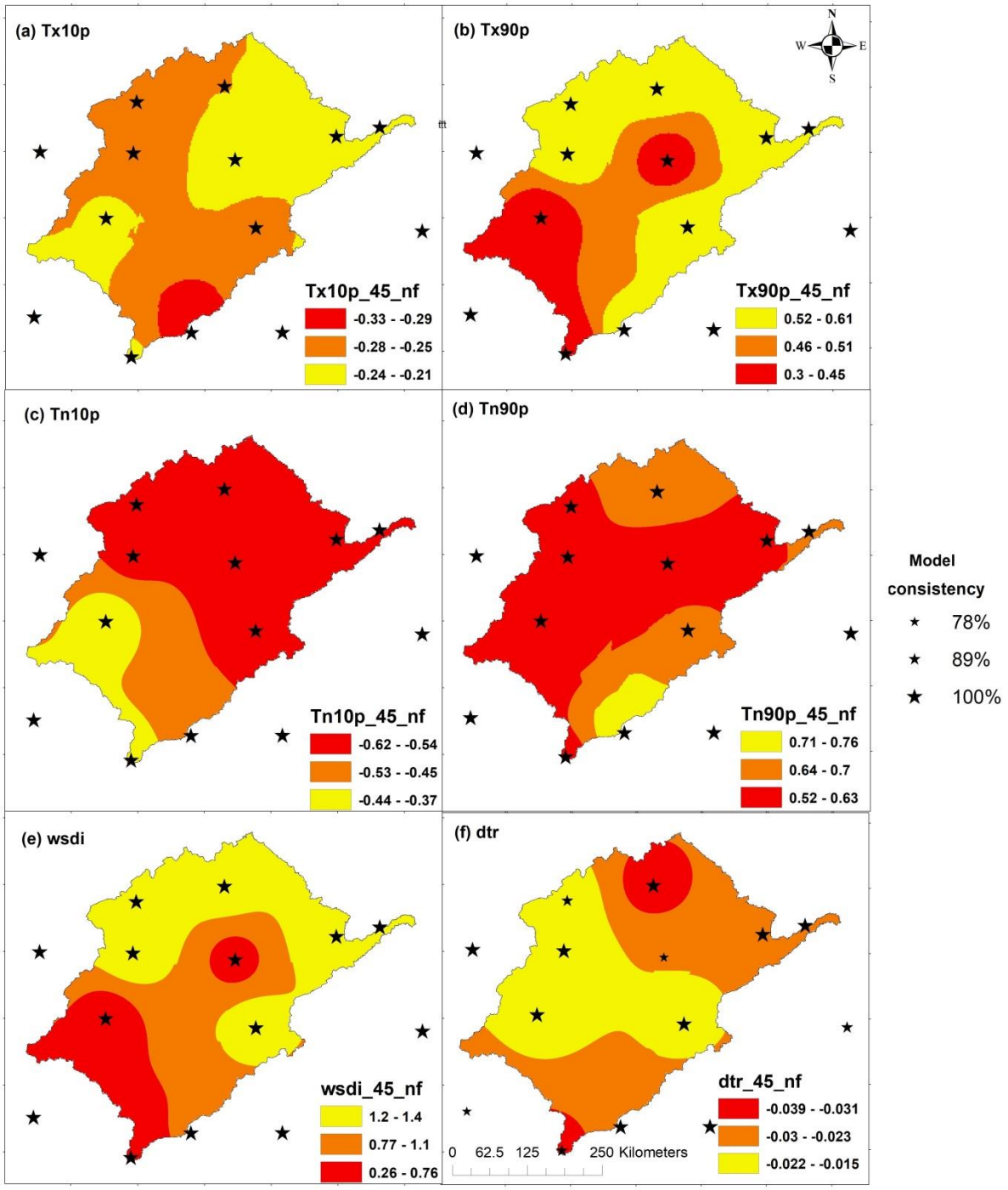

Figure 28: Spatial trends in temperature indices for the near future (202-2050) under RCP 4.5 (a) Cool day frequency (%/year), (b) Warm day frequency (%/year), (c) Cool night frequency (%/year), (d) Warm night frequency (%/year),(e) Warm spells duration (days/year), and (f) Diurnal temperature range (^{0}C/year).

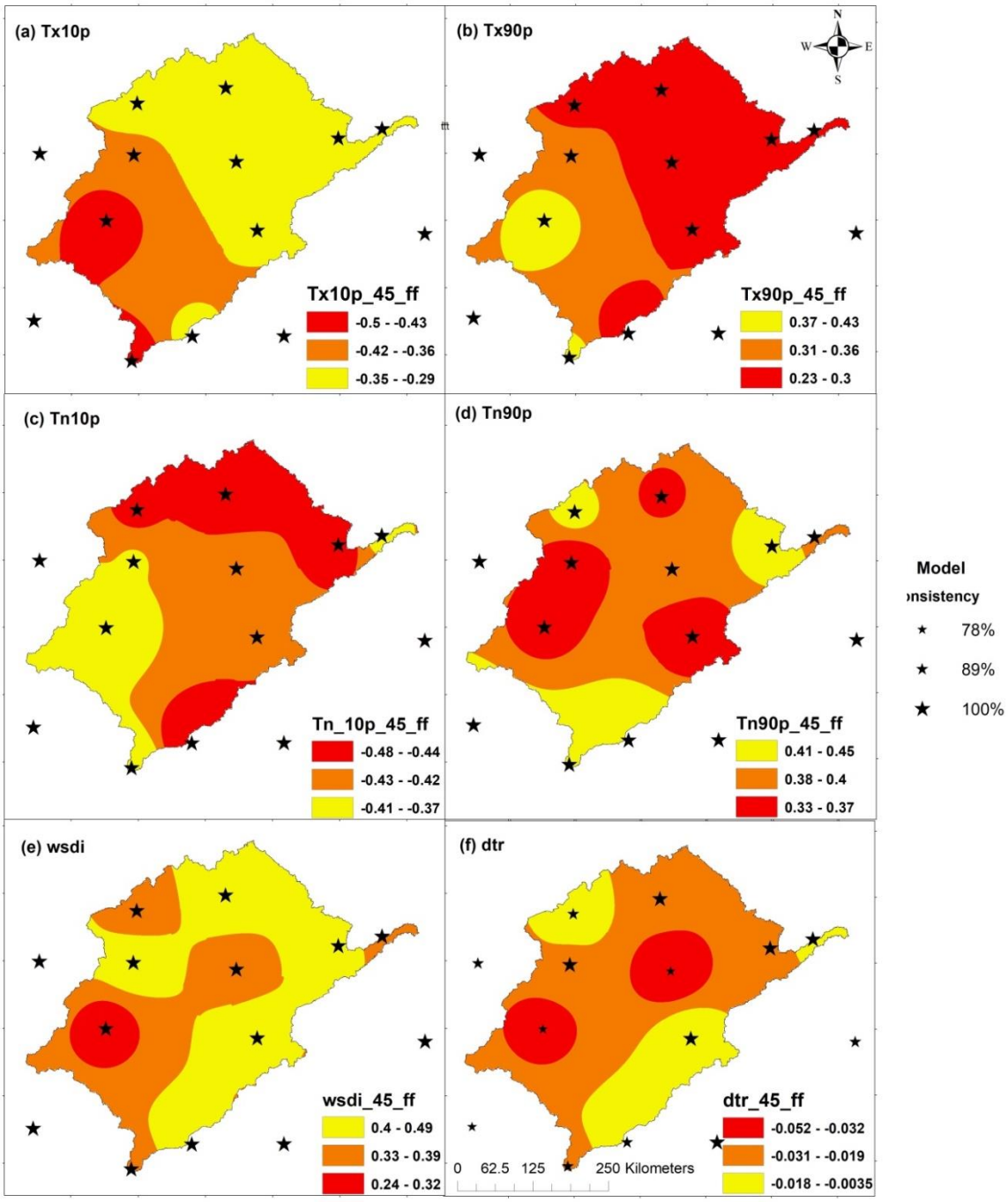

Figure 29: Spatial trends in temperature indices for the far future (2060-2090) under RCP 4.5 (a) Cool day frequency (%/year), (b) Warm day frequency (%/year), (c) Cool night frequency (%/year), (d) Warm night frequency (%/year),(e) Warm spells duration (days/year), and (f) Diurnal temperature range (^{0}C/year)

Temperature Indices Trend under RCP 8.5

Results of near future analysis under RCP 8.5 (Table 21 c) show significant negative trends in cool night frequency, cool day frequency and diurnal temperature range for all stations while all stations exhibited significant increasing trend in warm day frequency, warm night frequency and warm spell duration.

The spatial trend pattern (Figure 30) shows that highest values of negative trend in cool day frequency (-0.56 to -0.64%/year) is recorded in the south-western sector of the basin while the highest values for negative trend in cool night frequency (-0.71 to -0.81%/year) is seen in most parts of the basin. High positive trend in warm spell duration (0.88 to 1.60) is seen in most parts of the basin. The model consistency varies between 89% and 100% for diurnal temperature range while it retains 100% consistent rate for other temperature indices.

For far future analysis (Table 21 d), there is a negative trend in the diurnal temperature ranges and cool night and cool day frequencies. There is a positive trend in warm spell duration and warm day and warm night frequencies. The spatial pattern of the trend (Figure 31) shows that negative trend in cold day and cold night frequencies increases towards the southern part of the basin while the warm day and warm night frequencies positive trends also increase towards the southern part. The warm spell duration increases towards the northern part of the basin. The magnitude of trend analysis comparison of the historical extremes with RCP 4.5 both for near and far future shows an increasing magnitude of the temperature extreme events.

Precipitation Indices Trend under RCP 4.5

All precipitation indices except consecutive dry days are observed to have negative trends in the near future with the highest negative trend of -39.02 mm/year in annual total precipitation (Table *21* a). The negative trends in annual total precipitation are statistically significant in Bauchi, Gombe, Nguru and Potiskum stations. Negative trends are observed in maximum 5-days precipitation, consecutive wet days and annual total precipitation for near future time slice. However, some of these negative trends are not statistically significant. The consecutive dry days had all positive trends except for the negative trends at Diffa, Magaria and Zinder stations. The spatial trend (Figure 32) also suggested an overall negative trend in maximum 5-days precipitation, consecutive wet days, wet days, very wet days and annual total precipitation across the basin. However, the pattern of trend differs across the basin. For example, negative trend in maximum 5-days precipitation, consecutive wet days, very wet days, extremely wet days and annual total precipitation increase towards the south-west, while the negative trend in consecutive dry days increases towards the north-western part of the basin. The model consistency varies between 78% and 100%. For far future time slice, all trends turned positive for annual total precipitation, having the highest positive trend of 23.33 mm/year except for Goure Katsina and Zinder with negative trends of -1.67, -0.56 and -6.24 mm/year respectively. Nevertheless, other precipitation indices have mixed positive and negative trends for the stations. The spatial trend (Figure 33) shows that negative trends in precipitation indices are predominantly located at the north-western part of the basin except for consecutive dry days. The model consistency varies between 56% and 100%. The comparison of magnitude of trend for the historical and RCP 4.5 extremes shows a mixed pattern. For example, maximum 5-days precipitation, consecutive wet days, extremely wet days and annual total precipitation all had negative magnitudes while consecutive dry days had mixed

magnitude for all stations while very wet days had a negative magnitude except for Zinder station under RCP 4.5 for near future. For far future, there was generally a mixed magnitude of trend for all precipitation indices. Overall, there is a drying trend in the basin.

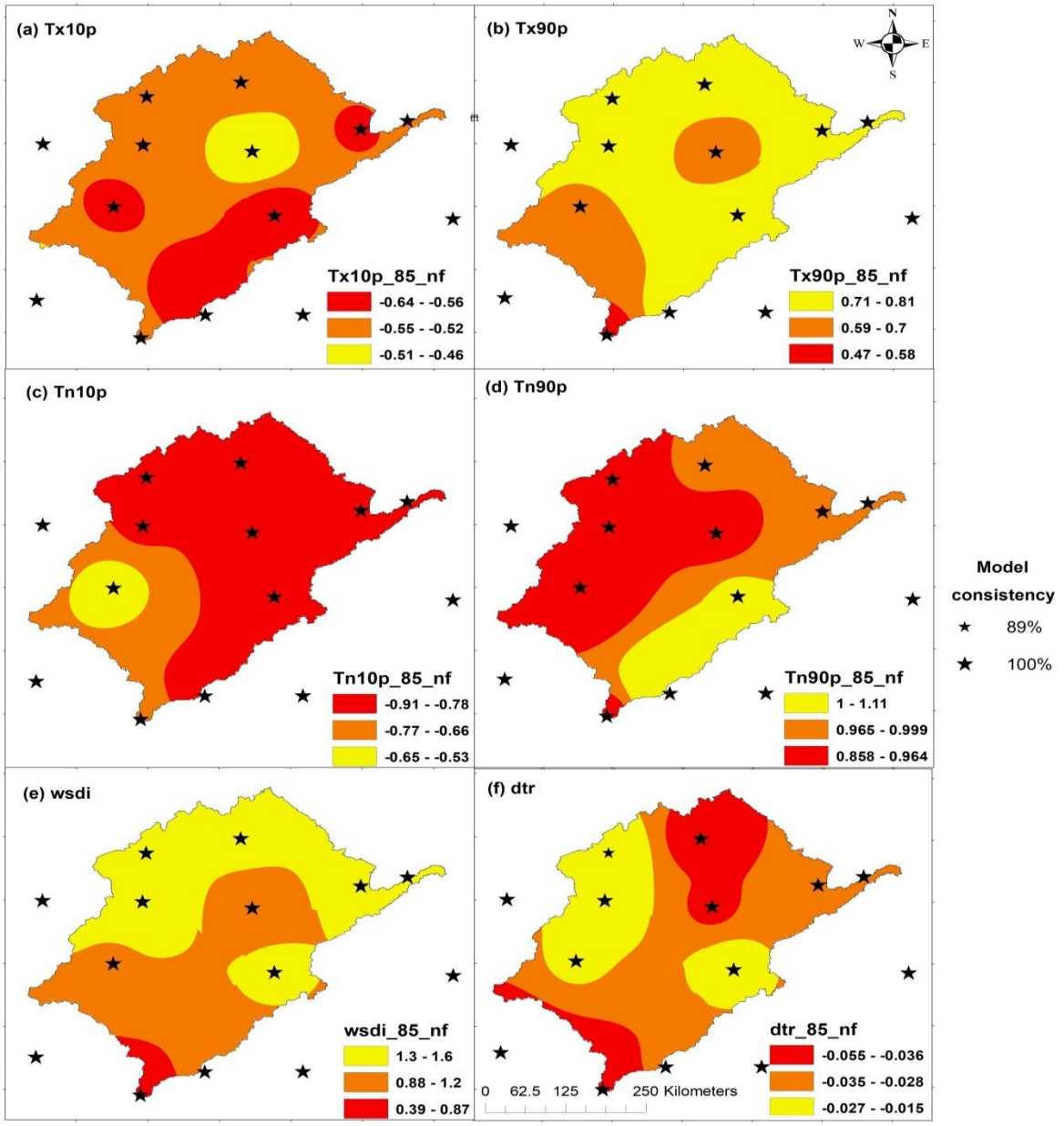

Figure 30: Spatial trends in temperature indices for the near future (2020-2050) under RCP 8.5 (a) Cool day frequency (%/year), (b) Warm day frequency (%/year), (c) Cool night frequency (%/year), (d) Warm night frequency (%/year),(e) Warm spells duration (days/year), and (f) Diurnal temperature range (^{0}C/year).

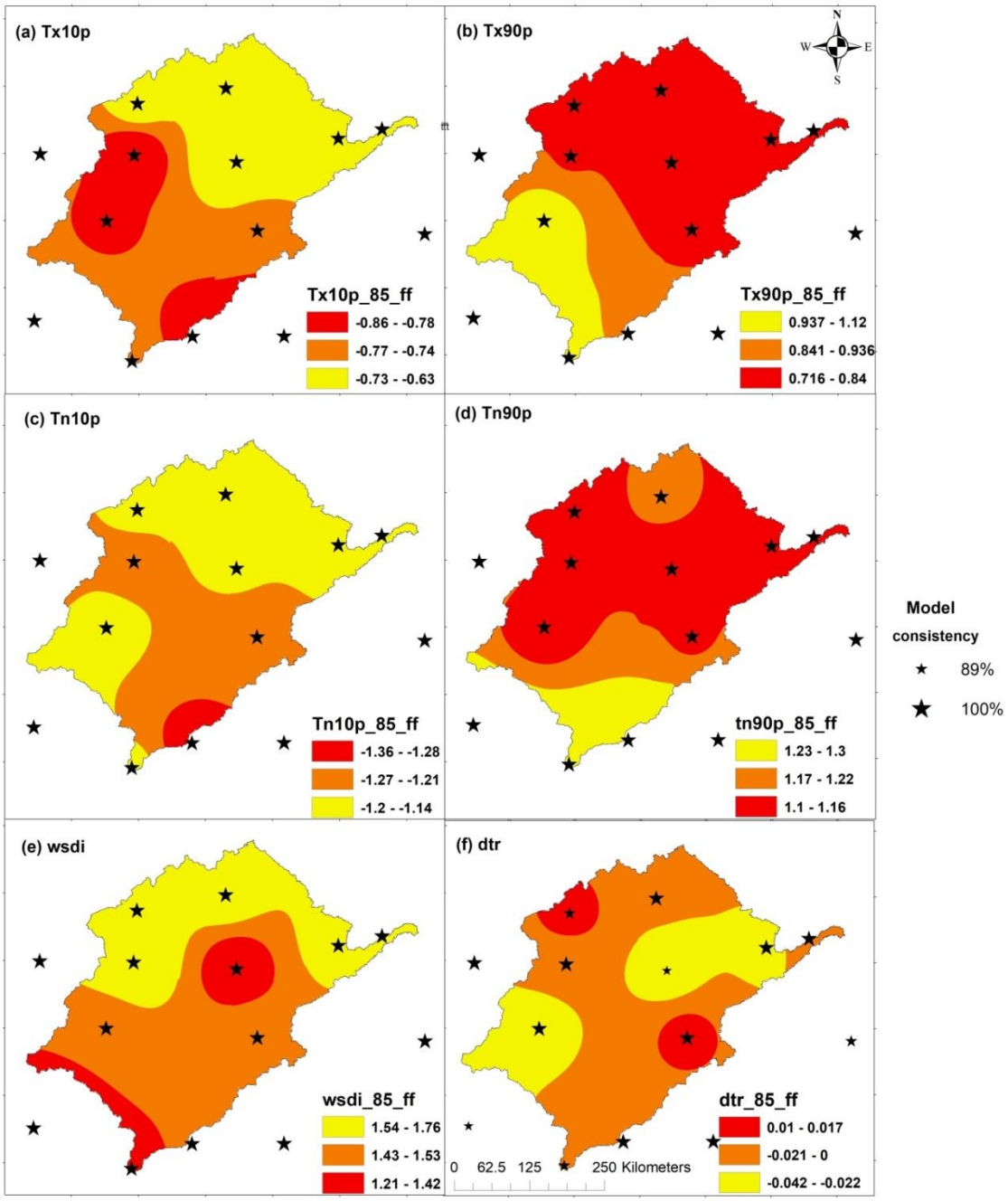

Figure 31: Spatial trends in temperature indices for the far future (2060-2090) under RCP 8.5 (a) Cool day frequency (%/year), (b) Warm day frequency (%/year), (c) Cool night frequency (%/year), (d) Warm night frequency (%/year),(e) Warm spells duration (days/year), and (f) Diurnal temperature range (^{0}C/year).

Precipitation Indices Trend under RCP 8.5

Under RCP 8.5 for near future (Table 21 c), all precipitation indices show negative trends except for the consecutive dry days with some positive trends. The highest negative trend of -36.46 mm/year was recorded in annual total precipitation. The negative trends in annual total precipitation are significant in all stations within the basin. Maximum 5-days precipitation, consecutive wet days, very

wet days and extremely wet days all have negative trends for every station, although with some degree of significance and non-significance. The spatial trends (Figure 34) in annual total precipitation, very wet days, extremely wet days and consecutive wet days all decreases towards the southern part of the basin. For far future (Table 21 d), all precipitation indices trend is positive except for consecutive wet days with a not-significant negative trend at Goure. The highest positive trend (48.35) is reported for annual total precipitation at Jos. There are mixed occurrences of both significant and not-significant trends for this time slice. The spatial trend (Figure 35) shows that all precipitation indices show increment towards the southern part of the basin except for consecutive dry days which shows an increment towards the north-western part of the basin.

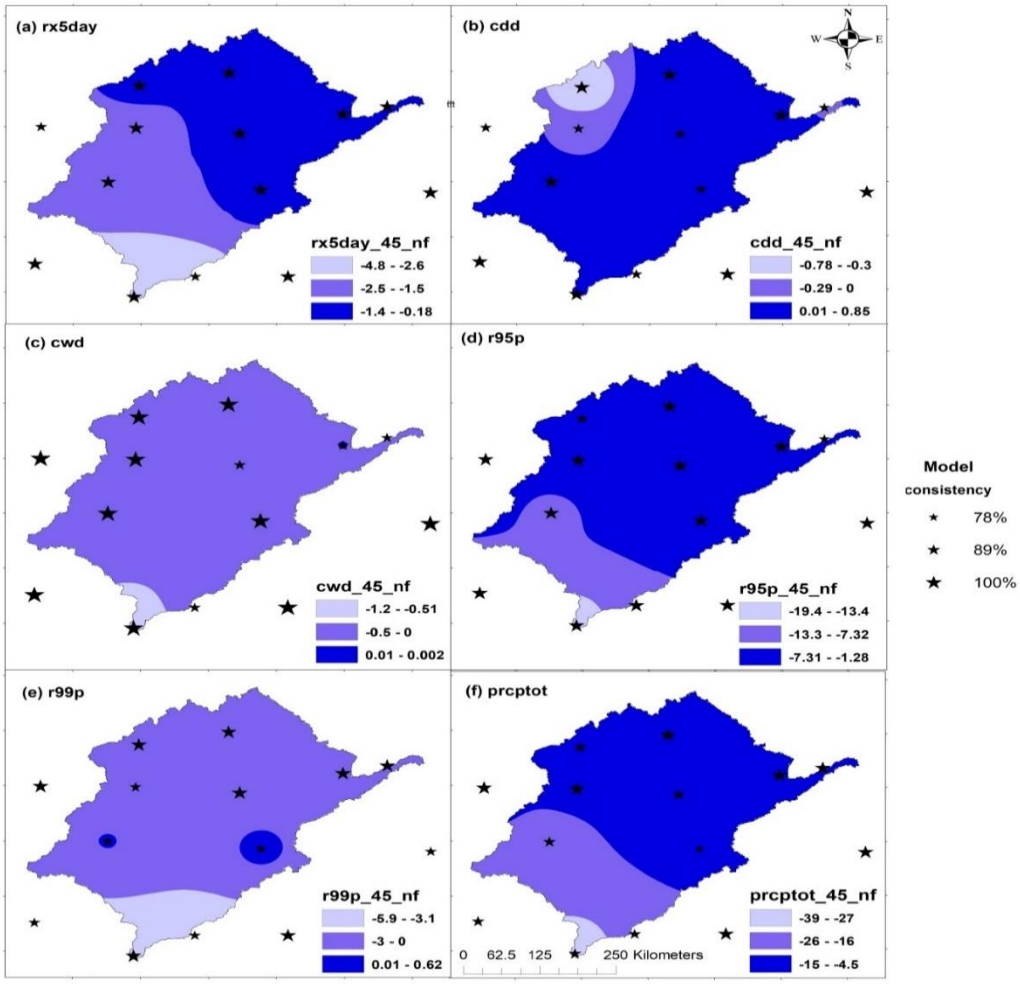

Figure 32: Spatial trends in precipitation indices for the near future (2020-2050) under RCP 4.5 (a) Maximum 5-day precipitation (mm/year), (b) Consecutive dry days (days/year), (c) Consecutive wet days (days/year), (d) Very wet days (mm/year),(e) Extremely wet days (mm/year), and (f) Annual total precipitation (mm/year)

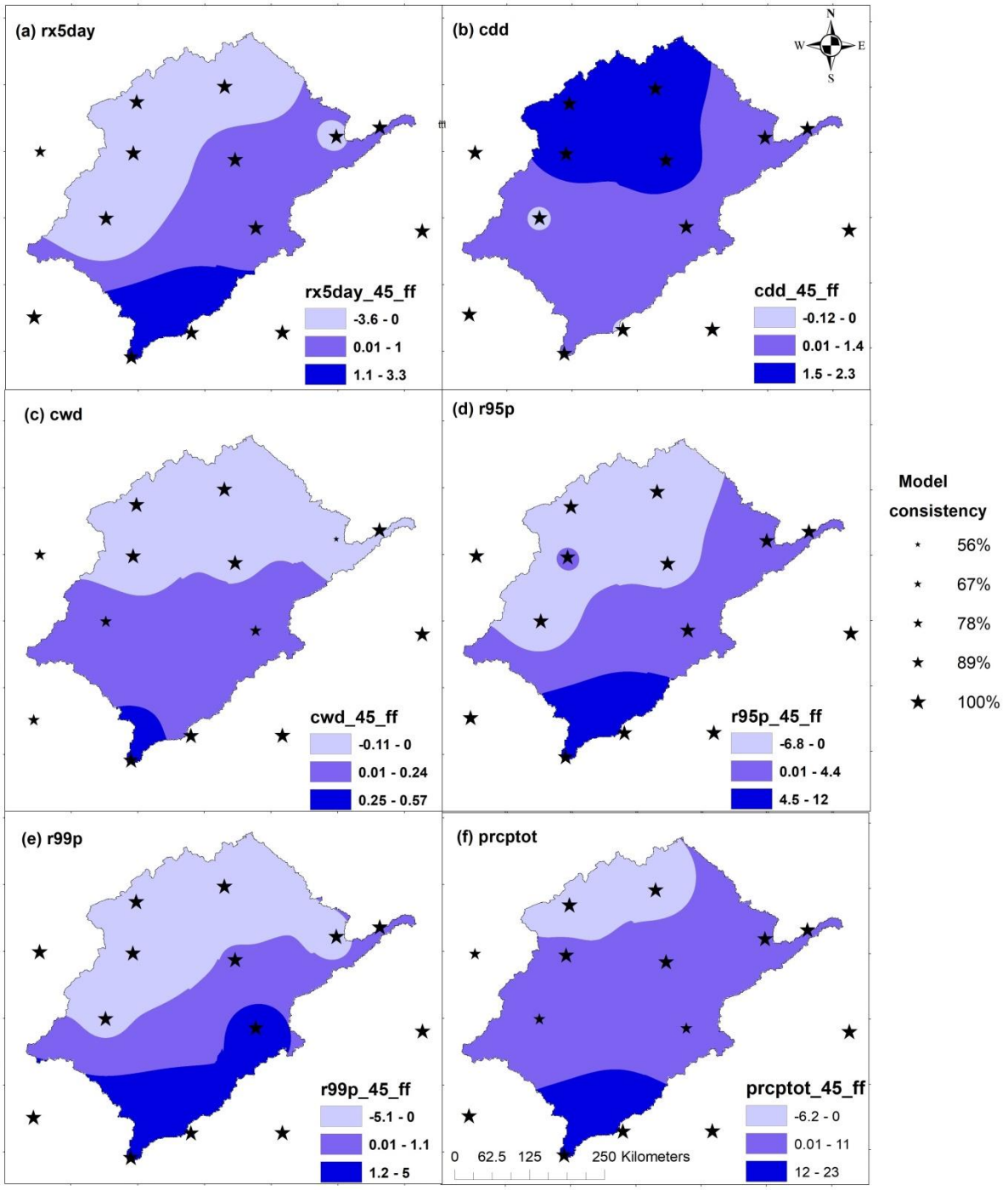

Figure 33: Spatial trends in precipitation indices for the far future (2060-2090) under RCP 4.5 (a) Maximum 5-day precipitation (mm/year), (b) Consecutive dry days (days/year), (c) Consecutive wet days (days/year), (d) Very wet days (mm/year),(e) Extremely wet days (mm/year), and (f) Annual total precipitation (mm/year).

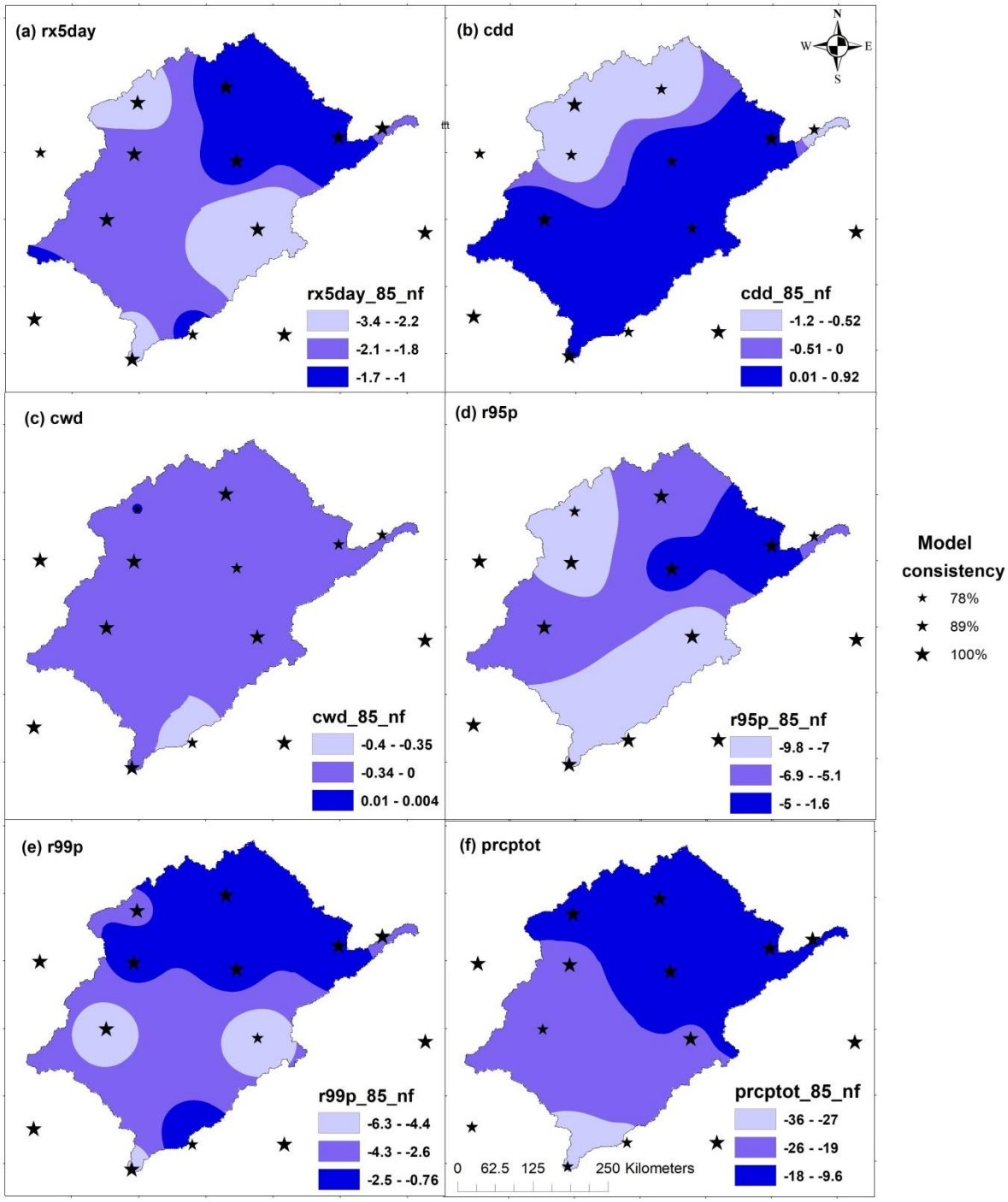

Figure 34: Spatial trends in precipitation indices for the near future (2020-2050) under RCP 8.5 (a) Maximum 5-day precipitation (mm/year), (b) Consecutive dry days (days/year), (c) Consecutive wet days (days/year), (d) Very wet days (mm/year),(e) Extremely wet days (mm/year), and (f) Annual total precipitation (mm/year).

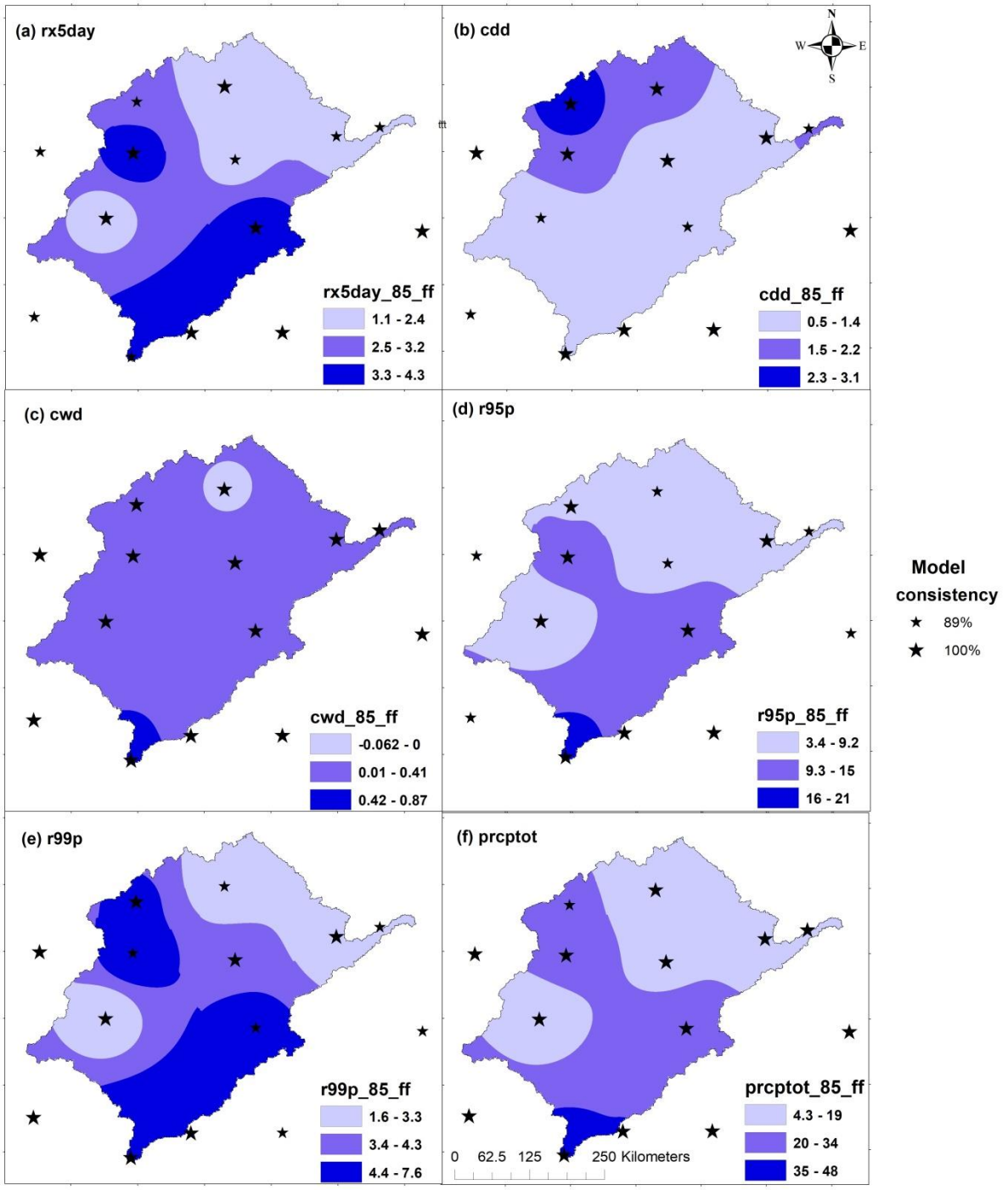

Figure 35: Spatial trends in precipitation indices for the far future (2060-2090) under RCP 8.5 (a) Maximum 5-day precipitation (mm/year), (b) Consecutive dry days (days/year), (c) Consecutive wet days (days/year), (d) Very wet days (mm/year),(e) Extremely wet days (mm/year), and (f) Annual total precipitation (mm/year).

The magnitude of trend comparison between historical extremes and RCP 8.5 shows a mixed change in the magnitude of the precipitation extreme events. For near future, all precipitation indices had negative magnitudes except consecutive dry days with a mixed magnitude. For far future scenarios, maximum 5-days precipitation had negative trend except for Kano, consecutive dry days had positive

magnitude except for Maiduguri, consecutive wet days had positive magnitude except for Goure, very wet days had positive magnitude except for Goure and Kano, extremely wet days had positive magnitude except for Bauchi and Kano and annual total precipitation had positive magnitude except for Kano.

In general, there is no global pattern in of precipitation extreme trends between RCP 4.5 and 8.5 because the pattern of magnitude and trend depends on the location of the station. However, most of the indices had an increasing magnitude from RCP 4.5 to 8.5.

Figure 36 and Figure 37 further quantify the uncertainties associated with the model projection. For example, in Figure 36, all models seem to have similar range for extremely wet days for most part of the projection period for Maine station while this is not same for diurnal temperature range. Figures for other stations are presented in the (Adeyeri 2019).

6.5 Discussion

In this study, climate extreme indices in the Komadougu-Yobe basin, Lake Chad region were analysed. To validate the ability of the ensemble climate model to capture present-day extremes and their trends, we analysed the results from the station controlled historical period, the raw CORDEX and bias-corrected CORDEX outputs. The results show a similar pattern of extreme climate indices over the basin. However, the raw CORDEX overestimated the trend of most indices while the significant magnitude was not captured. The bias-corrected CORDEX performed better as it was able to capture both pattern and significant magnitude in trends.

The temperature indices considered show a significant warming trend in the basin; hence, hypothesis two is confirmed. This result confounds with previous studies in other regions of Africa. For example, (Mouhamed et al. 2013) reported warming trend throughout the Sahel between 1960 and 2010. (Abatan et al. 2018b) also reported a warming trend over Nigeria between 1971 and 2012 with warming most pronounced in southern Nigeria. Our results in this study are consistent with these findings. However, (Abatan et al. 2018a) observed most significant warming trends in some stations located in the coastal areas. Though, there was no significant difference in the coastal and inland stations in our study area which may be attributed to the reduced ocean-land temperature gradient that characterized the monsoon region as reported by (Mouhamed et al. 2013).

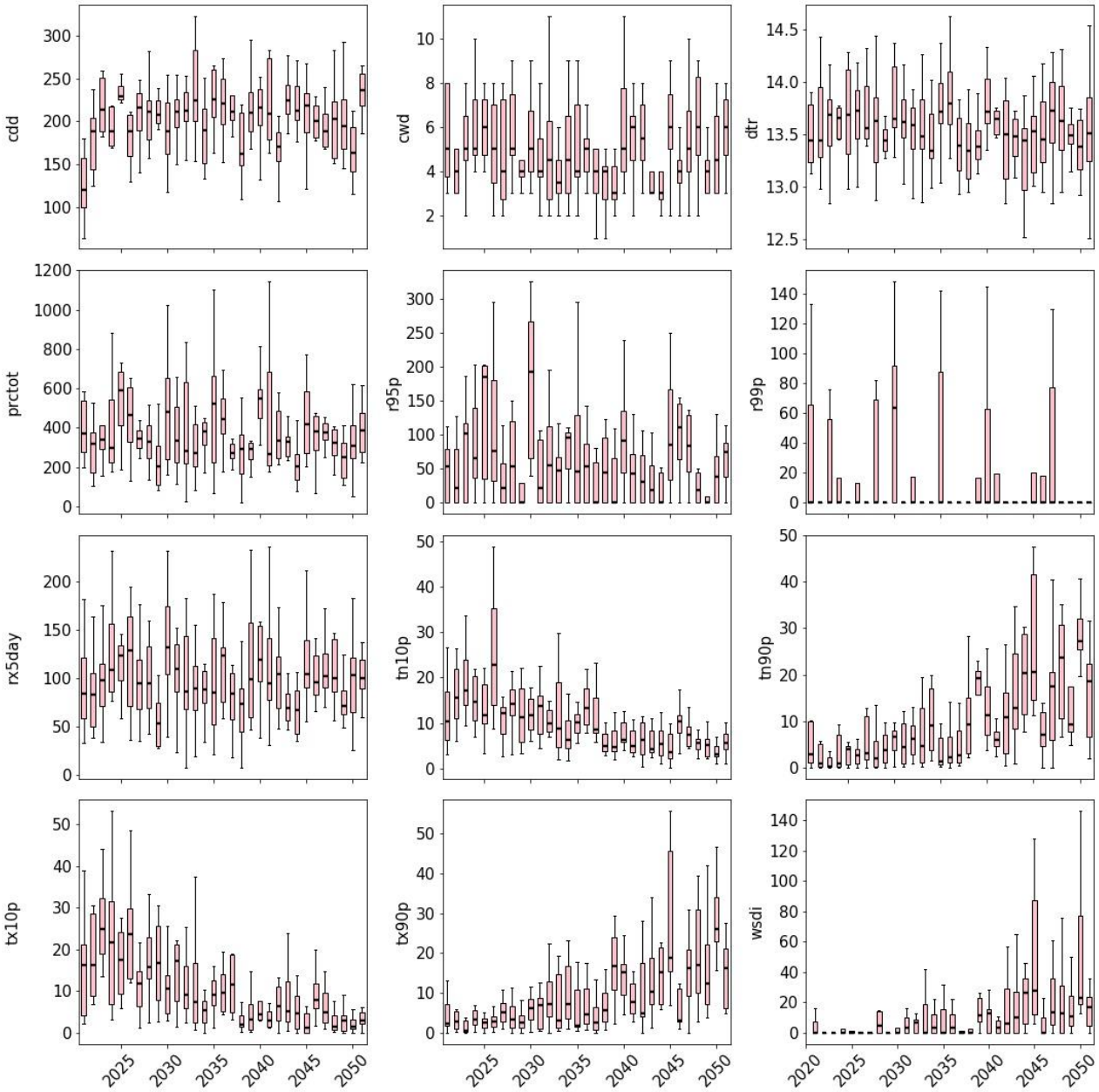

Figure 36: Boxplot of climate indices consisting of 8 climate models with the ensemble mean for Maine station for the near future under RCP4.5 (2020-2050)

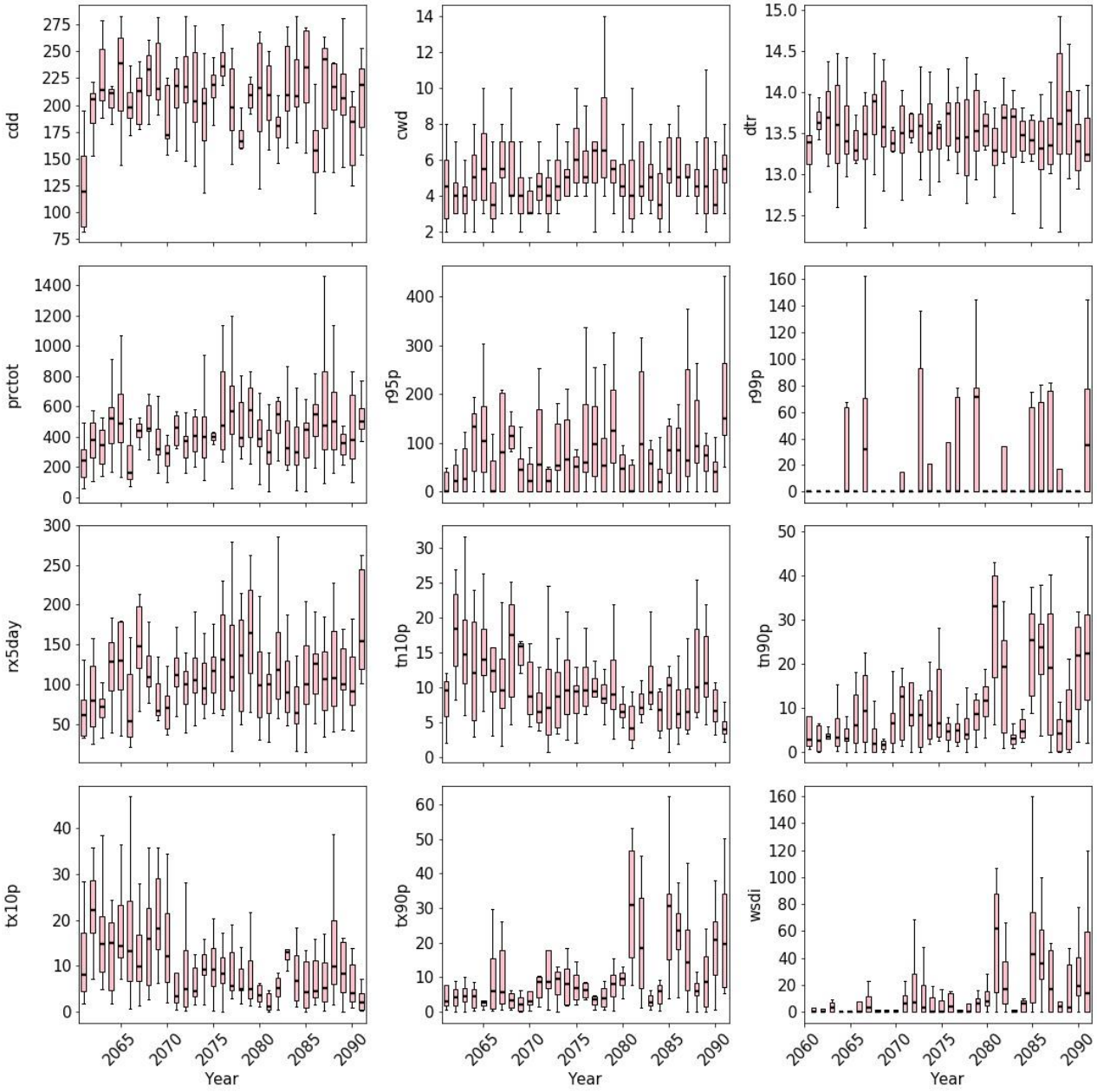

Figure 37: Boxplot of climate indices consisting of 9 models for Maine station for the far future under RCP4.5 (2060-2090)

The increase in the warm spell frequencies could be attributed to the increase in greenhouse gases concentration in the atmosphere which results in global warming. The negative trend of the diurnal temperature range in the study area could be caused by a faster warming of the minimum temperature even though there was an increase in both maximum and minimum temperatures (Mouhamed et al. 2013). The projected increase in a warm spell and the overall warming of the stations in the basin for near and far future under RCP4.5 and RCP8.5 is an indication that the future normal temperature may become more severe than the past if mitigation measures are not in place to abate the warming.

For precipitation indices, the increase in annual total precipitation in the basin is consistent with (Lebel and Ali 2009) which might have been caused by the Sahelian precipitation recovery

(Thompson and Polet 2000). The significant increasing trend of very wet days and extremely wet days observed in the study area is in line with the findings of (Sarr 2011) who reported an increase in the frequency of extreme precipitation events in the Sahel. However, it should be noted that despite the increasing frequency of extreme precipitation events, there was also an increasing trend in consecutive dry days with a decreasing consecutive wet day.

Due to the spatial variability of precipitation, the projected precipitation indices appear to follow different trends at different time slices under the two RCPs. For example, all annual total precipitation, extremely wet days, very wet days and maximum 5-day precipitation follow a negative trend for near future although not statistically significant for all stations under RCP4.5 and 8.5 near future scenarios but turned majorly positive for all indices under both scenarios for far future depicting a more intense extreme event in the future. This result is consistent with (Abiodun et al. 2017) who stated that the result of GCM projections showed a likely increase in extreme precipitation events over West Africa. (Abiodun et al. 2017) also documented a decrease in projected wet days frequency and annual total precipitation over Maputo between 2081 to 2100 under the RCP8.5 scenario. Same authors also noted an increase in annual total precipitation over Lagos between 2081 and 2100 under both RCP scenarios.

Whilst the projected decrease in the frequency and intensity of extreme precipitation especially over Kano for near future under both RCP scenarios will inevitably affect the levels of water in the two dams in the Kano (Tiga and Challawa dams), and also affect the water used for irrigation purposes in the Sahelian basin, the far future slices under the two RCP scenarios showed a projected increase in the frequency and intensity of extreme precipitation which suggests flooding as well as more water for hydro-electricity and irrigation, hence, more water supply to the drying Lake Chad. The projected increase in dry spells could reduce agricultural productivity, food security and a potential pressure on the available freshwater resources in the basin (Abiodun et al. 2017).

Although, the uncertainties associated with climate change impact assessment on extreme indices cannot be under-emphasised. This includes GCM and RCM configurations and the RCP scenarios. However, in this study, the uncertainty range was minimized by analysing the model ensemble mean as seen in the comparison results of the CORDEX historical period with validation period.

6.6 Conclusion

In order to understand the susceptibility of river basins to climate change, this study investigated the impact of climate change on climate extreme indices in the Komadougu-Yobe basin, Lake Chad region using homogenized observed stations' data for past climate extremes' characteristics and an ensemble mean of 8 bias-corrected CORDEX climate models for future projection of climate extremes under two RCP scenarios. The results show that there is a warming trend in temperature in

the basin while the precipitation indices do not have uniform trend conformity as this depends on the precipitation index of concern.

Generally, over the study area, the magnitude of the trends of hot extremes was greater than the cold extremes which imply that the distributions of the warm extremity associated with the increasing daily temperature are changing more rapidly than the cold ends. The increased positive trends in total annual precipitation and corresponding positive trends in the intensity of wet events coincide with the positive trends of hot extremes which indicate the capacity of the warmer air to hold more moisture resulting in a prolonged low-level moisture convergence and possible occurrence of storm activities in the region. Furthermore, the historical and future climate extreme characteristics revealed similar patterns of trends over the study area. However, the magnitude of the projected climate extremes, most importantly temperature, was continually greater in the latter years. These consistencies could be scaled with the RCP emission scenarios which have demonstrated a strong relationship between the anthropogenic GHG emissions and potential environmental impacts.

It is worth noting from current understanding that the environmental impacts associated with increasing extreme climate events and constrained by anthropogenic climate change will attract severe costs especially to vulnerable economies (like of the study area) in West Africa. Thus, to reach a more definitive conclusion, future work must seek to explore and improve individual regional climate simulation, especially of precipitation, to reduce uncertainties and discrepancies in model outputs.

Therefore, the attempts in this study to characterize areas in the river basin with the potential risk of climate extreme events will serve as a useful resource for assessments of the potential impacts of climate change on human and ecosystems, and in turn enhance regional adaptation, hazard preparedness, planning strategies, and decision making.

Chapter 7: Calibrating a conceptual hydrological model using multi-objective optimization techniques (Paper Five)

Having established some climate extremes conditions in the study for historical and future projections area in the previous chapter, it is therefore important to accurately represent the response of the stream flow to these extreme events which are caused by climate change. In order to precisely represent this response, there is a need for a robust hydrological modelling which will take into account the exact hydrological properties of the study area even in the face of climate extremes. To this regard, this chapter aims to calibrate a conceptual hydrological model using multi-objective optimization techniques over the trans-boundary Komadougu-Yobe Basin. The optimization techniques adopted are the Local Optimization-Multi Start (LOMS), Differential Evolution (DE), Multi-objective Particle Swarm Optimization (MPSO), Memetic Algorithm with Local Search Chains (MALS), Shuffled Complex Evolution-Rosenbrock's function (SCE-R), Bayesian Markov Chain Monte Carlo (MCMC) approach while the three combined objective functions include minimizing the root mean square error and maximizing both Kling-Gupta (KGE) and Nash-Sutcliffe efficiencies (NSE). This chapter only focuses on the calibration of the hydrological model at historical time scale as presented in section 7.6. Future work will seek to project the response of the stream flow to climate change at different climate scenarios. This manuscript is accepted by the Journal of Hydrology: Regional Studies.

Abstract

Computational and optimization processes of model parameters calibration influence the ability of hydrological models to simulate the water cycle for effective water resources management. In this study, the GR5J hydrological model parameters over the Komadougu-Yobe Basin of West Africa are calibrated using six optimization methods i.e. Local Optimization-Multi Start (LOMS), the Differential Evolution (DE), the Multi-objective Particle the Swarm Optimization (MPSO), the Memetic Algorithm with Local Search Chains (MALS), the Shuffled Complex Evolution-Rosenbrock's function (SCE-R), and the Bayesian Markov Chain Monte Carlo (MCMC) approach. Three combined objective functions i.e. Root Mean Square Error, Nash- Sutcliffe efficiency, Kling-Gupta efficiency are applied. A multi-objective function approach is used to correct the errors propagated by using a single objective function. The calibration process is divided into two separate episodes (1973-2013 and 1980-2010) so as to ascertain the robustness of the calibration approaches. Runoff simulation results are analysed with a time-frequency wavelet transform. For calibration and validation stages, all optimization methods simulate the base flow and high flow spells with a satisfactory level of accuracy. In all cases, the DE and the SCE-R methods perform better than others. The combination of multi-objective functions and multi-optimization techniques improve the model's parameters stability and the algorithms' optimization to represent the runoff in the basin.

Keywords: optimization techniques; wavelet analysis; base flow; high flow; GR5J; runoff

7.1 Introduction

Hydrological modelling is vital for effective water resources management (Bellin et al. 2016). The goal of a hydrological model is to accurately represent the hydrological systems in order to evaluate the impact assessment and risk evaluation related to water resources management in a river basin (Donnelly-Makowecki and Moore 1999). This involves the simplification of the real-world system by means of mathematical equations and assumptions concurrently with input and forcing data, model parameters, and their initial values (Gupta et al. 1998).

Each hydrological model has its constraints in terms of the number of input data, spatial variability representation, calibration parameters and duration. In particular, some hydrological models have been developed to represent a simplified representation, relationship and transformation of precipitation into runoff (Narasayya et al. 2013; Singh et al. 2003). These so-called precipitation-runoff models are created to characterize the physical components of a basin by assuming a simplified precipitation-runoff relationship; without explicit representation of the spatial variability in topography, vegetation and soil properties. The advantage of these models is that they require less input data. Additionally, they are simpler to set up and have fewer calibration parameters. As a consequence, they are widely used for operational applications (Lampert and Wu 2015) as well as for investigating the future changes in climate and land use (Beven 2011). In this type of model, the parameters selection is restricted to a predefined range in order to achieve a realistic representation of the basin properties. Furthermore, these parameters are indirectly estimated using calibration and optimization procedures (Gupta et al. 1998). The best model parameter sets during the calibration procedures are benchmarked on objective functions which indicate the degree of numerical agreement between basin observations and model simulations. Previous researches (Duan 2003; Lu et al. 2013) illustrate that calibrations based on a single-objective function are effective for emphasizing a definite characteristic of a system, however, causing increasing errors in other characteristics of the system (Wagener 2003). In hydrological simulations, for instance, calibration based on an objective function fine-tunes the model simulation in favour of the predetermined objective function which does not assure a better simulation with other objective function. A multi-objective calibration method seeks to address this limitation by quantifying the adjustments in maximizing or minimizing a number of objective functions, finding a representative set of the Pareto optimal solutions, as well as defining a single solution that maximizes or minimizes a specific independent preference (Gupta et al. 2009; van Werkhoven et al. 2009).

According to (Yapo et al. 1998), multi-objective calibrations are of great advantage as it ensures desired outcomes in hydrological applications. A detailed report of the advantages of this technique is summarized in (Efstratiadis and Koutsoyiannis 2010). Thenceforth, many hydrological studies have applied this technique by weighing various objective functions (Foglia et al. 2009; Li et al.

2010), population-based search method, and Pareto set search (Bekele and Nicklow 2007; Dumedah et al. 2010). In similar attempts, (Rakovec et al. 2016) calibrated the mesoscale Hydrologic Model (mHm) over 83 European basins using the Multi-scale Parameter Regionalization approach for improved physiographic and hydrologic regimes. (NING et al. 2015) calibrated the Hydrological Predictions for the Environment model (HYPE) (Lindström et al. 2010) over the Da River Basin of Vietnam using the Differential Evolution Markov Chain Monte Carlo (Braak 2006) step-wise calibration method. (Werth et al. 2009) applied the multi-objective calibration framework of Non-dominated-Sorting-Genetic-Algorithm-II (Deb et al. 2002) (NSGAII) to calibrate the WaterGAP Global Hydrology Model (Döll et al. 2003) over the Congo basin in Africa, the Amazon basin in South America, and the Mississippi basin of North America. (Xie et al. 2012) calibrated the Soil and Water Assessment Tool model (Arnold and Fohrer 2005) using the NSGAII technique to assess the total water storage variability over Sub-Saharan Africa basins.

While previous studies established the advantages of using multiple efficiency criteria over a single criterion, they do not consider the effect of using combined multi-optimization procedures and multiple-objective functions on model parameters set. The advantage of using various optimization methods lies in its ability to assess quality phases of the optimized solutions such as their accuracies, diversities and cardinalities (Riquelme et al. 2015).

In order to reduce the errors being propagated by the use of single objective function as well as generating good optimized solutions for the model parameter sets, this study attempts to calibrate a 5-parameter daily lumped precipitation-runoff model i.e. the *modèle du Génie Rural à 5 paramètres au pas de temps Journalier* (GR5J) (Coron et al. 2017) over the Komadougu-Yobe Basin (KYB) in West Africa using a combined multi-optimization procedures and multiple-objective functions. A detailed description of the study area is given in section 7.2. The GR5J model, the calibration, optimization methods, modelling strategies and time-frequency approach are presented in section 7.3, 7.4 and 7.5 respectively. Results are provided in section 7.6, followed by a summary and conclusion in section 7.7.

7.2 Study Area and Data

The study area and data used is as presented in section 4.2 and 5.3.1 respectively.

7.3 Hydrological model, calibration and optimization methods

In this section, the GR5J model, as well as the multi-objective and the multi-optimization methods are described. The schematic of the methodology is presented in Figure 38.

7.3.1 The GR5J Model

The GR5J model (Lavenne et al. 2016) is a precipitation-runoff model that focuses on soil moisture partition. The general model structure is presented in Figure 39. Five model parameters can be caralibted, namely the maximum capacity production store, X1 (mm) and a maximum capacity routing store, X3 (mm) which are the two store compartments fed by the time base of a unit hydrograph, X4 (days). The two other parameters, i.e. the inter-catchment exchange coefficient, X2 (mm/d) and the inter-catchment exchange threshold, X5, which quantifies the inter-catchment groundwater flows. X1 and X2 are connected to water balance (Table 22). The degree-day snow module (Valéry et al. 2014) is not activated in this study, as there is no snow in our application study. X1 and X3 are positive real numbers, X2 accepts both positive and negative numbers while X4 is always greater than 0.5 (Perrin et al. 2003). The primary inputs for the model are precipitation and evapotranspiration. Additionally, the ordinary krigging method (Li and Heap 2014) is used to calculate the area mean basin rainfall

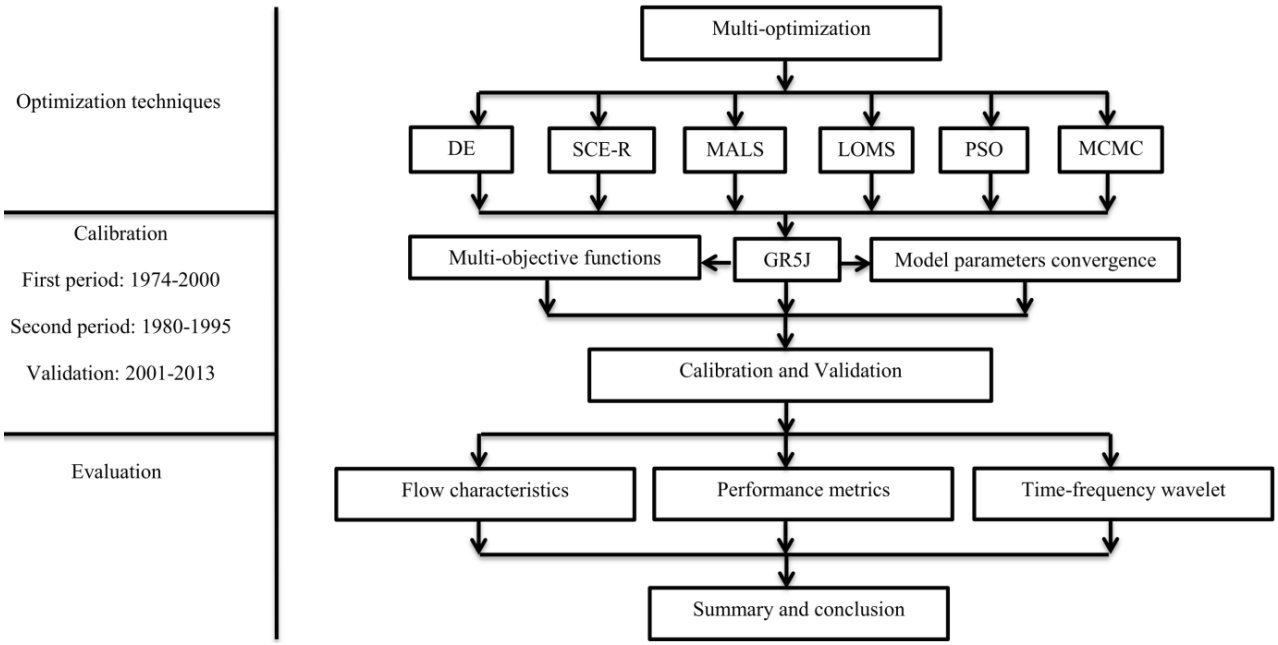

Figure 38: Methodology flow chart

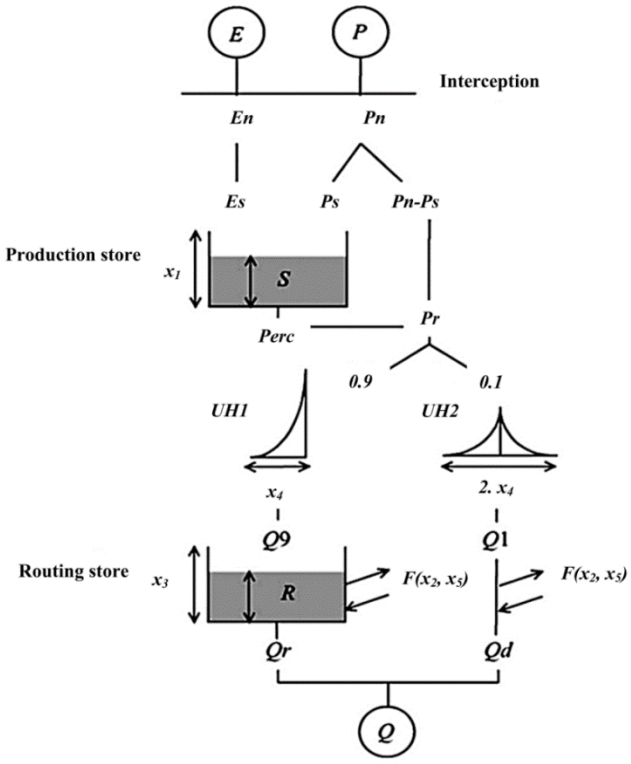

Figure 39: GR5J model set up (Lavenne et al. 2016)

P is the areal basin precipitation, E is the mean of inter-annual potential evapotranspiration, Pn is the net precipitation, En is the net evapotranspiration, S is the production store, Perc is percolation amount, R is the routing store, Q9 and Q1 are the outputs of the unit hydrographs UH1 and UH2 respectively, Q is the total runoff

Table 22: Model parameters

Parameters	Meaning	Unit
X1	production store capacity	mm
X2	Inter-catchment exchange coefficient	mm/day
X3	Routing store capacity	mm
X4	Unit hydrograph time constant	day
X5	Inter-catchment exchange threshold	-

7.3.2 Multi-objective calibration

A multi-objective model calibration is based on objective functions suitable for various hydrological processes such as peak flows, general and low flows (Madsen 2000). This reduces the errors being propagated by the use of single objective function.

A multi-objective calibration problem can be expressed as:

$$min[F_1(\emptyset), F_2(\emptyset), \ldots, F_m(\emptyset)], \emptyset \in \ominus \quad \textit{Equation 30}$$

where $F_m(\emptyset)$ are the different objective functions.

$\emptyset$ is the model parameters while $\ominus$ is the parameter space. The model parameters are restricted to a physically plausible parameter space. The upper and lower bounds of the model parameters are specified as a hypercube function of the parameter space. Equation (28) reaches a Pareto set of solutions given an optimal trade-off among the different objective functions (Gupta et al. 2009).

The multi-objective method selected for this study consists in minimizing the root mean square error and maximizing both, the Nash-Sutcliffe and the Kling-Gupta efficiencies. The Root Mean Square Error (RMSE) is a commonly used statistic that provides a good overall measure of how close modelled values are to predicted values.

$$RMSE = \sqrt[2]{\frac{\sum_{i=1}^{n}(M_i - O_i)^2}{n}} \quad \textit{Equation 31}$$

where O_i represents the ith observed value and M_i represents the ith model value for a total of n observations. The Nash and Sutcliffe Efficiency (NSE) compares the relative magnitude of the residual variance to observation variance (Nash and Sutcliffe 1970).

$$NSE = \frac{\sum_{i=1}^{n}(Q_o - Q_{av})^2 - \sum_{i=1}^{n}(Q_o - Q_s)^2}{\sum_{i=1}^{n}(Q_o - Q_{av})^2} \quad \textit{Equation 32}$$

Q_o is the observed discharge, Q_{av} is the average observed discharge, Q_s is the simulated discharge. NSE varies between -∞ and 1 with the optimum value being 1. However, due to the quadratic nature of NSE, it provides information on the model's ability to simulate high flows. However, NSE can also return optimum values as a result of periodicity, thereby providing a misleading interpretation of the model's ability. As a result of these lapses, many studies (Criss and Winston 2008; Mathevet 2006) decomposed the NSE into a ratio of standard deviations (αNSE), relative bias (βNSE) and the ratio of the correlation coefficient (r). (Gupta et al. 2009) showed that optimizing αNSE underestimates the variability of simulated flows because the optimum NSE is attained when αNSE = r. In view of this, (Gupta et al. 2009) and (Kling et al. 2012) recommended the Kling-Gupta efficiency (KGE) in order to circumvent the connections between the variation coefficient and bias and ratios.

$$KGE = 1 - \sqrt{(rc - 1)^2 + (\beta_{KGE} - 1)^2 + (\gamma_{KGE} - 1)^2} \quad \textit{Equation 33}$$

where rc is the linear Pearson correlation coefficient, β_{KGE} is the bias and γ_{KGE} is the variation coefficient ratio.

7.3.3 Multi-optimization methods

In this study, six different multi-optimization methods are used for the calibration of the model parameters. The results of the multi-optimization technique provide a set of solutions which

concurrently optimize conflicting objective functions in a population set, leading to a Pareto-optimal solution of the model parameters (Savic 2002). The six methods are briefly explained in the following.

Particle Swarm Optimization (PSO)

The PSO is a population-based stochastic optimization procedure (Kennedy and Eberhart 1995). In this method, the population of potential solutions is called a swarm while particles are the members in the swarm. These particles change positions in a multi-dimensional search space depending on the position of other particles in the swarm as well as their own relative positioning. The process involves the adjustment of the system based on a set of arbitrary solutions while the optimization search is maintained as the generations are updated. The history of the best positions of the particles is retained by the neighbouring particles while considering their fitness level after each iteration. This helps in refining the final solution. The process reaches finest optimization when all particles converge. The advantages of this method include its ability to converge fast, high efficiency in finding global optimal and its ability to run parallel computation. The disadvantages include its ability to converge prematurely and subsequently be stuck into a local minimum. Further details can be found in (Clerc and Kennedy 2002). While this method has been widely used in fields like neuro-computing and some environmental science field, it is scarcely used in hydrology.

Shuffled Complex Evolution with Rosenbrock's function (SCE-R)

The advantage of this method lies in its ability to combine both local and global optimization techniques. It starts with a direct local search (Rosenbrock 1960). When the value of the objective function is decreasing, the length of the search vector is increased in order to have an optimum solution. The iteration stops when the initial parameter setting is retained, a new minimum is reached or all axes are explored. The global search combines the shuffling of complexes i.e. partitioning the sample points from a population into distinct groups, competitive evolution and controlled random search with simplex search (Duan et al. 1993). These enhance information sharing about the search space created individually by each complex. However, iteration takes time on instances of many parameters while trying to maintain a satisfactory level of diversity. This method has been used widely to locate the global optimum for precipitation-runoff models (Cooper et al. 2007).

Memetic Algorithms with Local Search Chains (MALS)

MALS is a steady-state memetic algorithm with improved genetic algorithms per local search techniques (Molina et al. 2010). They are particularly suitable for uninterrupted optimization, as they combine the strength of evolutionary algorithms with a local search routine to find the local optimum of a likely region. The local search intensity is increased to get the most likely solution. In MALS, the worst solution is substituted in the population instead of substituting every individual after iterations. This retains the improvement of the solution after the local search (Bergmeir et al. 2016)

and subsequently controls the local search procedure to the most likely solutions. However, this method does not perform well if the numbers of parameters to optimize are many.

Differential Evolution (DE)

DE is based on a global population stochastic search procedure suitable to find the global optimum in a continuous search domain (Storn and Price 1997). DE does not require derivatives of the objective function. In DE procedure, a good optimized solution requires a trial-and-error search to adjust its related parameter values. This method is useful in conditions where the objective functions are difficult to differentiate. However, DE is inefficient on smooth functions which are mostly derivative based. This method has been successfully applied for pattern recognition (Ilonen et al. 2003), communications (Storn 1996) and engineering (Joshi and Sanderson 1999). Details of this method are presented in (Qin et al. 2010).

Bayesian Markov Chain Monte Carlo simulation (MCMC)

This method uses an adaptive metropolis algorithm and a delayed rejection procedure in implementing a Markov Chain Monte Carlo simulation. MCMC aims to generate parameter values' samples by simulating random processes having the posterior distribution as stationary distribution. This posterior distribution is the probability distribution on the parameter space. MCMC further explores the posterior distribution by creating random processes with the stationary distribution as the parameters' posterior distribution. The new parameters in the adaptive metropolis are created with a covariance matrix which adjusts to the size and shape of the object distribution. This permits a more proficient posterior distribution exploration. The new parameters generated during delayed rejection are from the scaled covariance matrix jump arising from the last accepted value. This preserves the reversibility of the Markov chain. Advantages of the MCMC include its computational and statistical efficiency. Additionally, tuning the scheme does not require trial runs. However, scaling is poor when there is an infinite target distribution variance. This is not revealed during the inspection of the target density which makes it difficult to detect analytically. Furthermore, it takes time for MCMC to recover from distorted preliminary information because it adapts too closely to the preliminary information from the output. Details are documented in (Haario et al. 2005; Haario et al. 2006).

Local Optimization-Multi Start approach (LOMS)

The Local Optimization-Multi Start approach (LOMS) is a simple bounded and box-constrained general optimization technique (Gay 1990). In LOMS, the performance of optimization is affected by scale vector chosen in computing the sample's trial values and in testing the convergence of parameters. This strategy requires setting up the start point in transformed parameter space. However, the multi-start approach assesses the consistency in the local optimization method. The details of this method are documented in (Gay 1990).

7.4 Modelling strategy

To ascertain the robustness of the optimization techniques, calibration methods and model output, the analysis period is divided into two different episodes (Table 23). This provides worthwhile information on the model's ability to replicate the runoff at different times. The calibration period for episode 1 is between 1974 and 2000 and the validation period is between 2001 and 2013 while episode 2 has the calibration period between 1980 and 1995 and the validation period is between1996 and 2001. In calibrating the GR5J model, the initial model parameters are fine-tuned with a set of trial-and-error experiments before the start of the optimization objectives. In the modelling set up, each optimization technique is run separately in the hydrological model using the multi-objective calibration technique for each calibration and validation periods. The number of iteration and simulated needed for each model parameters to converge for each optimization method is also reported. Furthermore, the properties of the runoff generated by each optimization techniques are analysed and compared with the observation.

Table 23: Analysis period

Episode	Warm up period	Calibration period	Validation period
1	1971-1973	1974-2000	2001-2013
2	1974-1979	1980-1995	1996-2011

7.5 Time-frequency wavelet

The transient behaviour of the runoff is examined with a time frequency wavelet analysis. The wavelet transform decomposes signals in a way in which the signal trends and details are represented as a function of time. This shows areas with high common power in the time-frequency space i.e., a transient and localized behaviour at different time scales. In this transform, a two-parameter basis $\{\psi_{a,\tau}(t), (a,\tau)\ \epsilon\ (R_+^* \times R)\}$ replaces the Fourier basis where 'τ' is the shift in time and 'a' is the scale. The Fourier basis expresses a signal in terms of power and frequency of its decomposed sine waves but gives no account of the time the frequencies occur. However, this replacement facilitates the time-scale discrimination process during analysis. The continuous time signal $x(t)$ in the transform has coefficients which are defined by a linear integral operator:

$$C_x(a,\tau) = \int_{-\infty}^{+\infty} x(t)\psi_{a,\tau}^*(t)dt \qquad (31)$$

where $\psi_{a,\tau}^*(t) = \frac{1}{\sqrt{a}}\psi\left(\frac{t-\tau}{a}\right)$, * is the complex conjugate and $\psi(t)$ is the wavelet.

In this multi-resolution analysis, equation (31) is discretized because hydrological signals are discrete in time. This enables the orthogonal decomposition of the runoff signal by detailing the increasing order of resolution as well as its approximation. The wavelet power spectrum of the runoff local covariance across different time scales is generated based on the wavelet energy stress of the time series (Veleda et al. 2012). The advantage of this transform lies in its ability to deconstruct complex signals into basic signals of finite bandwidth without a phase shifting or signal leakage of the primary signal.

7.6 Results

In this section, the results of the multi-objective optimization approaches are described. Further results include the model parameters convergence, flow characteristics, performance metrics as well as the wavelet decomposition of the simulated runoff.

7.6.1 Multi-objective optimization calibration

The summary of the multi-objective optimization computation is presented in Table 24. It is observed that the global optimization approach of MALS exhibits the highest number of iterations while the PSO has the highest number of simulations for both calibration episodes. The lowest iterations and simulations are exhibited by the SCE-R approach in all cases.

Table 24: Statistics of the multi-objective calibration approaches

	Episode 1(1974-2000)		**Episode 2(1980-1995)**	
Strategy	**Iterations**	**Simulations**	**Iterations**	**Simulations**
SCE-R	41	629	52	745
DE	200	402	200	402
PSO	113	4520	110	4400
MALS	2248	2747	2320	2675
LOMS	75	420	69	451
MCMC	40	2992	56	2986

The optimum model parameters generated during calibration for each optimization method (Table 25) is used in running the model during validation for the two episodes. The result for the first episode shows that SCE-R, DE, PSO and MALS methods have the NSE, KGE and RMSE of 0.89, 0.81 and 0.24 respectively for the calibration period (1974-2000) while the validation period (2001-2013) seem to be an improvement over the calibration period. The NSE, KGE and RMSE generated during this period are 0.91, 0.84 and 0.23 respectively. The correlation plot for the calibration period (1974-2000) for the first episode (Figure 40a) shows the simulated runoff generated by PSO optimization

method has the highest correlation with the observed runoff (QOBS) with a value of 0.79. However, there is a degree of correlation between simulated runoff generated by all optimization methods.

The correlation plot for the validation period (2001-2013) shows a high degree of correlation between the observed runoff and the simulated runoff from SCE-R, DE, PSO and MALS optimization methods (Figure 40b). However, SCE-R optimization method has the highest correlation value of 0.73 while MCMC has the lowest value of 0.67. The graphical comparison of the simulated runoff with observed runoff for the entire period of calibration and validation (Figure not shown due to overlapping graphs) shows a degree of representativeness and agreement with the observed runoff. However, for a sub-set period of calibration (1999-2000) and validation (2001-2002), there are some overestimations of the peak by some optimization techniques (e.g. MCMC) and the underestimation of the base flow by some other optimization techniques (e.g. SCE-R and DE) (Figure 41). In contrast, MCMC represented the base flow well. The anomaly (Figure 41) shows the deviations of the simulated run-off from the observed runoff. The highest deviation is seen in MCMC result while the lowest is seen in DE and SCE-R. However, the degree of anomaly seems to be lesser during the validation period. Furthermore, SCE-R, DE, PSO and MALS returned reasonable optimized objective functions for both calibration and validation periods (Table 25). For the second episode of the calibration (1980-1995) (Table 25), the results show SCE-R, DE, PSO and MALS provide the best parameters. They have the NSE, KGE and RMSE values of 0.89, 0.79 and 0.23 respectively. LOMS and MCMC have lower NSE and KGE values. This same behaviour is exhibited during the validation period (1996-2011). In both cases, LOMS and MCMC have the lowest performance.

It is worthy to note that changing the calibration episodes has little to no effect on the generated model parameters. For example, in SCE-R method for both calibration episodes, X1 is between 100.25 to 101.78mm, X2 is between -14.96 to -14.98mm while X3, X4 and X5 do not change. For MALS, X1 does not change, X2 ranges from -14.95 to -14.96mm, X3 is from 998.68 to 1000.14 mm while X4 and X5 do not change. The range of these similar calibration parameters during both episodes for the different optimization techniques shows the robustness of the calibration efficiencies of these methods. Furthermore, the applied calibration methods show reasonable abilities to simulate runoff with a satisfactory level of accuracy.

Table 25:Multi-objective sets of calibration parameters during the calibration and validation periods for the two analysis epochs

Episode 1											
	Calibration Best Parameters					**Calibration (1974-2000)**			**Validation (2001-2013)**		
Strategy	X1 (mm)	X2 (mm)	X3 (mm)	X4 (day)	X5	NSE	KGE	RMSE	NSE	KGE	RMSE
SCE-R	100.25	-14.96	1000.52	20	0.40	0.89	0.81	0.24	0.91	0.84	0.23
DE	100.25	-14.96	998.68	20	0.40	0.89	0.81	0.24	0.91	0.84	0.23
PSO	100.25	-14.98	999.18	20	0.40	0.89	0.81	0.24	0.91	0.84	0.23
MALS	100.25	-14.96	998.68	20	0.40	0.89	0.81	0.24	0.91	0.84	0.23
LOMS	800.83	-14.77	200.35	30	0.09	0.67	0.72	0.65	0.74	0.74	0.61
MCMC	800.95	-14.25	200.35	30	0.08	0.67	0.72	0.65	0.74	0.74	0.61
Episode 2											
	Calibration Best Parameters					**Calibration (1980-1995)**			**Validation (1996-2011)**		
SCE-R	101.78	-14.98	1000.52	20	0.40	0.89	0.79	0.23	0.92	0.84	0.21
DE	101.78	-14.95	1000.14	20	0.40	0.89	0.79	0.23	0.92	0.84	0.21
PSO	101.98	-14.96	1000.18	20	0.40	0.89	0.79	0.23	0.92	0.84	0.21
MALS	100.25	-14.95	1000.14	20	0.40	0.89	0.79	0.23	0.92	0.84	0.21
LOMS	800.46	-10.95	200.35	30	0.44	0.71	0.69	0.66	0.73	0.73	0.53
MCMC	800.95	-10.11	200.35	30	0.44	0.71	0.69	0.66	0.73	0.73	0.53

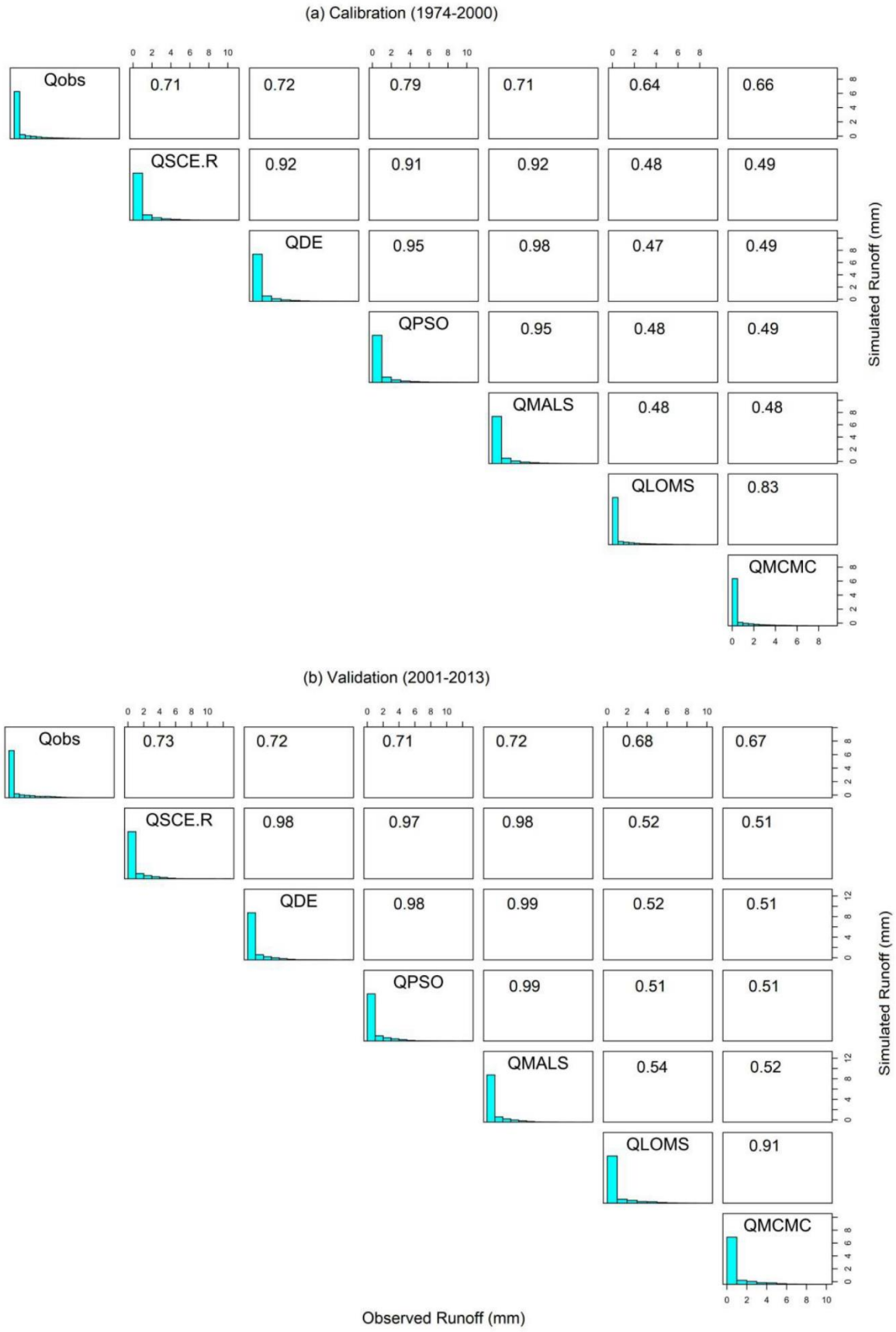

Figure 40: Correlation plot for the (a) calibration period (1974-2000) (b) validation period (2001-2013)

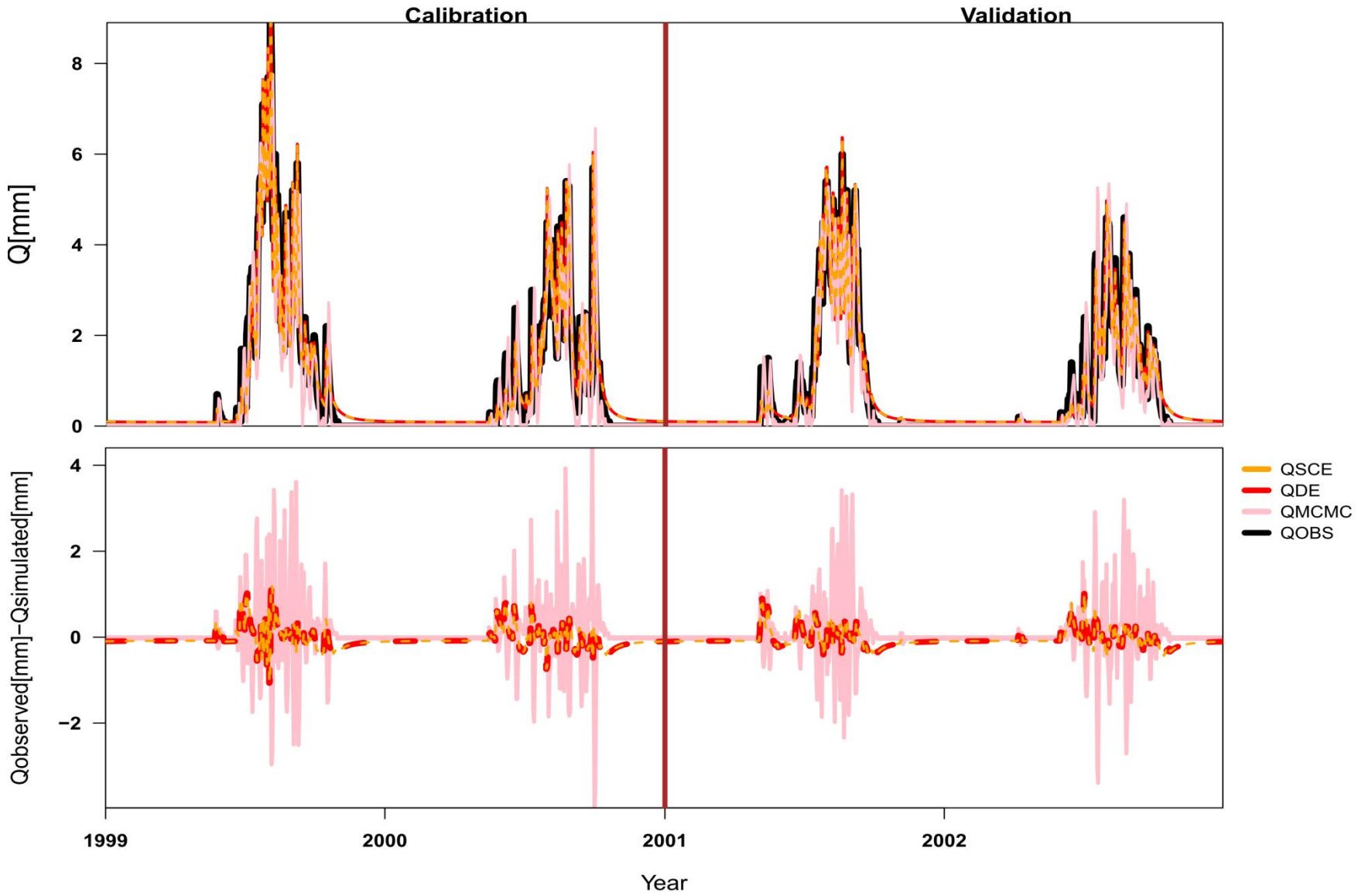

Figure 41: Above: Comparison of daily observed runoff with GRJ5-simulated runoff using different optimization methods. Below: GR5J-simulated runoff anomaly with observation for sub-calibration period (1999-2000) and sub-validation period (2001-2002). Q is daily runoff

7.6.2 Convergence of model parameters

The assessment of the model parameters convergence shows the number of iterations needed for the model parameters to converge towards a good optimized solution. To evaluate these convergences, the parameters are transformed into real space and the first 200 iterations are analysed based on the trade-off between computational period and simulation accuracy. The result for all optimization methods shows that X4 converges faster than the rest of the parameters. X4 converges at about 30 iterations while the slowest converging parameter is X1, which do not converge at 200 iterations. This means that it takes longer for every individual in the X1 population to be identical in order to reach an optimized solution. Hence, the computation time is prolonged. As illustration, the convergence for model parameters generated from the DE optimization method is presented in Figure 42.

Table 26: Base flow statistics

Base Flow (mm/day)			
Calibration (1974-2000)			
Strategy	Mean Daily Flow	Median Daily Flow	Mean Base flow Volume
OBS	0.59	0.00	0.08
SCE-R	0.65	0.12	0.18
DE	0.65	0.12	0.18
PSO	0.65	0.12	0.18
MALS	0.65	0.12	0.18
LOMS	0.52	0.05	0.02
MCMC	0.52	0.04	0.02
Validation (2001-2013)			
OBS	0.68	0.00	0.09
SCE-R	0.74	0.13	0.20
DE	0.74	0.13	0.20
PSO	0.74	0.13	0.20
MALS	0.74	0.13	0.20
LOMS	0.63	0.04	0.05
MCMC	0.62	0.04	0.04

7.6.3 Flow characteristics

In an attempt to further understand the hydrological properties of the basin as simulated by individual optimization methods, the statistics of the base flow and high flow spells is computed. The base flow separation method follows (Ladson et al. 2013).

Base flow

In Table 26, the base flow is generated for both calibration and validation periods for the two phases. For calibration period, SCE-R, DE, MALS and PSO clearly overestimate the mean daily base flow by 0.06 mm/day while LOMS and MCMC underestimate it by -0.07 mm/day. The overestimation by SCE-R, DE, PSO, MALS and the underestimation by LOMS and MCMC is seen to persist for the median daily base flow and mean base flow volume. For the validation period, SCE-R, DE, PSO and MALS continue to overestimate the base flow parameters while LOMS and MCMC continue with the underestimation.

High flow spells

The number of high flow spell events is underestimated by SCE-R, DE, PSO, MALS while LOMS and MCMC overestimated it for both calibration and validation period (Table 27). However, the highest overestimation is seen LOMS (112) during calibration and in MCMC (52) during validation. The same trend is repeated for the spell event frequency. LOMS and MCMC underestimated the maximum duration of high flow spell days during calibration by -2 days while SCE-R, DE, PSO and MALS overestimated it by +13 days. During validation, all optimization methods underestimated this event by at least -11 days. The average annual maximum flows and flood skewness (the ratio of average annual maximum to mean daily flow) is overestimated by all methods during calibration and validation periods. The highest overestimation in flood skewness is by LOMS during the calibration period (12.43) and MCMC during the validation period (11.23). All calibration techniques fairly predicted the correct average day of the year on which maximum flows occur during the calibration period with a degree of ± 2 days. However, LOMS and MCMC overestimated it by +5 days during the validation period.

Table 27: High flow spells statistics

High flow spells							
Calibration (1974-2000)							
Strategy	No of spell events	Spell event frequency (no/year)	Maximum duration of spell events (days)	average annual maximum flow(mm)	coefficient of variation of annual maximum flows	flood skewness	average day of the year on which maximum flows occur (day)
OBS	91	3.37	77	6.19	27.60	10.43	229
SCE-R	72	2.67	90	7.02	32.57	10.88	228
DE	71	2.63	90	7.03	32.58	10.90	228
PSO	72	2.67	90	7.03	32.57	10.88	228
MALS	71	2.63	90	7.03	32.58	10.90	228
LOMS	112	4.15	68	6.48	26.60	12.43	231
MCMC	110	4.07	68	6.45	26.46	12.34	231
Validation (2001-2013)							
OBS	37	2.85	79	6.85	22.83	10.01	231
SCE-R	34	2.62	68	7.84	28.80	10.61	231
DE	34	2.62	68	7.84	28.80	10.61	231
PSO	34	2.62	68	7.84	28.78	10.61	231
MALS	34	2.62	68	7.84	28.80	10.61	231
LOMS	50	3.85	66	6.98	22.88	11.15	236
MCMC	52	4.00	66	7.00	22.82	11.23	236

Flood Skewness is the ratio of average annual maximum to mean daily flow

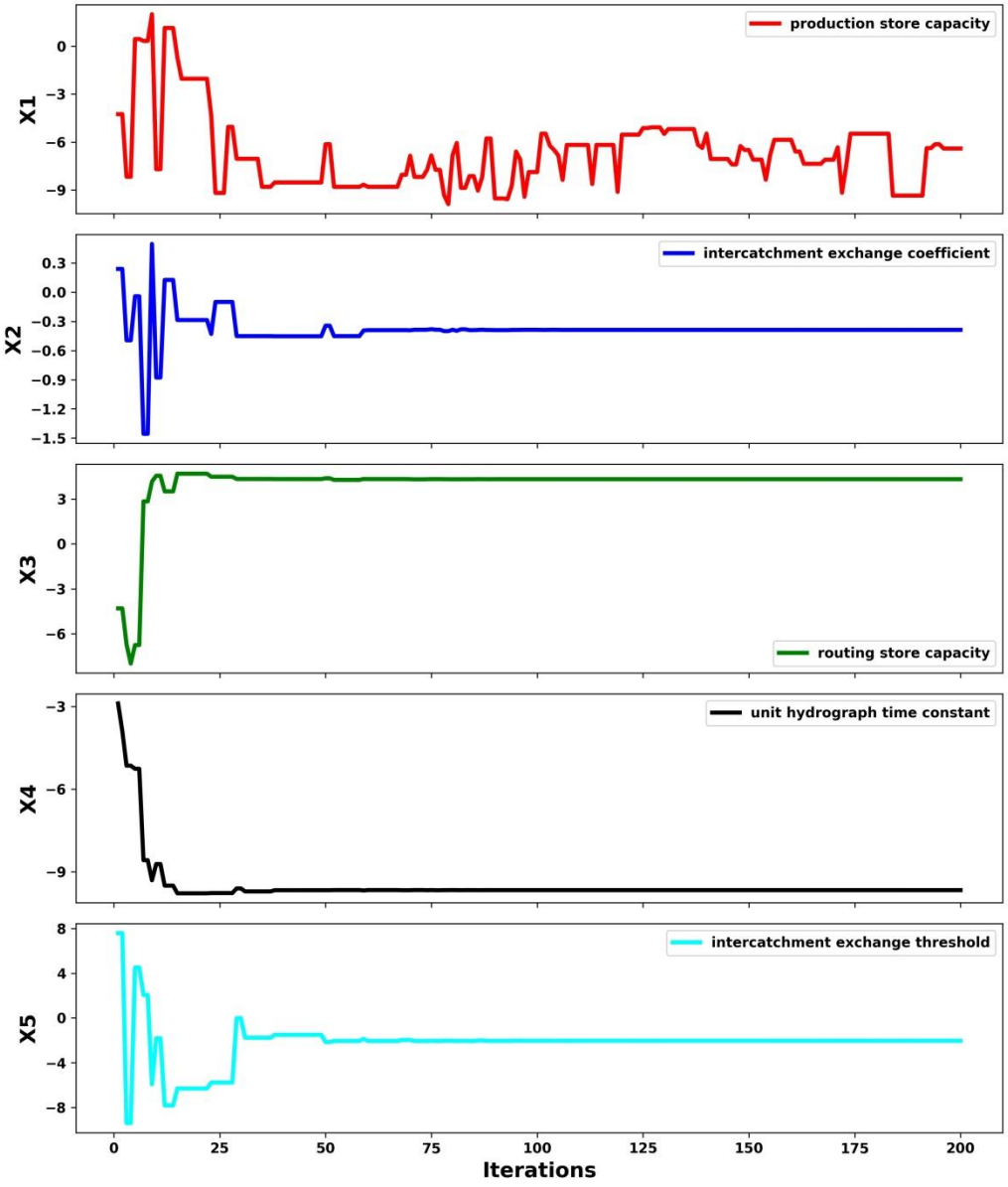

Figure 42: Convergence of model parameters from the DE optimization method

7.6.4 Performance metrics

The summary of the numerical performance metrics for each of the optimization technique implemented is shown in Figure 43. The performance metric is for the entire calibration and validation period. The performance evaluation shows that MCMC has the highest values of mean absolute error (0.28) and mean square error (0.40) while LOMS and MCMC recorded a low volumetric efficiency of 0.56 (Figure 43). This means that these two optimization techniques mismatched the fractional volume of water delivered per unit time. However, all other techniques perform better in the fraction of water delivered.

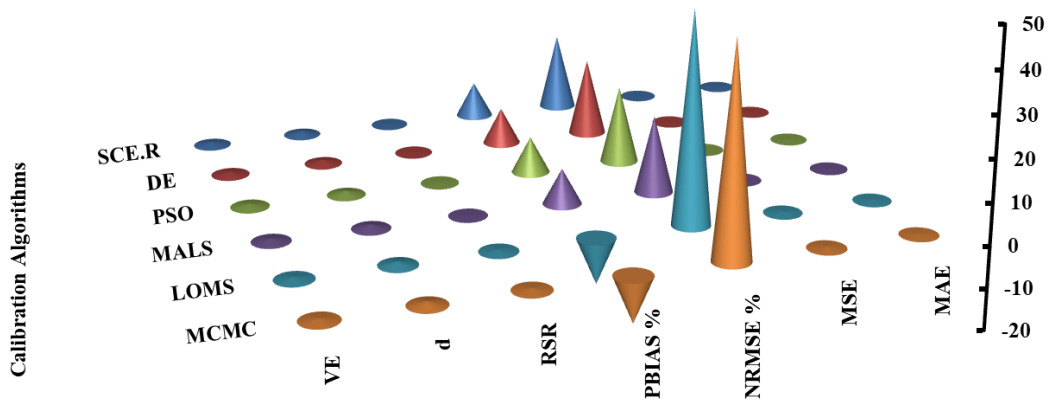

Performance metrics

	MAE	MSE	NRMSE %	PBIAS %	RSR	d	VE
SCE.R	0.16	0.05	18.4	8.4	0.18	0.99	0.74
DE	0.17	0.06	18.5	8.6	0.19	0.98	0.73
PSO	0.16	0.05	18.4	8.6	0.18	0.99	0.74
MALS	0.16	0.05	18.4	8.4	0.18	0.99	0.74
LOMS	0.27	0.39	50	-10.9	0.5	0.93	0.56
MCMC	0.28	0.4	50.1	-11	0.51	0.93	0.56

Figure 43: Performance evaluation of each calibration algorithms between 1974 and 2013. MAE is the mean absolute error, MSE is the mean square error, NRMSE is the normalized root mean square error, PBIAS is the percentage of bias, RSR is the ratio of root mean square error to the standard deviation, d is the index of agreement and VE is the volumetric efficiency.

7.6.5 Joint time-frequency signal

The wavelet spectra plot of the runoff variance across different time scales for the first simulation phase (1974-2013) shows slight differences in the results of the optimization techniques (Figure 44). The wavelet coefficients estimates are only reliable in the areas within the cone of influence i.e. the solid black lines which represent the 95% confidence level. For the observation (OBS), there is 3 to 4 years periodicity of high-frequency power from 1974 to 1992. However, this periodicity is only significant between 1979-1992 and 2005-2008. The highest wavelet power of between 11 and 12 years is captured by all techniques. This high periodicity is assumed to be caused by high precipitation variability as well as the impact of human activities in the runoff in the basin (Adeyeri et al. 2019b; Nicholson 2001; Umar and Ankidawa 2016). Furthermore, the significant power between 1989 and 1997 in the OBS is underestimated by DE, PSO, MALS and LOMS methods. These phenomena are captured by different optimization techniques. Likewise, the span of significant powers varies from

one method to the other. For example, MALS underestimated the span of powers while MCMC overestimated it. A dominant episode of significant power between 6 and 7 years is observed between 1990 and 2000. This is accurately replicated by the SCE-R while other techniques apart from MCMC underestimated it. Furthermore, the wavelet phases (blue arrows) are accurately captured by all techniques. Arrows pointing up (down) show a lead (lag) of 90^o from the first time series to the second time series. If the time series move together, there is a zero-phase difference. If the arrows are pointing left (right), it means the time series are anti-phase (in-phase) i.e. negatively (positively) correlated. In general, the magnitude of the wavelet coefficient is accurately represented by all optimization techniques.

7.7 Summary and conclusion

Different multi-objective and multi-optimization techniques have been evaluated in this study for the GR5J hydrological model applied to the case of the Komadougu-Yobe basin KYB. The calibration process involved the use of six evolutionary optimization methods (SCE-R, DE, PSO, MALS, LOMS and MCMC) and three combined objective functions (i.e. minimizing RMSE, maximizing both NSE and KGE). The robustness of the calibration approaches was validated by considering two episodes (1973-2013 and 1980-2010) for the analysis.

The applied calibration methods showed reasonable abilities to simulate runoff with a satisfactory level of accuracy. The results of the flow statistics were not universally consistent as some optimization methods overestimates while others continually underestimate the flow representation. For example, MCMC underestimated the maximum duration of high flow spell by -2 days while MALS overestimated it by +13 days. For the particular case of KYB, we found that the DE and the SCE-R methods performed best. The multi-objective computational assessment for each optimization methods to reach the optimal Pareto solutions showed that MALS exhibits the highest number of iterations while the PSO had the highest number of simulations for both calibration periods. The lowest iterations and simulations were exhibited by the SCE-R approach in all cases. Comparing the computational period and the performance metric of SCE-R indicated of the trade-off balance between computational period and simulation accuracy. Based on these evaluations, it is concluded that the combination of multi-objective functions and multi-optimization techniques for optimal Pareto sets for GR5J model parameters over the KYB do not only improve the stability of the model parameters during calibration, but also improve the optimization ability of the calibration algorithms towards more accurate and robust representation of the river runoff in the basin.

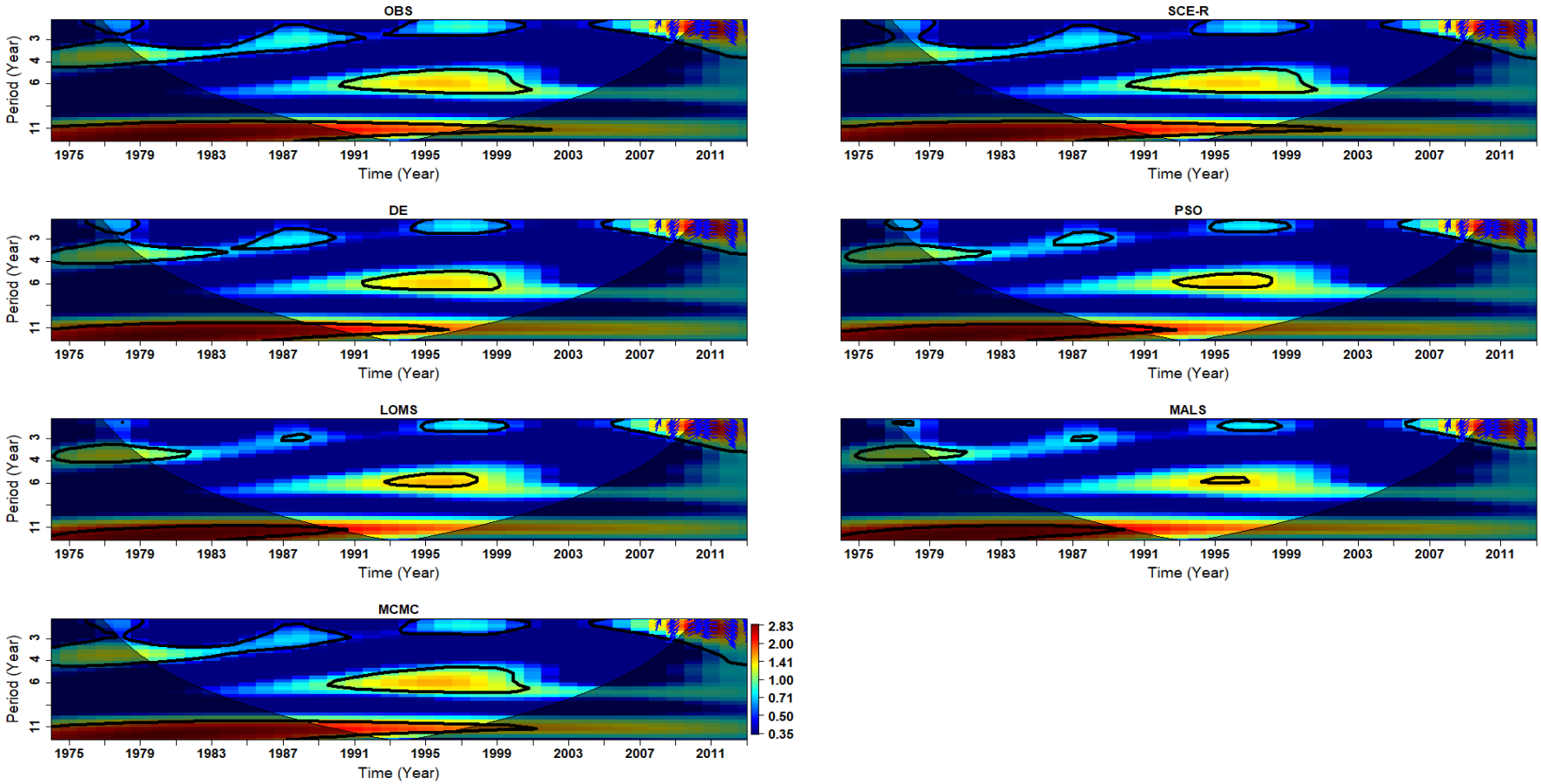

Figure 44: Wavelet spectra plot for runoff generated by observation, the Differential Evolution (DE),the Local Optimization-Multi Start (LOMS), the Bayesian Markov Chain Monte Carlo (MCMC), the Shuffled Complex Evolution-Rosenbrock's function (SCE-R), the Multi-objective Particle the Swarm Optimization (PSO), and the Memetic Algorithm with Local Search Chains (MALS) optimization method between 1974 and 2013. Solid black line represents the 95% confidence level

Chapter 8: General discussion of the results

This study investigated the hydrological response of the trans-boundary Komadougu-Yobe basin of West Africa to climate change.

8.1 Paper One Discussion

The study started with the spatio-temporal trends and homogeneity analysis of precipitation in the basin using data from Nigerian Meteorological Agency (NiMet), Department of National Meteorology Niger (DMN) and a 10 km resolution gridded observation data from Princeton University (PGF) for the period 1979 and 2015. However, due to low density of station data, the station data were assimilated into the gridded dataset. This was done to improve the quality of the gridded dataset for good representation of climatic features of locations with data paucity. The analysis was however performed on the grid scale. In the analysis, abrupt change points were detected by the different homogeneity tests at different periods and location but these change points were not corrected. This, coupled with the overall quality of the gridded dataset inadvertently affected the quality of the results.

Results from the initial analysis of precipitation show that mean annual precipitation ranges from 240 mm in the northern part and 1060mm in the southern part. This is in agreement with (IUCN 2011; Thompson and Polet 2000) who established that the southern part of the basin experiences more precipitation due to the southward shifts of the average isohyets. The coefficient of variation (CV) ranges from 41.49% to 13.47% with an average CV of 25.06% in the whole basin. This is in line with (Odunuga et al. 2011b), who reported such CV over the Hadeija-Jama'are basin which is a sub-basin of the KYB. However, more variations in precipitation values are established in areas with lower precipitation. This result agrees with (Taxak et al. 2014) who reported that zones with least variations are located on heavy precipitation zones. In all the seasons, precipitation increases from the north to the south due to the African monsoon which brings humidity from the Atlantic Ocean (IUCN 2011; Thompson and Polet 2000; USGS 2012).

The Mann-Kendall statistic showed a mixed trend of precipitation in most grids over the basin. A shift in seasonal precipitation was also established. Furthermore, the rising and falling trends of precipitation were observed at higher elevation and at lower elevation respectively. The result also revealed a temporal and spatial variation in precipitation over the basin.

8.2 Paper Two Discussion

As an improvement over the previous result, the study furthered the investigation of the hydrometeorological variables in the study area by analysing the spatiotemporal trends as well

as the relationship between precipitation, river discharge, maximum and minimum temperature over between 1971 and 2013. The data used in this analysis were limited to observed station data. The abrupt change points were corrected using a recently developed methodology for change point correction in climate time series. Hence, a new homogenized data was generated. Furthermore, the relationship between hydrometeorological variables was established.

The monthly analysis of temperature variables showed the monthly range of maximum and minimum temperature varied from 24 to 41 ^{o}C and 11 to 27 ^{o}C respectively. The highest values of maximum temperature were seen from March to June. These months precede the rain months and months with high river discharge (Adeyeri et al. 2019b). This may be attributed to the intensification of convective precipitation at high temperatures (Berg et al. 2013) especially in conditions where the ocean drives the atmosphere. For minimum temperature, the highest values are seen from March to October while the lowest values are seen from December to February. Higher values of minimum temperature may be attributed to the formation of stratiform cloud in the mornings (Janiga and Thorncroft 2014). There was also an increasing trend in both annual maximum and minimum temperature for the period of study. However, the rate of increase in minimum temperature (0.05 ^{o}C/year) was higher than the rate of increase maximum temperature (0.03 ^{o}C/year).

The monthly trend showed a non-significant decrease in the trend of discharge for all months except the months of June, July, August, September and November. This was confirmed by (Adeyeri et al. 2019b) that the river discharge in these months was between 20 to 100 mm/month while the other months have decreasing discharge. However, for the seasonal trends, there are significantly increasing trends of discharge in both wet and annual seasons. The dry season had a non-significant decreasing trend. For the precipitation time series, there is a non-significant decreasing trend in May, June and July. The seasonal analysis shows an increasing trend of precipitation for all seasons. These findings agree with (USGS 2012) who reported an increasing trend of temperature in the Sahel as a consequence of the warming of the northern Atlantic Ocean and the Mediterranean, thereby, increasing the meridional convergence of external moisture at of low-levels. This eventually increases the precipitation in the region and creating a partial precipitation recovery especially in the 1990s. Consequently, yearly variations in precipitation are greatly influenced by local moisture recycling rate which is controlled by planetary flow configurations linked with the El Niño-Southern Oscillation.

To further understand the relationship between precipitation, river discharge, minimum and maximum temperature, the correlation plot among these variables are examined.

In the dry season, a positive correlation was established between precipitation, minimum temperature, maximum temperature and years. However, river discharge shows a negative

correlation with the temperature variables. During the wet season, a positive correlation was established among all variables except for the negative correlation between river discharge and the two temperature variables. For the annual season, all variables show positive correlations except for the correlation between discharge and maximum temperature while there is no correlation between discharge and minimum temperature. In all seasons, the river discharge and precipitation have strong positive correlations. Spatially, there was a latitudinal increase (decrease) in the basin temperature (precipitation) from lower to higher latitudes. Additionally, there was an overall increasing temperature and precipitation trend in the basin.

8.3 Paper Three Discussion

To further understand how the trend observed above affects the river discharge in the basin, the variations in river discharge as a result of the contributory effects of precipitation variability and human influences was examined using daily homogenised precipitation and discharge data between 1971 and 2013. Results of the LULC classification reveals some level of alterations in the LULC classes from 1975 to 2013. Accordingly, there has been an increase in bare surface, plantation, settlements and water bodies from 1975 to 2013, together with a decrease in the forest, and grassland coverage. Irrigated agriculture increased from 1975 to 2000 before declining from 2000 to 2013. For the entire period, i.e. from 1975 to 2013, there is a continuous decrease in forest and grassland while there are gains in other LULC classes. Overall, plantation has the highest gain of 41% while grassland has the highest loss of 38%. Results from other studies (Hundecha and Bárdossy 2004) have shown that the transformations in basin's LULC classes have significant effects on the river discharge. There was also an increasing trend of precipitation and river discharge. Furthermore, it was established that the increasing precipitation trend is as a result of the precipitation recovery after the droughts episodes which subsequently led to an increase in river discharge.

The assessment of LULC revealed that the period with the highest discharge means coincided with the periods of reduced irrigated agriculture, forest and grassland. This means that a reduced irrigated agriculture, forest and grassland potentially reduced the rate of evapotranspiration and infiltration as well as interception loss, hence, making more water available for discharge downstream.

Using the DCC, the relationship between discharge and precipitation should exhibit a straight line without breakages, provided that there are no external influences. The DCC and GEV result identified three major breakpoints in 1974 and 1993, suggesting that the changes in discharge were not only from precipitation variability but also from human influences. These change points correspond to the years when the different dams and the large-scale irrigation schemes

became fully operational. Further results showed that the impact of human activities and precipitation variability on river discharge was equally shared.

8.4 Paper Four Discussion

In an attempt to further understand the susceptibility of KYB to climate change, especially how the extreme conditions affect precipitation and temperature variation from historical to future projections at two climate scenarios, the climate extreme indices were analysed using homogenized observed stations' data for past climate extremes' characteristics and an ensemble mean of 8 bias-corrected CORDEX climate models for future projection of climate extremes under two RCP scenarios.

The climate extreme indices considered are the warm day frequency (tx90p), cool night frequency (tn10p), warm night frequency (tn90p), warm spell duration indicator (wsdi), diurnal temperature range (dtr), maximum 5-days precipitation (rx5day), consecutive dry days (cdd), consecutive wet days (cwd), very wet days (r95p), extremely wet days (r99p), and annual total precipitation (prctot).

There was an overall positive trend is observed in warm day frequency, warm night frequency and warm spell duration while the cold night frequency has an overall negative trend over the entire stations for the observed historical period (1971-2017). To test the ability of the bias-corrected CORDEX data to reproduce the spatial trends of the temperature indices, the spatial trend of the bias-corrected CORDEX data is analysed between 1979 and 2005. The result showed a similar trend with the station-controlled historical temperature indices, however, with different magnitudes.

Unlike temperature, the variations in the trend of precipitation were dependent on local and regional characteristics. The spatial pattern of the trends validation period and bias-corrected CORDEX data between 1979 and 2005 showed an increasing trend of maximum 5-days precipitation, consecutive dry days, very wet days and annual total precipitation while the consecutive wet days and extremely wet days had decreasing trends in most parts of the basin.

The bias-corrected CORDEX performed better than the raw CORDEX in reproducing the trends of the climate indices for the station controlled historical period between 1979 and 2005. It was also able to capture the significant observed direction and magnitude in the indices. This provides the basis and confidence in using the bias correction method for future projections.

The results of climate indices over the basin under two representative concentration pathways (RCP4.5 and RCP 8.5) projections for global warming for two-time slices are also discussed. The time slices are given near future (2020-2050) and far future (2060-2090). Under RCP4.5, the near future trends in cool day frequency, cool night frequency and diurnal temperature range

were seen to be significantly decreasing in all stations except for three stations with non-significant negative trend in diurnal temperature range. The trend in warm day frequency, warm night frequency and warm spells duration were seen to be significantly positive in all stations except for two stations with non-significant positive trend in warm night frequency. All precipitation indices except consecutive dry days are observed to have negative trends in the near future with the highest negative trend of -39.02 mm/year in annual total precipitation.

For far future, cool day frequency and cool night frequency still exhibited significant negative trend in for all stations in the basin. However, diurnal temperature range both significant and non-significant negative trend although with some stations like Bauchi, Gombe, Potiskum and Zinder having no trend. Positive trend in warm day and warm night frequencies was evident in all stations. All trends turned positive for annual total precipitation, having the highest positive trend of 23.33 mm/year except for Goure Katsina and Zinder with negative trends of -1.67, -0.56 and -6.24 mm/year respectively. Nevertheless, other precipitation indices have mixed positive and negative trends for the stations. Overall, there is a drying trend in the basin.

Under RCP8.5, results of near future analysis showed significant negative trends in cool night frequency, cool day frequency and diurnal temperature range for all stations while all stations exhibited significant increasing trend in warm day frequency, warm night frequency and warm spell duration.

All precipitation indices showed negative trends except for the consecutive dry days with some positive trends. The highest negative trend of -36.46 mm/year was recorded in annual total precipitation. The negative trends in annual total precipitation are significant in all stations within the basin. Maximum 5-days precipitation, consecutive wet days, very wet days and extremely wet days all have negative trends for every station, although with some degree of significance and non-significance.

For far future analysis, there was a negative trend in the diurnal temperature ranges and cool night and cool day frequencies. There was a positive trend in warm spell duration and warm day and warm night frequencies. The spatial pattern of the trend showed that negative trend in cold day and cold night frequencies increases towards the southern part of the basin while the warm day and warm night frequencies positive trends also increase towards the southern part. The warm spell duration increases towards the northern part of the basin. The magnitude of trend analysis comparison of the historical extremes with RCP 4.5 both for near and far future shows an increasing magnitude of the temperature extreme events.

All precipitation indices trend was positive except for consecutive wet days with a not-significant negative trend at Goure. The highest positive trend (48.35 mm/year) was reported for annual total precipitation at Jos. There are mixed occurrences of both significant and not-

significant trends for this time slice. The spatial trend showed that all precipitation indices show increment towards the southern part of the basin except for consecutive dry days which shows an increment towards the north-western part of the basin.

In general, there was no global pattern in of precipitation extreme trends between RCP 4.5 and 8.5 because the pattern of magnitude and trend depends on the location of the station. However, most of the indices had an increasing magnitude from RCP 4.5 to 8.5.

However, the uncertainties associated with climate change impact assessment on extreme indices cannot be under-emphasised. This includes GCM and RCM configurations and the RCP scenarios. The uncertainties associated with GCMs and RCMs are usually from parameterisation, climate approximations, boundary and initial conditions (IPCC 2013).

(Kyselý and Beranová 2009) established that the simulated outputs from precipitation extremes depend on the model, most especially, the parameterisation of convective processes. The practicality of any GCM, RCM simulations as well as RCP scenarios is under constant questioning due to several sources of uncertainties. However, in this study, the uncertainty range was minimized by the model ensemble experiments.

To quantify the uncertainties associated with the model projection, for example, all models seem to have similar range for extremely wet days for most part of the projection period for Maine station while this is not same for diurnal temperature range.

Generally, over the study area, the magnitude of the trends of hot extremes was greater than the cold extremes which imply that the distributions of the warm extremity associated with the increasing daily temperature are changing more rapidly than the cold ends. The increased positive trends in total annual precipitation and corresponding positive trends in the intensity of wet events coincide with the positive trends of hot extremes which indicate the capacity of the warmer air to hold more moisture resulting in a prolonged low-level moisture convergence and possible occurrence of storm activities in the region. Furthermore, the historical and future climate extreme characteristics revealed similar patterns of trends over the study area. However, the magnitude of the projected climate extremes, most importantly temperature, was continually greater in the latter years. These consistencies could be scaled with the RCP emission scenarios which have demonstrated a strong relationship between the anthropogenic GHG emissions and potential environmental impacts.

8.5 Paper Five Discussion

Having established some climate extremes conditions in the study area for historical and future projections in the above discussion, it is therefore important to accurately represent the response of the stream flow to these extreme events which are caused by climate change. In order to

precisely represent this response, there is a need for a robust hydrological modelling which will take into account the exact hydrological properties of the study area even in the face of climate extremes. To this regard, the calibration of a conceptual hydrological model was done using six evolutionary optimization methods (SCE-R, DE, PSO, MALS, LOMS and MCMC) and three combined objective functions (i.e. minimizing RMSE, maximizing both NSE and KGE) over the study area. The robustness of the calibration approaches was validated by considering two episodes (1974-2013 and 1980-2013) for the analysis. It is worth to note that changing the calibration episodes has little to no effect on the generated model parameters. This ascertains the robustness of the optimization and calibration approaches. Results from this analysis revealed that the applied calibration methods showed reasonable abilities to simulate runoff with a satisfactory level of accuracy. The results of the flow statistics were not universally consistent as some optimization methods overestimates while others continually underestimate the flow representation. The performance evaluation showed that MCMC has the highest values of mean absolute error (0.28) and mean square error (0.40) while LOMS and MCMC recorded a low volumetric efficiency of 0.56. This means that these two optimization techniques mismatched the fractional volume of water delivered per unit time. However, all other techniques perform better in the fraction of water delivered. For the particular case of KYB, we found that the DE and the SCE-R methods performed best. The multi-objective computational assessment for each optimization methods to reach the optimal Pareto solutions showed that MALS exhibits the highest number of iterations while the PSO had the highest number of simulations for both calibration periods. The lowest iterations and simulations were exhibited by the SCE-R approach in all cases. Comparing the computational period and the performance metric of SCE-R indicated a trade-off balance between computational period and simulation accuracy. The wavelet spectra plot of the runoff variance across different time scales for the first simulation phase showed slight differences in the results of the optimization techniques. For the observation, there was 3 to 4 years periodicity of high-frequency power from 1974 to 1992. However, this periodicity is only significant between 1979-1992 and 2005-2008. The highest wavelet power of between 11 and 12 years is captured by all techniques. This high periodicity is assumed to be caused by high precipitation variability as well as the impact of human activities in the runoff in the basin (Adeyeri et al. 2019b; Nicholson 2001). A dominant episode of significant power between 6 and 7 years was observed between 1990 and 2000. This was accurately replicated by the SCE-R while other techniques apart from MCMC underestimated it. Furthermore, the wavelet phases were accurately captured by all techniques. In general, the magnitude of the wavelet coefficient is accurately represented by all optimization techniques.

Based on these evaluations, it is concluded that the combination of multi-objective functions and multi-optimization techniques for optimal Pareto sets for GR5J model parameters over the KYB do not only improve the stability of the model parameters during calibration, but also improve the optimization ability of the calibration algorithms towards more accurate and robust representation of the river runoff in the basin.

Chapter 9: General conclusion and perspectives

This study investigated the hydrological response of the trans-boundary Komadougu-Yobe basin of West Africa to climate change. There is an overall increasing trend of temperature and precipitation in the basin.

This temperature increase could reduce the availability of pastures to feed livestock, affect crop yield and intensify the impact of droughts (Hatfield and Prueger 2015). On the other hand, increasing precipitation as a result of the Sahelian precipitation recovery could revive the wetlands in the basin thereby maintaining the food chain balance and preserving the ecosystem. However, excess water could lead to flooding, thus, farmlands, farm produce and properties could be affected. This could have significant impacts on water management and the socio-economic activity in the basin. Furthermore, the impacts of drought on water demand and supply by natural systems and humans could be aggravated by the warming climate (Cook et al. 2015).

The river discharge also had an increasing trend, which might be related to the ability of the constructed dams to retain water in the wet season and later release it evenly throughout the year. This is in agreement with the findings of (Adams 1993). Furthermore, the increasing precipitation trend as a result of the precipitation recovery after the droughts episodes can also lead to an increase in discharge (Guo et al. 2014).

The distribution of LULC also affects the volume of river discharge. For example, volume of discharge increased as with a reduction in irrigated agriculture, forest and grassland. This means that a reduced irrigated agriculture, forest and grassland potentially reduced the rate of evapotranspiration and infiltration as well as interception loss, hence, making more water available for discharge downstream, as also suggested by e.g. (Jia et al. 2009) and (Spracklen et al. 2012). Additionally, our result is in line with several studies reporting that basin's discharge significantly increased after deforestation while it decreases with afforestation (Tuteja et al. 2007), as an increase in water bodies increases the discharge coefficient, despite a higher evaporation rate caused by the LULC change (Li and Shi 2015). As reported by (Wang and Hejazi 2011), climate variability and human activities are generally seen as the main forces causing an alteration in river discharge. On the other hand, there was an increasing trend of extreme events in the basin.

In order to precisely represent the hydrological response of the basin to climate change, a robust hydrological modelling strategy was developed to take into account the exact hydrological properties of the study area even in the face of climate extremes. The combination of multi-objective functions and multi-optimization techniques for optimal Pareto sets for hydrological

modelling strategy over the KYB do not only improve the stability of the model parameters during calibration, but also improve the optimization ability of the calibration algorithms towards more accurate and robust representation of the river discharge in the basin in the context of climate change, climate extremes and water resources.

The environmental impacts associated with increasing extreme climate events and constrained by anthropogenic climate change will attract severe costs especially to vulnerable economies (like of the study area) in West Africa.

Therefore, the attempts in this study to characterize areas in the river basin with the potential risk of climate extreme events will serve as a useful resource for assessments of the potential impacts of climate change on human, ecosystems, water resources, and in turn enhance regional adaptation, hazard preparedness, planning strategies, and decision making. Adequate measures and relevant developmental practices should be put in place to mitigate the warming trend as well as flooding that could arise as a result of the increased precipitation. However, in an attempt to secure the basin resources from climate change and climate extreme events, feasibility studies and environmental impact assessment should be prioritised before embarking on relevant developmental projects.

Thus, to reach a more definitive conclusion, future work must seek to explore and improve individual regional climate simulation, especially of precipitation, to reduce uncertainties and discrepancies in model outputs.

Future work should seek to project the response of the river discharge in the basin to climate change for future climate scenarios. A more robust bias-correcting technique should be implored in order to accurately represent the basin's climatic properties in the regional climate model outputs.

Reference

Abatan AA, Abiodun BJ, Gutowski WJ, Rasaq-Balogun SO (2018a) Trends and variability in absolute indices of temperature extremes over Nigeria: linkage with NAO. Int. J. Climatol 38:593–612. doi: 10.1002/joc.5196

Abatan AA, Osayomi T, Akande SO, Abiodun BJ, Gutowski WJ (2018b) Trends in mean and extreme temperatures over Ibadan, Southwest Nigeria. Theor Appl Climatol 131:1261–1272. doi: 10.1007/s00704-017-2049-1

Abbaspour KC, Faramarzi M, Ghasemi SS, Yang H (2009) Assessing the impact of climate change on water resources in Iran. Water Resour. Res. 45:413–425.

Abiodun BJ, Adegoke J, Abatan AA, Ibe CA, Egbebiyi TS, Engelbrecht F, Pinto I (2017) Potential impacts of climate change on extreme precipitation over four African coastal cities. Climatic Change 143:399–413. doi: 10.1007/s10584-017-2001-5

Acquaotta F, Fratianni S (2014) The importance of the quality and reliability of the historical time series for the study of climate change. ABClima 14:1–10.

Acquaotta F, Fratianni S, Venema V (2016) Assessment of parallel precipitation measurements networks in Piedmont, Italy. Int. J. Climatol. 36:3963–3974. doi: 10.1002/joc.4606

Adams WM (1993) Indigenous Use of Wetlands and Sustainable Development in West Africa. The Geographical Journal 159:209–220. doi: 10.2307/3451412

Adeniyi MO, Oladiran EO (2000) Air sea interaction: ENSO phenomenon as it affects periodicity of flooding in Nigeria. Sci. Res. 2:30–35

Adeyeri OE, Okogbue EC, Ishola KA (2017a) Climate Change and Coastal Floods: The Susceptibility of Coastal Areas of Nigeria. J Coast Zone Manag 20:1–8.

Adeyeri OE, Akinsanola AA, Ishola KA (2017b) Investigating surface urban heat island characteristics over Abuja, Nigeria: Relationship between land surface temperature and multiple vegetation indices. Remote Sensing Applications: Society and Environment 7:57–68. doi: 10.1016/j.rsase.2017.06.005

Adeyeri OE, Lamptey B, Lawin AE, Sanda IS (2017c) Spatio-Temporal Precipitation Trend and Homogeneity Analysis in Komadougu-Yobe Basin, Lake Chad Region. J Climatol Weather Forecasting 05:1-10. doi: 10.4172/2332-2594.1000214

Adeyeri OE, Okogbue EC, Akinluyi FO, Ishola KA (2017d) Spatio-Temporal Trend of Vegetation Cover over Abuja using Landsat Datasets. International Journal of Agriculture and Environmental Research: 3:1–8.

Adeyeri OE, Lawin AE, Laux P, Ishola KA, Ige SO (2019a) Analysis of climate extreme indices over the Komadougu-Yobe basin, Lake Chad region: Past and future occurrences. Weather and Climate Extremes 23:100194. doi: 10.1016/j.wace.2019.100194

Adeyeri OE, Laux P, Lawin AE, Arnault J (2019b) Assessing the impact of human activities and precipitation variability on the river discharge of Komadugou-Yobe Basin, Lake Chad Area. Environmental Earth Sciences (Submitted)

Aguilar E (2003) Guidelines on climate metadata and homogenization. WMO/TD, no. 1186. World Meteorological Organization, Geneva. 60pp.

Akinsanola AA, Ajayi VO, Adejare AT, Adeyeri OE, Gbode IE, Ogunjobi KO, Nikulin G, Abolude AT (2018) Evaluation of rainfall simulations over West Africa in dynamically downscaled CMIP5 global circulation models. Theor Appl Climatol 132:437–450.

Akinsanola AA, Ogunjobi KO (2017) Recent homogeneity analysis and long-term spatio-temporal rainfall trends in Nigeria. Theor Appl Climatol 128:275–289.

Alamou EA, Obada E, Afouda A (2017) Assessment of Future Water Resources Availability under Climate Change Scenarios in the Mékrou Basin, Benin. Hydrology 4:51–62.

Alexandersson H (1986) A homogeneity test applied to precipitation data. J. Climatol. 6:661–675. doi: 10.1002/joc.3370060607

Arnold JG, Fohrer N (2005) SWAT2000: current capabilities and research opportunities in applied watershed modelling. Hydrol. Process. 19:563–572. doi: 10.1002/hyp.5611

Ati OF, Stigter CJ, Oladipo EO (2002) A comparison of methods to determine the onset of the growing season in northern Nigeria J. Climatol. 22:12–20.

Attogouinon A, Lawin Agnidé, E., M'Po Yèkambèssoun, N'Tcha, Houngue R (2017) Extreme Precipitation Indices Trend Assessment over the Upper Oueme River Valley-(Benin). Hydrology 4:36–60. doi: 10.3390/hydrology4030036

Awotwi A, Anornu GK, Quaye-Ballard J, Annor T, Forkuo EK (2017) Analysis of climate and anthropogenic impacts on runoff in the Lower Pra River Basin of Ghana. Heliyon 3: e00477–e00490. doi: 10.1016/j.heliyon. 2017.e00477

Babamaaji RA, Lee J (2014) Land use/land cover classification of the vicinity of Lake Chad using NigeriaSat-1 and Landsat data. Environ Earth Sci 71:4309–4317.

Baines PG, Folland CK (2007) Evidence for a Rapid Global Climate Shift across the Late 1960s. J. Climate 20:2721–2744. doi: 10.1175/JCLI4177.1

Bechtold P, Bazile E, Guichard F, Mascart P, Richard E (2001) A mass-flux convection scheme for regional and global models. Q.J Royal Met. Soc. 127:869–886.

Bekele EG, Nicklow JW (2007) Multi-objective automatic calibration of SWAT using NSGA-II. Journal of Hydrology 341:165–176. doi: 10.1016/j.jhydrol.2007.05.014

Bellin A, Majone B, Cainelli O, Alberici D, Villa F (2016) A continuous coupled hydrological and water resources management model. Environmental Modelling & Software 75:176–192. doi: 10.1016/j.envsoft.2015.10.013

Berg P, Moseley C, Haerter JO (2013) Strong increase in convective precipitation in response to higher temperatures. Nature Geosci 6:181–185. doi: 10.1038/ngeo1731

Bergmeir C, Molina D, Benítez JM (2016) Memetic Algorithms with Local Search Chains in R : The Rmalschains Package. J. Stat. Soft. 75:1–10. doi: 10.18637/jss.v075.i04

Beven KJ (2011) Rainfall-runoff modelling: The primer, 2nd ed. Wiley-Blackwell, Chichester, West Sussex, Hoboken, NJ. 120pp.

Bian GD, Du JK, Song MM, Xu YP, Xie SP, Zheng WL, Xu C-Y (2017) A procedure for quantifying runoff response to spatial and temporal changes of impervious surface in Qinhuai River basin of southeastern China. CATENA 157:268–278.

Braak CJFT (2006) A Markov Chain Monte Carlo version of the genetic algorithm Differential Evolution: easy Bayesian computing for real parameter spaces. Statistics Computing 16:239–249.

Buishand TA (1982) Some methods for testing the homogeneity of rainfall records. Journal of Hydrology 58:11–27. doi: 10.1016/0022-1694(82)90066-X

Buma W, Lee S-I, Seo J (2016) Hydrological Evaluation of Lake Chad Basin Using Space Borne and Hydrological Model Observations. Water 8:205–220. doi: 10.3390/w8050205

Caussinus H, Lyazrhi F (1997) Choosing a Linear Model with a Random Number of Change-Points and Outliers, vol 49. Springer, Netherlands, 100pp.

Chaney NW, Sheffield J, Villarini G, Wood EF (2014) Development of a High-Resolution Gridded Daily Meteorological Dataset over Sub-Saharan Africa: Spatial Analysis of Trends in Climate Extremes. J. Climate 27:5815–5835. doi: 10.1175/JCLI-D-13-00423.1

Charney J, Quirk WJ, Chow S–h, Kornfield J (1977) A Comparative Study of the Effects of Albedo Change on Drought in Semi–Arid Regions. J. Atmos. Sci. 34:1366–1385.

Chattopadhyay S, Edwards D (2016) Long-Term Trend Analysis of Precipitation and Air Temperature for Kentucky, United States. Climate 4:10–20. doi: 10.3390/cli4010010

Chien H, Yeh PJ-F, Knouft JH (2013) Modeling the potential impacts of climate change on streamflow in agricultural watersheds of the Midwestern United States. Journal of Hydrology 491:73–88. doi: 10.1016/j.jhydrol.2013.03.026

Christensen JH, Christensen OB (2007) A summary of the PRUDENCE model projections of changes in European climate by the end of this century. Climatic Change 81:7–30.

Chu H-J (2012) Assessing the relationships between elevation and extreme precipitation with various durations in southern Taiwan using spatial regression models. Hydrol. Process. 26:3174–3181. doi: 10.1002/hyp.8403

Clerc M, Kennedy J (2002) The particle swarm - explosion, stability, and convergence in a multidimensional complex space. IEEE Trans. Evol. Computat. 6:58–73.

Cleveland WS (1979) Robust Locally Weighted Regression and Smoothing Scatterplots. Journal of the American Statistical Association 74:829–836.

Cleveland WS (1984) Graphs in Scientific Publications. The American Statistician 38:261–270.

Coe MT, Foley JA (2001) Human and natural impacts on the water resources of the Lake Chad basin. Geographical Research: Atmospheres 106:1–18.

Cook BI, Ault TR, Smerdon JE (2015) Unprecedented 21st century drought risk in the American Southwest and Central Plains. Sci Adv 1: e1400082–e1400099.

Cooper VA, Nguyen V-T-V, Nicell JA (2007) Calibration of conceptual rainfall–runoff models using global optimisation methods with hydrologic process-based parameter constraints. Journal of Hydrology 334:455–466. doi: 10.1016/j.jhydrol.2006.10.036

Coron L, Thirel G, Delaigue O, Perrin C, Andréassian V (2017) The suite of lumped GR hydrological models in an R package. Environmental Modelling & Software 94:166–171.

Cotillon SE (2017) West Africa land use and land cover time series. U.S. Geological Survey Fact Sheet:2017–3004. doi: 10.3133/fs20173004

Criss RE, Winston WE (2008) Do Nash values have value? Discussion and alternate proposals. Hydrol. Process. 22:2723–2725. doi: 10.1002/hyp.7072

Cunderlik JM, Burn DH (2004) Linkages between Regional Trends in Monthly Maximum Flows and Selected Climatic Variables. J. Hydrol. Eng. 9:246–256.

Deb K, Pratap A, Agarwal S, Meyarivan T (2002) A fast and elitist multiobjective genetic algorithm: NSGA-II. IEEE Trans. Evol. Computat. 6:182–197. doi: 10.1109/4235.996017

Destouni G, Jaramillo F, Prieto C (2013) Hydroclimatic shifts driven by human water use for food and energy production. Nature Clim Change 3:213–217. doi: 10.1038/nclimate1719

Diallo I, Giorgi F, Deme A, Tall M, Mariotti L, Gaye AT (2016) Projected changes of summer monsoon extremes and hydroclimatic regimes over West Africa for the twenty-first century. Clim Dyn 47:3931–3954. doi: 10.1007/s00382-016-3052-4

Doğu E, Kocakoç İD (2011) Estimation of Change Point in Generalized Variance Control Chart. Communications in Statistics - Simulation and Computation 40:345–363.

Döll P, Kaspar F, Lehner B (2003) A global hydrological model for deriving water availability indicators: model tuning and validation. Journal of Hydrology 270:105–134.

Domonkos P, Coll J (2017) Homogenisation of temperature and precipitation time series with ACMANT3: method description and efficiency tests. Int. J. Climatol. 37:1910–1921.

Donders TH, Wagner F, Visscher H (2005) Quantification Strategies for Human-Induced and Natural Hydrological Changes in Wetland Vegetation, Southern Florida, USA. Quat. res. 64:333–342. doi: 10.1016/j.yqres.2005.08.016

Donnelly-Makowecki LM, Moore RD (1999) Hierarchical testing of three rainfall–runoff models in small forested catchments. Journal of Hydrology 219:136–152.

Dosio A (2017) Projection of temperature and heat waves for Africa with an ensemble of CORDEX Regional Climate Models. Clim Dyn 49:493–519.

Dosio A, Panitz H-J (2016) Climate change projections for CORDEX-Africa with COSMO-CLM regional climate model and differences with the driving global climate models. Clim Dyn 46:1599–1625. doi: 10.1007/s00382-015-2664-4

Duan Q (2003) Calibration of watershed models. Water science and application American Geophysical Union, Washington, D.C. 6:1–12.

Duan QY, Gupta VK, Sorooshian S (1993) Shuffled complex evolution approach for effective and efficient global minimization. J Optim Theory Appl 76:501–521.

Dumedah G, Berg AA, Wineberg M, Collier R (2010) Selecting Model Parameter Sets from a Trade-off Surface Generated from the Non-Dominated Sorting Genetic Algorithm-II. Water Resour Manage 24:4469–4489. doi: 10.1007/s11269-010-9668-y

Efstratiadis A, Koutsoyiannis D (2010) One decade of multi-objective calibration approaches in hydrological modelling: a review. Hydrological Sciences Journal 55:58–78.

Ejieji CJ, Amodu MF, Adeogun AG (2016) Prediction of the streamflow of Hadejia-Jama'are-Komadougu-Yobe-River Basin, North Eastern Nigeria, using swat model. Ethiop. J. Env Stud & Manag 9:209–220. doi: 10.4314/ejesm.v9i2.8

Ekpoh IJ, Nsa E (2011) Extreme Climatic Variability in North-western Nigeria: An Analysis of Rainfall Trends and Patterns. JGG 3:20–30. doi: 10.5539/jgg.v3n1p51

Engelbrecht FA, McGregor JL, Engelbrecht CJ (2009) Dynamics of the Conformal-Cubic Atmospheric Model projected climate-change signal over southern Africa. Int. J. Climatol. 29:1013–1033. doi: 10.1002/joc.1742

Fasona M, Tadross M, Abiodun B, Omojola A (2011) Local Climate Forcing and Eco-Climatic Complexes in the Wooded Savannah of Western Nigeria. NR 02:155–166.

Fasona MJ, Omojola AS (2005) Climate Change, Human Security and Communal Clashes in Nigeria. International Workshop on Human Security and Climate Change 5:21–23.

Foglia L, Hill MC, Mehl SW, Burlando P (2009) Sensitivity analysis, calibration, and testing of a distributed hydrological model using error-based weighting and one objective function. Water Resour. Res. 45:1053–1075. doi: 10.1029/2008WR007255

Funk C, Peterson P, Landsfeld M, Pedreros D, Verdin J, Shukla S, Husak G, Rowland J, Harrison L, Hoell A, Michaelsen J (2015) The climate hazards infrared precipitation with stations—a new environmental record for monitoring extremes. Sci Data 2:1–15.

Gao P, Mu X-M, Wang F, Li R (2011) Changes in streamflow and sediment discharge and the response to human activities in the middle reaches of the Yellow River. Hydrol. Earth Syst. Sci. 15:1–10. doi: 10.5194/hess-15-1-2011

Gay D (1990) Usage summary for selected optimization routines. Computing Science Technical Report 5:20-35.

Gbobaniyi E, Sarr A, Sylla MB, Diallo I, Lennard C, Dosio A, Dhiédiou A, Kamga A, Klutse NAB, Hewitson B, Nikulin G, Lamptey B (2014) Climatology, annual cycle and interannual variability of precipitation and temperature in CORDEX simulations over West Africa. Int. J. Climatol. 34:2241–2257. doi: 10.1002/joc.3834

Giannini A, Saravanan R, Chang P (2003) Oceanic forcing of Sahel rainfall on interannual to interdecadal time scales. Science 302:1027–1030. doi: 10.1126/science.1089357

Giorgi F, Colin J, Ghassem, R, Asrar (2009) Addressing climate information needs at the regional level: the CORDEX framework. World Meteorological Organization (WMO) Bulletin, 175pp.

Gudmundsson L, Bremnes JB, Haugen JE, Engen-Skaugen T (2012) Technical Note: Downscaling RCM precipitation to the station scale using statistical transformations – a comparison of methods. Hydrol. Earth Syst. Sci. 16:3383–3390.

Guo Y, Li Z, Amo-Boateng M, Deng P, Huang P (2014) Quantitative assessment of the impact of climate variability and human activities on runoff changes for the upper reaches of Weihe River. Stoch Environ Res Risk Assess 28:333–346. doi: 10.1007/s00477-013-0752-8

Gupta HV, Kling H, Yilmaz KK, Martinez GF (2009) Decomposition of the mean squared error and NSE performance criteria: Implications for improving hydrological modelling. Journal of Hydrology 377:80–91. doi: 10.1016/j.jhydrol.2009.08.003

Gupta HV, Sorooshian S, Yapo PO (1998) Toward improved calibration of hydrologic models: Multiple and noncommensurable measures of information. Water Resour. Res. 34:751–763. doi: 10.1029/97WR03495

Haario H, Saksman E, Tamminen J (2005) Componentwise adaptation for high dimensional MCMC. Computational Statistics 20:265–273. doi: 10.1007/BF02789703

Haario H, Laine M, Mira A, Saksman E (2006) DRAM: Efficient adaptive MCMC. Stat Comput 16:339–354. doi: 10.1007/s11222-006-9438-0

Hamed KH, Ramachandra Rao A (1998) A modified Mann-Kendall trend test for autocorrelated data. Journal of Hydrology 204:182–196.

Hao FH, Chen LQ, Liu CM, Dai D (2004) Impact of land use change on runoff and sediment yield. Journal of Soil and Water Conservation 8:5–8.

Hatfield JL, Prueger JH (2015) Temperature extremes: Effect on plant growth and development. Weather and Climate Extremes 10:4–10. doi: 10.1016/j.wace.2015.08.001

Hoerling M, Hurrell J, Eischeid J, Phillips A (2006) Detection and Attribution of Twentieth-Century Northern and Southern African Rainfall Change. J. Climate 19:3989–4008.

Hundecha Y, Bárdossy A (2004) Modeling of the effect of land use changes on the runoff generation of a river basin through parameter regionalization of a watershed model. Journal of Hydrology 292:281–295. doi: 10.1016/j.jhydrol.2004.01.002

Huntington TG (2006) Evidence for intensification of the global water cycle: Review and synthesis. Journal of Hydrology 319:83–95. doi: 10.1016/j.jhydrol.2005.07.003

Ige SO, Ajayi VO, Adeyeri OE, Oyekan KSA (2017) Assessing remotely sensed temperature humidity index as human comfort indicator relative to landuse landcover change in Abuja, Nigeria. Spat. Inf. Res. 25:523–533. doi: 10.1007/s41324-017-0118-2

Ilonen J, Kamarainen J-K, Lampinen J (2003) Differential evolution training algorithm for feed-forward neural networks. Neural Processing Letters 17:93–105.

IPCC (2013) Climate change 2013: The physical science basis : summary for policymakers, a report of Working Group I of the IPCC, technical summary, a report accepted by Working Group I of the IPCC but not approved in detail and frequently asked questions : part of the Working Group I contribution to the fifth assessment report of the Intergovernmental Panel on Climate Change. Intergovernmental Panel on Climate Change, New York

IUCN (2011) International Union for Conservation of Natural Resources (IUCN) and Hadejia Nguru Wetland Conservation Project (HNWCP). The Hadejia - Nguru Wetlands Report, 124pp.

Janiga MA, Thorncroft CD (2014) Convection over Tropical Africa and the East Atlantic during the West African Monsoon: Regional and Diurnal Variability. J. Climate 27:4159–4188.

Jia Y, Zhao H, Niu C, Jiang Y, Gan H, Xing Z, Zhao X, Zhao Z (2009) A WebGIS-based system for rainfall-runoff prediction and real-time water resources assessment for Beijing. Computers & Geosciences 35:1517–1528. doi: 10.1016/j.cageo.2008.10.004

Jones, Colin F, Giorgi G, Asrar (2011) The Coordinated Regional Downscaling Experiment: CORDEX–an international downscaling link to CMIP5. CLIVAR exchanges 16.2:34–40

Jones JR, Schwartz JS, Ellis KN, Hathaway JM, Jawdy CM (2015) Temporal variability of precipitation in the Upper Tennessee Valley. Journal of Hydrology: Regional Studies 3:125–138. doi: 10.1016/j.ejrh.2014.10.006

Joshi R, Sanderson AC (1999) Minimal representation multisensor fusion using differential evolution. IEEE Trans. Syst., Man, Cybern. A 29:63–76. doi: 10.1109/3468.736361

Karl TR, Knight RW (1998) Secular Trends of Precipitation Amount, Frequency, and Intensity in the United States. Bull. Amer. Meteor. Soc. 79:231–241.

Kennedy J, Eberhart RC (1995) Particle swarm optimization. In Proceedings of IEEE International Conference on Neural Networks 5:1942–1948

Khatiwada K, Panthi J, Shrestha M, Nepal S (2016) Hydro-Climatic Variability in the Karnali River Basin of Nepal Himalaya. Climate 4:17-25. doi: 10.3390/cli4020017

Kim J, Waliser DE, Mattmann CA, Goodale CE, Hart AF, Zimdars PA, Crichton DJ, Jones C, Nikulin G, Hewitson B, Jack C, Lennard C, Favre A (2014) Evaluation of the CORDEX-Africa multi-RCM hindcast: systematic model errors. Clim Dyn 42:1189–1202.

Kjellström E, Bärring L, Nikulin G, Nilsson C, Persson G, Strandberg G (2016) Production and use of regional climate model projections - A Swedish perspective on building climate services. Clim Serv 2-3:15–29. doi: 10.1016/j.cliser.2016.06.004

Klein Tank AMG, Zwiers FW, Zhang X (2009) Guidelines on analysis of extremes in a changing climate in support of informed decisions for adaptation. WMO/TD, vol 1500. WMO, Geneva, 66pp.

Kling H, Fuchs M, Paulin M (2012) Runoff conditions in the upper Danube basin under an ensemble of climate change scenarios. Journal of Hydrology 424-425:264–277.

Klutse NAB, Sylla MB, Diallo I, Sarr A, Dosio A, Diedhiou A, Kamga A, Lamptey B, Ali A, Gbobaniyi EO, Owusu K, Lennard C, Hewitson B, Nikulin G, Panitz H-J, Büchner M (2016) Daily characteristics of West African summer monsoon precipitation in CORDEX simulations. Theor Appl Climatol 123:369–386. doi: 10.1007/s00704-014-1352-3

Kyselý J, Beranová R (2009) Climate-change effects on extreme precipitation in central Europe: uncertainties of scenarios based on regional climate models. Theor Appl Climatol 95:361–374. doi: 10.1007/s00704-008-0014-8

Ladson AR, Brown R, Neal B, Nathan R (2013) A standard approach to baseflow separation using the Lyne and Hollick filter. AJWR 17:1–15. doi: 10.7158/W12-028.2013.17.1

Lampert DJ, Wu M (2015) Development of an open-source software package for watershed modeling with the Hydrological Simulation Program in Fortran. Environmental Modelling & Software 68:166–174. doi: 10.1016/j.envsoft.2015.02.018

Lamptey BL (2008) Comparison of Gridded Multisatellite Rainfall Estimates with Gridded Gauge Rainfall over West Africa. J. Appl. Meteor. Climatol. 47:185–205.

Lavenne A de, Thirel G, Andréassian V, Perrin C, Ramos M-H (2016) Spatial variability of the parameters of a semi-distributed hydrological model. Proc. IAHS 373:87–94.

Le L, Galle S (2005) How Changing Rainfall Regimes May Affect the Water Balance: A Modelling Approach in West Africa. 7th Congress of International Association of Hydrological Sciences 6:203–210

Lebel T, Ali A (2009) Recent trends in the Central and Western Sahel rainfall regime (1990–2007). Journal of Hydrology 375:52–64. doi: 10.1016/j.jhydrol.2008.11.030

Legesse D, Vallet-Coulomb C, Gasse F (2003) Hydrological response of a catchment to climate and land use changes in Tropical Africa: case study South Central Ethiopia. Journal of Hydrology 275:67–85. doi: 10.1016/S0022-1694(03)00019-2

Li X, Weller DE, Jordan TE (2010) Watershed model calibration using multi-objective optimization and multi-site averaging. Journal of Hydrology 380:277–288.

Li J, Shi W (2015) Effects of alpine swamp wetland change on rainfall season runoff and flood characteristics in the headwater area of the Yangtze River. CATENA 127:116–123.

Li WH, He YT, Yang LT (2001) A summary and perspective of forest vegetation impacts on water yield. Nat. Resources 8:398–406.

Li KY, Coe MT, Ramankutty N, Jong R de (2007) Modeling the hydrological impact of land-use change in West Africa. Journal of Hydrology 337:258–268.

Lindström G, Pers C, Rosberg J, Strömqvist J, Arheimer B (2010) Development and testing of the HYPE (Hydrological Predictions for the Environment) water quality model for different spatial scales. Hydrology Research 41:295–319. doi: 10.2166/nh.2010.007

Longobardi A, Villani P (2009) Trend analysis of annual and seasonal rainfall time series in the Mediterranean area. Int. J. Climatol. 40:12–20. doi: 10.1002/joc.2001

Lopez T, Antoine R, Kerr Y, Darrozes J, Rabinowicz M, Ramillien G, Cazenave A, Genthon P (2016) Subsurface Hydrology of the Lake Chad Basin from Convection Modelling and Observations. Surv Geophys 37:471–502. doi: 10.1007/s10712-016-9363-5

Lu D, Ye M, Meyer PD, Curtis GP, Shi X, Niu X-F, Yabusaki SB (2013) Effects of error covariance structure on estimation of model averaging weights and predictive performance. Water Resour. Res. 49:6029–6047. doi: 10.1002/wrcr.20441

Lus M de, Ravents J, Gonzlez-Hidalgo JC, Snchez JR, Cortina J (2000) Spatial analysis of rainfall trends in the region of Valencia (east Spain). Int. J. Climatol 20:1451–1469.

Lyon B, DeWitt DG (2012) A recent and abrupt decline in the East African long rains. Geophys. Res. Lett. 39:44–52. doi: 10.1029/2011GL050337

Madden RA, Williams J (1978) The Correlation between Temperature and Precipitation in the United States and Europe. Monthly Weather Rev 22:454–466.

Madsen H (2000) Automatic calibration of a conceptual precipitation-runoff model using multiple objectives. Journal of Hydrology 235(3):276–288

Maidment DR (1993) Handbook of hydrology. McGraw-Hill, New York, 120pp.

Mann HB (1945) Nonparametric Tests Against Trend. Econometrica 13:245–260.

Mao Y, Nijssen B, Lettenmaier DP (2015) Is climate change implicated in the 2013-2014 California drought? A hydrologic perspective. Geophys. Res. Lett. 42:2805–2813.

Mason S, Joubert A (1997) Simulated changes in extreme precipitation over southern Africa. Int. J. Climatol. 8:291–301.

Matalas NC, Langbein WB (1962) Information content of the mean. J. Geophys. Res. 67:3441–3448. doi: 10.1029/JZ067i009p03441

Mathevet T (2006) A bounded version of the Nash-Sutcliffe criterion for better model assessment on large sets of basins. IAHS 5:211–219.

Mearns LO, Gutowski W, Jones R, Leung R, McGinnis S, Nunes A, Qian Y (2009) A Regional Climate Change Assessment Program for North America. Eos Trans. AGU 90:311–317.

Mironov DV (2008) Parameterization of lakes in numerical weather prediction: Description of a lake model. Technical report, vol 11. DWD, Offenbach am Main, 50pp.

Molina D, Lozano M, García-Martínez C, Herrera F (2010) Memetic algorithms for continuous optimisation based on local search chains. Evol Comput 18:27–63.

Moss RH, Edmonds JA, Hibbard KA, Manning MR, Rose SK, van Vuuren DP, Carter TR, Emori S, Kainuma M, Kram T, Meehl GA, Mitchell JFB, Nakicenovic N, Riahi K, Smith SJ, Stouffer RJ, Thomson AM, Weyant JP, Wilbanks TJ (2010) The next generation of scenarios for climate change research and assessment. Nature 463:747–756.

Mouhamed L, Traore SB, Alhassane A, Sarr B (2013) Evolution of some observed climate extremes in the West African Sahel. Weather and Climate Extremes 1:19–25.

Muhammad J, Chiroma K, Yahaya D, Gashua, Abba, J. (2015) Water Management Issues in the Hadejia-Jama'are-Komadougu-Yobe Basin: DFID-JWL and Stakeholders Experience in Information Sharing, Reaching Consensus and Physical Interventions. Intergovernmental Panel on Climate Change. doi: 10.1088/1751-8113/44/8/085201

Murtaugh PA (2014) In defense of P values. Ecology 95:611–617. doi: 10.1890/13-0590.1

Nair US (2003) Impact of land use on Costa Rican tropical montane cloud forests: Sensitivity of cumulus cloud field characteristics to lowland deforestation. J. Geophys. Res. 108:541–551. doi: 10.1029/2001JD001135

Narasayya K, Roman UC, Meena BL, Sreekanth S, Naveed AS (2013) Prediction of storm-runoff using physically based hydrological model for burhanpur watershed, India:76–85

Nash JE, Sutcliffe JV (1970) River flow forecasting through conceptual models part I — A discussion of principles. Journal of Hydrology 10:282–290.

Nicholls N (2004) The Changing Nature of Australian Droughts. Climatic Change 63:323–336.

Nicholson SE (2001) Climatic and environmental change in Africa during the last two centuries. Clim. Res. 17:123–144. doi: 10.3354/cr017123

Nikulin G, Jones C, Giorgi F, Asrar G, Büchner M, Cerezo-Mota R, Christensen OB, Déqué M, Fernandez J, Hänsler A, van Meijgaard E, Samuelsson P, Sylla MB, Sushama L (2012) Precipitation Climatology in an Ensemble of CORDEX-Africa Regional Climate Simulations. J. Climate 25:6057–6078. doi: 10.1175/JCLI-D-11-00375.1

Ning S, Ishidaira H, Wang J (2015) Calibrating a hydrologic model by step-wise method using GRACE TWS and discharge data. J. JSCE, Ser. B1 71: I_85-I_90.

Odunuga S, Okeke I, Omojola A (2011) Hydro-climatic variability of the Hadejia Jama'are river systems in north-central Nigeria. IAHS 7:163–168

Oguntunde PG, Abiodun BJ, Lischeid G (2011) Rainfall trends in Nigeria, 1901–2000. Journal of Hydrology 411:207–218. doi: 10.1016/j.jhydrol.2011.09.037

Onamuti OY, Okogbue EC, Orimoloye IR (2017) Remote sensing appraisal of Lake Chad shrinkage connotes severe impacts on green economics and socio-economics of the catchment area. R Soc Open Sci 4:171–190. doi: 10.1098/rsos.171120

Onoz B, Bayazit M (2003) The power of statistical tests for trend detection. Turkish J. Eng. Environ. Sc. 8:247–251.

Oudin L, Michel C, Anctil F (2005) Which potential evapotranspiration input for a lumped rainfall-runoff model? Journal of Hydrology 303:275–289.

Oyebande L (2001) Stream flow regime change and ecological response in the Lake Chad Basin in Nigeria. In Acreman, M (ed.) Hydro-ecology: Linking hydrology to Aquatic Ecology. Int. assoc. hydrol. Science 5:1–12.

Pant GB (2003) Long-term climate variability and change over monsoon. Asia. J. Indian Geophys. Union 5:125–134

Parsons WT, Cuthbertson EG (1992) Noxious Weeds of Australia. Inkata Press, Victoria, B.C., 120pp.

Perrin C, Michel C, Andréassian V (2003) Improvement of a parsimonious model for streamflow simulation. Journal of Hydrology 279:275–289.

Pettitt AN (1979) A Non-Parametric Approach to the Change-Point Problem. Applied Statistics 28:126–138. doi: 10.2307/2346729

Philandras CM, Nastos PT, Kapsomenakis J, Douvis KC, Tselioudis G, Zerefos CS (2011) Long term precipitation trends and variability within the Mediterranean region, vol 11. Copernicus GmbH, 450pp.

Pinto I, Lennard C, Tadross M, Hewitson B, Dosio A, Nikulin G, Panitz H-J, Shongwe ME (2016) Evaluation and projections of extreme precipitation over southern Africa from two CORDEX models. Climatic Change 135:655–668. doi: 10.1007/s10584-015-1573-1

Qin H, Zhou J, Lu Y, Li Y, Zhang Y (2010) Multi-objective Cultured Differential Evolution for Generating Optimal Trade-offs in Reservoir Flood Control Operation. Water Resour Manage 24:2611–2632. doi: 10.1007/s11269-009-9570-7

Qiu L, Peng D, Xu Z, Liu W (2015) Identification of the impacts of climate changes and human activities on runoff in the upper and middle reaches of the Heihe River basin, China. J Water Climate Change 2:115–225. doi: 10.2166/wcc.2015.115

Rakovec O, Kumar R, Attinger S, Samaniego L (2016) Improving the realism of hydrologic model functioning through multivariate parameter estimation. Water Resour. Res. 52:7779–7792. doi: 10.1002/2016WR019430

Reynolds LV, Shafroth PB, LeRoy Poff N (2015) Modeled intermittency risk for small streams in the Upper Colorado River Basin under climate change. J. Hydrology 523:768–780.

Riquelme N, Lucken C von, Baran B (2015) Performance metrics in multi-objective optimization. IEEE Trans. Syst., Man, Cybern. A:1–11. doi: 10.1109/CLEI.2015.7360024

Rosenbrock HH (1960) An Automatic Method for Finding the Greatest or Least Value of a Function. The Computer Journal 3:175–184. doi: 10.1093/comjnl/3.3.175

Rusticucci M, Penalba O (2000) Precipitation seasonal cycle over Southern South America. Climate Research 8:1–15.

Samuelsson P, Jones CG, WillÃ©n U, Ullerstig A, Gollvik S, Hansson U, Jansson C, KjellstrÃ¶m E, Nikulin G, Wyser K (2011) The Rossby Centre Regional Climate model RCA3: model description and performance. TELLUSA, 8:12-23.

Sarkar S, Kafatos M (2004) Interannual variability of vegetation over the Indian sub-continent and its relation to the different meteorological parameters. Remote Sensing of Environment 90:268–280. doi: 10.1016/j.rse.2004.01.003

Sarr B (2011) Return of heavy downpours and floods in a context of changing climate. AGRHYMET Monthly Bulletin 12:9–11

Savic D (2002) Single-objective vs. multiobjective optimisation for integrated decision support. In Proceedings of the First Biennial Meeting of the International Environmental Modelling and Software Society 8:7–12

Searcy JK, Hardison CH (1960) Double-mass curves. General Surface-Water Techniques. USGS water supply paper 1541:1-15.

Sen PK (1968) Estimates of the Regression Coefficient Based on Kendall's Tau. Journal of the American Statistical Association 63:1379–1392. doi: 10.2307/2285891

Sheen KL, Smith DM, Dunstone NJ, Eade R, Rowell DP, Vellinga M (2017) Skilful prediction of Sahel summer rainfall on inter-annual and multi-year timescales. Nat Commun 8:14966–14977. doi: 10.1038/ncomms14966

Shepard D (1968) A two-dimensional interpolation function for irregularly-spaced data. In: Blue RB, Rosenberg AM (eds) the 1968 23rd ACM national conference, pp 517–524.

Shongwe ME, van Oldenborgh GJ, van den Hurk BJJM, Boer B de, Coelho CAS, van Aalst MK (2010) Projected changes in mean and extreme precipitation in Africa under global warming. Part 1: Southern Africa. J. Climate 8:12–20. doi: 10.1175/2008JCLI2317.1

Singh VP, Ramachandra Rao A, Hamed KH, Chen H-L (2003) Nonstationarities in Hydrologic and Environmental Time Series, vol 45. Springer Netherlands, Dordrecht, 80pp.

Sobowale A, Adewumi JK, Otun JA, Adie DB (2010a) Water resources potentials of Hadejia River Subcatchment of Komadougu Yobe River Basin in Nigeria. Agric Eng Int: CIGR Journal 5:1–6.

Spracklen DV, Arnold SR, Taylor CM (2012) Observations of increased tropical rainfall preceded by air passage over forests. Nature 489:282–285. doi: 10.1038/nature11390

Sriwongsitanon N, Taesombat W (2011) Effects of land cover on runoff coefficient. Journal of Hydrology 410:226–238. doi: 10.1016/j.jhydrol.2011.09.021

Storn R (1996) On the usage of differential evolution for function optimization. In: North American Fuzzy Information Processing 8:519–523.

Storn R, Price K (1997) Differential evolution-A simple and effcient heuristic for global optimization over continuous Spaces. Journal of Global Optimization 11:341–359.

Tafida AA, Galtima M (2016) An Assessment of Rural Household Vulnerability in the Hadejia Nguru Wetlands Region, Northeastern Nigeria. Journal of Global Initiatives: Policy, Pedagogy, Perspective 11:109–124.

Tang J, Yin X-A, Yang P, Yang Z (2014) Assessment of Contributions of Climatic Variation and Human Activities to Streamflow Changes in the Lancang River, China. Water Resour Manage 28:2953–2966. doi: 10.1007/s11269-014-0648-5

Tanko AI (2007) Improving Land and Water Resources Management in the Komadougu Yobe River Basin. Northern Eastern FMWR-IUCN-NCF Komadougu Yobe B Project 234, 6pp.

Taxak AK, Murumkar AR, Arya DS (2014) Long term spatial and temporal rainfall trends and homogeneity analysis in Wainganga basin, Central India. Weather Climate Ext 4:50–61.

Teutschbein C, Seibert J (2012) Bias correction of regional climate model simulations for hydrological climate-change impact studies: Review and evaluation of different methods. Journal of Hydrology 456-457:12–29. doi: 10.1016/j.jhydrol.2012.05.052

Teutschbein C, Seibert J (2013) Is bias correction of regional climate model (RCM) simulations possible for non-stationary conditions? Hydrol. Earth Syst. Sci. 17:5061–5077.

Theil H (1950) A Rank-Invariant Method of Linear and Polynomial Regression Analysis. Nederl. Akad. Wetensch. Proc. 23:345–381. doi: 10.1007/978-94-011-2546-8_20

Thompson JR, Polet G (2000) Hydrology and land use in a sahelian floodplain wetland. Wetlands 20:639–659. doi: 10.1672/0277-5212(2000)020[0639:HALUIA]2.0.CO;2

Trenberth KE, Shea DJ (2005) Relationships between precipitation and surface temperature. Geophys. Res. Lett. 32:40–50. doi: 10.1029/2005GL022760

Tuteja NK, Vaze J, Teng J, Mutendeudzi M (2007) Partitioning the effects of pine plantations and climate variability on runoff from a large catchment in southeastern Australia. Water Resour. Res. 43:80–95. doi: 10.1029/2006WR005016

Uluocha NO, Okeke IC (2004) Implications of wetlands degradation for water resources management: Lessons from Nigeria. GeoJournal 61:151–154.

Umar AS, Ankidawa BA (2016) Climate Variability and Basin Management: A Threat to and from Wetlands of Komadougu Yobe Basin, North Eastern. Asian J. Eng. Tech 7:25–36.

USGS (2012) Famine Early Warning Systems Network-Informing Climate Change Adaptation Series. A Climate Trend Analysis of Niger. Fact Sheet: 2012:3070–3080.

Valéry A, Andréassian V, Perrin C (2014) 'As simple as possible but not simpler': What is useful in a temperature-based snow-accounting routine? Part 2 – Sensitivity analysis of the Cemaneige snow accounting routine on 380 catchments. Journal of Hydrology 517:1176–1187. doi: 10.1016/j.jhydrol.2014.04.058

van der Linden P, Mitchell JE (2009) ENSEMBLES: Climate Change and its Impacts: Summary of research and results from the ENSEMBLES project. Met Office Hadley Canter, Exeter, UK, 160pp.

van Werkhoven K, Wagener T, Reed P, Tang Y (2009) Sensitivity-guided reduction of parametric dimensionality for multi-objective calibration of watershed models. Advances in Water Resources 32:1154–1169. doi: 10.1016/j.advwatres.2009.03.002

Vano JA, Das T, Lettenmaier DP (2012) Hydrologic Sensitivities of Colorado River Runoff to Changes in Precipitation and Temperature. J. Hydrometeor. 13:932–949.

Veleda D, Montagne R, Araujo M (2012) Cross-Wavelet Bias Corrected by Normalizing Scales, vol 29. American Meteorological Society, Boston, Mass., 20pp.

Wagener T (2003) Evaluation of catchment models. Hydrol. Process. 17:3375–3378.

Wang D, Hejazi M (2011) Quantifying the relative contribution of the climate and direct human impacts on mean annual streamflow in the contiguous United States. Water Resour. Res. 47:1080-1099. doi: 10.1029/2010WR010283

Warner TT (2004) Desert meteorology. Cambridge University Press, Cambridge, New York

Werth S, Güntner A, Petrovic S, Schmidt R (2009) Integration of GRACE mass variations into a global hydrological model. Earth and Planetary Science Letters 277:166–173.

Williams AP, Seager R, Abatzoglou JT, Cook BI, Smerdon JE, Cook ER (2015) Contribution of anthropogenic warming to California drought during 2012–2014. Geophys. Res. Lett. 42:6819–6828. doi: 10.1002/2015GL064924

Xie H, Longuevergne L, Ringler C, Scanlon BR (2012) Calibration and evaluation of a semi-distributed watershed model of Sub-Saharan Africa using GRACE data. Hydrol. Earth Syst. Sci. 16:3083–3099. doi: 10.5194/hess-16-3083-2012

Xu ZX, Takeuchi K, Ishidaira H, Li JY (2005) Long-term trend analysis for precipitation in Asian Pacific FRIEND river basins. Hydrol. Process. 19:3517–3532.

Yapo PO, Gupta HV, Sorooshian S (1998) Multi-objective global optimization for hydrologic models. Journal of Hydrology 204:83–97. doi: 10.1016/S0022-1694(97)00107-8

Yue S, Hashino M (2003) Long term trends of annual and monthly precipitation in Japan. J.Am. Water Resour. Assoc 12:587–596

Yue S, Pilon P, Cavadias G (2002) Power of the Mann–Kendall and Spearman's rho tests for detecting monotonic trends in hydrological series. Journal of Hydrology 259:254–271.

Yue S, Pilon P, Phinney B (2003) Canadian streamflow trend detection: impacts of serial and cross-correlation. Hydrological Sciences Journal 48:51–63.

Zhang X, Yang F (2004) RClimDex (1.0) User Manual. Climate Research Branch Environment, 12pp.

Zhang Y, Xu Y, Dong W, Cao L, Sparrow M (2006) A future climate scenario of regional changes in extreme climate events over China using the PRECIS climate model. Geophys. Res. Lett. 33: D05109–D05115. doi: 10.1029/2006GL027229

Zhang S, Lu XX (2009) Hydrological responses to precipitation variation and diverse human activities in a mountainous tributary of the lower Xijiang, China. CATENA 77:130–142.

Zhang A, Zhang C, Fu G, Wang B, Bao Z, Zheng H (2012) Assessments of Impacts of Climate Change and Human Activities on Runoff with SWAT for the Huifa River Basin, Northeast China. Water Resour Manage 26:2199–2217. doi: 10.1007/s11269-012-0010-8

Ziegler AD, Sheffield J, Maurer EP, Nijssen B, Wood EF, Lettenmaier DP (2003) Detection of Intensification in Global- and Continental-Scale Hydrological Cycles: Temporal Scale of Evaluation: Temporal scale of evaluation. 16:12–18.

Annex

List of published papers

1. **Adeyeri O.E**., Lawin A.E., Laux P., Ishola K.A & Ige S.O. (2019). Analysis of climate extreme indices over the Komadougu-Yobe basin, Lake Chad region: Past and future occurrences. *Journal of Weather and Climate Extremes*. https://doi.org/10.1016/j.wace.2019.100194.
2. **Adeyeri O.E**., Laux P., Lawin A.E., Arnault J., & Kunstmann H. (2019). Calibrating a conceptual hydrological model using multi-objective optimization techniques over the Komadougu-Yobe Basin. *Journal of Hydrology: Regional Studies*. https://doi.org/10.1016/j.ejrh.2019.100655
3. **Adeyeri O.E**., Laux P., Lawin A.E., Ige S.O. & Kunstmann H. (2019). Analysis of hydrometeorological variables over Komadougu-Yobe Basin, Lake Chad region. *Journal of Water and Climate Change*. https://doi.org/10.2166/wcc.2019.283.
4. **Adeyeri O.E.**, Lamptey B.L., Lawin A.E. & Sanda I.S. (2017). Spatio-temporal precipitation trend and homogeneity analysis in Komadougu-Yobe Basin, Lake Chad region. *Journal of Climatology and Weather Forecasting*. https://doi.org/10.4172/2332-2594.1000214.
5. **Adeyeri O.E.**, Akinsanola A.A. & Ishola K.A. (2017). Investigating surface urban heat island characteristics over Abuja, Nigeria: Relationship between land surface temperature and multiple vegetation indices. *Remote Sensing Applications: Society and Environment.* https://doi.org/10.1016/j.rsase.2017.06.005.
6. **Adeyeri O.E.**, Ishola K.A. & Okogbue E.C. (2017). Climate change and coastal floods: The susceptibility of coastal areas of Nigeria. *Journal of Coastal Zone Management*. https://doi.org/10.4172/2473-3350.1000443.
7. **Adeyeri O. E**., Okogbue E.C., Akinluyi F.O. & Ishola K.A (2017). Spatio-temporal trend of vegetation cover over Abuja using Landsat datasets. *International Journal of Agriculture and Environmental Research*. ISSN: 2455-6939.
8. **Adeyeri O.E.**, Laux P., Lawin A.E. & Arnault J. (Submitted). Assessing the impact of human activities and rainfall variability on the river discharge of Komadougu-Yobe Basin, Lake Chad Area. *Environmental Earth Sciences*.
9. **Adeyeri O.E.**, Lawin A.E., Laux P. & Ishola K.A. (Submitted). An approach to homogenise daily maximum air temperature over the trans-boundary Komadougu-Yobe Basin, Lake Chad Region, West Africa. *Scientific African.*

10. **Adeyeri O.E.**, Laux, Lawin A.E., Oyekan K.S.A. (Submitted). Multiple bias-correction of climate models temperature projection and trend: A case study of the transboundary Komadougu-Yobe river basin, Lake Chad region, West Africa. *SN Applied Sciences.*

List of co-authored papers

1. Gbode I.E., **Adeyeri O.E.,** Menang K.P., Insitful J.D., Ajayi V.O., Omotosho J.B., Akinsanola A.A. (2019). Observed changes in climate extremes in Nigeria. *Meteorological Applications*. https://doi.org/10.1002/met.1791.
2. Laux P., Lorenz M., Bliefernicht J., Faye B., Webber H., Dieng D., **Adeyeri O.E.** & Kunstmann H.(2018). Performance of various post-processing bias correction methods for climate change impact studies. *European Geophysical Union (EGU) Research Abstract*. EGU20:2018-18406.
3. Ishola K.A., Fealy R., Mills G., Fealy R., Green S., Casteneda A.J. & **Adeyeri O.E.** (2018). Developing regional calibration coefficients for estimation of hourly global solar radiation in Ireland. *International Journal of Sustainable Energy*. https://doi.org/10.1080/14786451.2018.1499645.
4. Adejato K.O., **Adeyeri O.E**. & Salubi O. (2018). Use of remote sensing and geographical information system in accessing the spatial distribution of Bitumen in Dahomey sub-basin, Southwestern Nigeria. *Journal of Applied Geology and Geophysics*. https://doi.org/10.9790/0990-0601022031.
5. Ige S.O., Ajayi V.O., **Adeyeri O.E.** & Oyekan K.S.A. (2017). Assessing remotely sensed temperature humidity index as human comfort indicator relative to land-use landcover change in Abuja, Nigeria. *Spatial Information Research*. https://doi.org/10.10007/s41324-017-0118-2.
6. Akinsanola A.A., Ajayi V.O., Adejare A.T., **Adeyeri O.E**., Gbode I.E., Ogunjobi K.O. & Nikulin G. & Abolude A.T. (2017). Evaluation of rainfall simulations over West Africa in dynamically downscaled CMIP5 global circulation models. *Journal of Theoretical and Applied Climatology*. https://doi.org/10.1007/s00704-017-2087-8.
7. Ishola K.A., Okogbue E.C. & **Adeyeri O.E.** (2016). Dynamics of surface urban biophysical compositions and its impact on land surface thermal field. *Modeling Earth Systems and Environment Journal*. https://doi.org/10.1007/s40808-016-0265-9.
8. Larbi I., Mama D., Hountondji F.C., **Adeyeri O.E.**, Odoom P.R (Submitted). Climate change projections and impact on water balance components in the Vea catchment, West Africa. Watershed Ecology and the Environment.

Candidate biography

Adeyeri Oluwafemi Ebenezer was born in the city of Akure, Ondo State, Nigeria. He attended the Federal University of Technology Akure where he bagged his Bachelor of Technology (Hons) and Master of Technology in Meteorology in the year 2011 and 2015 respectively. He proceeded to the University of Abomey-Calavi for his doctoral studies, fully sponsored by the German Federal Ministry of Education (BMBF) under the West African Science Canter on Climate Change and Adapted Land Use (WASCAL) initiative. During his doctoral studies, he secured various international fellowships like the Karlsruhe Institute of Technology doctoral fellowship, International Center of Theoretical Physics fellowship, Committee on Space Research fellowship and the Netherlands government fellowship in order to pursue different niche of researches which is broadly related to his doctoral studies. His research interests include hydrological and climate modelling; statistical downscaling and bias correction of climate models; atmospheric, satellite meteorology, climate and hydrology extreme studies; remote sensing and geographical Information system in urban climate and environmental studies and regional climate variability impact on water resources.

Abstract: This study was carried out to investigate the hydrological response of the Komadougu-Yobe basin to climate change using daily observed data and outputs from regional climate models. Analyses carried out in this study include (a) the spatiotemporal trends and correlation in daily hydrometeorological variable as well as climate extremes, (b) the quantification and segregation of the contributory effects of precipitation variability and human influences on the variations in river discharge, (c) the calibration of and conceptual hydrological model using six evolutionary optimization methods and three combined objective functions over the study area. Results from this study showed an increasing trend of climate extremes, temperature, precipitation and river discharge. The distribution of LULC also affected the volume of river discharge. However, the impact of human activities and precipitation variability on river discharge was seen to be equally shared in the basin. Furthermore, the applied model parameters' optimization methods showed reasonable abilities to simulate runoff with a satisfactory level of accuracy towards more accurate representation of the river discharge in the basin in the context of climate change, climate extremes and water resources. Therefore, the attempts in this study to characterize areas in the river basin with the potential risk of climate extreme events will serve as a useful resource for assessments of the potential impacts of climate change on human, ecosystems, water resources.

Keywords: climate change, water resources, hydrological modelling, homogeneity, bias-correction, landuse landcover.

PhD	
Candidate Name	**Adeyeri Oluwafemi Ebenezer**
Thesis Title	**Modelling the hydrological response of the Komadougu area of Lake Chad basin to climate change**
GRP/CCWR/INE/WASCAL – UAC	
Month, Year	**December, 2019**